Characterizing Antibody Escape Variants in the Respiratory Syncytial Virus Fusion Glycoprotein

A Thesis

Presented in Partial Fulfillment of the Requirements for the

Degree of Master of Science

with a

Major in Biology

in the

College of Graduate Studies

University of Idaho

by

Laura E. Hutchison

Major Professor: Tanya Miura, Ph.D.

Committee Members: Paul Rowley, Ph.D.; Jill Johnson, Ph.D.;

Daniel Weinreich, Ph.D.

Department Administrator: James Nagler, Ph.D.

August 2021

Authorization to Submit Thesis

This thesis of Laura E. Hutchison submitted for the degree of Master of Science with a Major in Biology and titled “Characterizing Antibody Escape Variants in the Respiratory Syncytial Virus Fusion Glycoprotein,” has been reviewed in final form. Permission, as indicated by the signatures and dates below, is now granted to submit final copies to the College of Graduate Studies for approval.

Major Professor: _____ Date: _____

Tanya Miura, Ph.D.

Committee Members: _____ Date: _____

Paul Rowley, Ph.D.

_____ Date: _____

Jill Johnson, Ph.D.

_____ Date: _____

Daniel Weinreich, Ph.D.

Department Administrator: _____ Date: _____

James Nagler, Ph.D.

Abstract

Monoclonal antibodies (mAbs) are becoming more commonly used as prophylactics or therapeutics for viral infections. While the binding specificity of the mAb may provide adequate protection against the wild-type virus, natural selection will favor viral genomes that acquire mutations leading to amino acid changes in viral proteins where mAbs normally bind. This results in a phenomenon known as antibody escape. This thesis project focuses on the mAb D25 and its interaction with the respiratory syncytial virus (RSV) fusion glycoprotein (F). F mediates viral entry into host cells and fusion between neighboring cells, while D25 neutralizes the ability of F to function in entry kinetics. However, F readily mutates to evade the neutralizing effects of mAbs including D25, resulting in variants that lead to antibody escape. A D25 mutational library encompassing 30 sites within the D25 binding epitope of F was built with the help of molecular modeling. We developed a high-throughput pipeline to screen these variants for antibody escape using methodologies such as deep mutational scanning and retroviral gene expression systems. Several individual variants within the D25 library were also assessed for antibody binding differences using flow cytometry and in-cell ELISA. Along with molecular modeling predictions of F mutations that give rise to antibody escape, our lab previously identified three mutations via deep sequencing after several passages of RSV in HEp-2 cells with varying concentrations of the D25 mAb. These mutations, Q202R, N208Y, and N208K were identified, where N208Y and N208K were both predicted by molecular modeling. This project allows for the identification and characterization of potential escape mutations in F by screening all potential amino acid variants at the 30 sites within the D25 binding epitope. We can use our findings to assist in viral variant surveillance for RSV, first using a broad deep mutational scanning – based screen to find potential escape mutants and then by validating those findings using individual-based binding assays.

Acknowledgements

I would first like to thank my major professor, Dr. Tanya Miura. Your guidance and mentorship have been imperative to the success in my graduate career. I appreciate your patience and willingness to work with me through the navigation of this project. You are one of the most knowledgeable scientists I have had the privilege to work with and am grateful for my time spent working in your lab.

I would like to thank Dr. Paul Rowley, members of our MoVIES working group, as well as Dr. Jagdish Patel. Thank you, Dr. Rowley, for your enthusiasm and excellent ideas that helped to develop the course of this project and for your ability to push my knowledge boundaries. Thank you to the MoVIES working group for your invaluable input and brainstorming of ideas. Thanks to Dr. Jagdish Patel for performing molecular modeling experiments as the basis of my project.

Dr. Jill Johnson and Dr. Weinreich, thank you for your contribution to this project. Your feedback has helped shaped the course of this degree and given me ideas to discuss related to future experiments or alternative strategies to answer questions. I appreciate the time and effort spent on evaluating me and testing my knowledge. Dr. Lee Fortunato, I would like to thank you for your assistance and guidance in helping to make my MLV library stocks. Without you, I would not have been able to make the system work.

I would next like to thank Sierra Beach, Manny Ijezie, Kevin Hutchison, McKenna Hull, and Frankie Scholz for their continuous support. Thank you to Frankie for your work on the D25 evolution experiments. I want to thank Melissa Oatley at WSU for her assistance with FACS for sorting library-transduced cells. I would also like to thank National Science Foundation EPSCoR Research Infrastructure Improvement Program: Track-2, award number OIA-1736253 for the opportunity to be involved in this work.

Lastly, I want to thank Tim Steffens for a wonderful three semesters of working with microbiology students and for being a fantastic mentor for me. My time spent as a TA has led me to pursue a career in science education and am grateful for the experiences I have gained working with Tim.

Dedication

I want to thank my parents Pete and Angie, who have supported and encouraged me when I felt like all my experiments were going wrong. They have always been a great sounding board to help me make the tough decisions. I want to thank my brother Josh, who has been incredibly supportive and very encouraging with everything I pursue in life, including this degree.

I want to thank my in-laws for being so welcoming, understanding, and supportive during my time in this program. I am very thankful for their advice and insight.

To my dear friend Rachel – thank you for always being a phone call away when I needed you most. You helped me push through some of my lowest points and celebrated with me during my highest points.

To my husband – Kevin, I dedicate this degree to you. I could not have completed this degree without your constant love and support.

Table of Contents

List of Tables

List of Figures

CHAPTER 1: LITERATURE REVIEW

RSV Characteristics

Respiratory syncytial virus (RSV) is a member of the *Pneumoviridae* family and *Orthopneumovirus* genus. It has a negative sense, single stranded RNA genome, and is enveloped by a lipid bilayer that it derives from host cells and uses to aid in membrane fusion processes in early stages of infection. There are two known subtypes of RSV (A and B) that tend to co-circulate together during the same RSV season. The RSV season typically peaks between mid-December to late February (1). Researchers have shown differing results among disease severity when comparing the two subtypes, but many studies provide evidence that subtype A infections cause more severe disease (2-4).

RSV particles are known to exist in both spherical and filamentous forms, but it is unknown whether spherical or filamentous is more common or causes more severe disease in infected individuals. Contained within the RSV particles, whether spherical or filamentous, is the RNA genome that is surrounded by nucleoprotein for protection against detection and RNA degradation within the host cell environment. Phosphoprotein and an associated RNA-dependent RNA polymerase make up part of the genome-nucleoprotein complex within the core of the virus particles. Phosphoprotein helps to link the RNA polymerase to the genome-nucleoprotein complex and aids in replication and transcription by interaction with various other proteins (5). The role of the RNA polymerase is to replicate the RNA genome to be packaged into new budding virions as well as participate in 5’ capping and cap methylation of mRNAs (6). These proteins associated with the RNA genome are encased in a mesh of matrix protein that serves as a primary capsid structure for the RSV particles. Matrix protein is involved in viral assembly and budding. It is also found to localize to the host cell nucleus during early infection stages to play a role in inhibiting transcription processes of the cell (7-9).

Surrounding the virion is a lipid bilayer that is studded with three different glycoproteins: the small hydrophobic protein (SH), the attachment glycoprotein (G), and the fusion glycoprotein (F). SH is thought to act as a viroporin, allowing transport

of ions in and out of the viral capsid. The precise role of these ion channels in the context of viruses is not fully understood and holds true in the case of the SH protein of RSV (10, 11). The G protein exists as both a transmembrane protein involved in attaching virions to host cells via receptor interactions and as a secreted protein that is known to act as an antigenic decoy to thwart the host immune system (12-14). F mediates fusion between the viral lipid bilayer and the lipid bilayer of host cells and functions to fuse nearby cells together when expressed on infected cells, forming large syncytia *in vitro* (15, 16). This protein is a type I transmembrane fusion protein that is synthesized as a precursor called F_0 that is approximately 574 amino acids in length. A proteolytic cleavage event takes place within the Golgi apparatus, where full length F is cleaved by furin-like proteases of the host to yield two subunits called F_1 and F_2. These subunits are linked by two disulfide bonds to make the heterodimeric protomer of F. Three of these protomers come together to form the fusion protein trimer that is present on the surface of the virion. The F protein sequence is highly conserved between the different RSV subtypes, which is important to consider when designing vaccines, therapeutics, and prophylactics.

RSV Replication Cycle

RSV particles need to initially attach to a host cell before proceeding with downstream infection steps. Both F and G glycoproteins are known to interact with host cell surface proteins that aid in attachment. G has been shown to bind many different proteins on the surface of cells, including glycosaminoglycans as well as heparin sulfate proteoglycans through the heparin-binding domain of G (17, 18). Heparin sulfate proteoglycans are not found on the surface of ciliated human airway epithelial cells though, the primary cell type that RSV infects (16, 19). This indicates that these interactions could be an *in vitro* artifact. G has also been shown to interact with CX3C chemokine receptor 1 that is expressed on the surface of ciliated bronchial epithelial cells (20-22). Though the G protein is not required for cellular attachment *in vitro*, studies have demonstrated that the interaction between G and CX3C chemokine receptor 1 are important for downstream signaling resulting from host cell receptor interactions, leading to the chemotaxis of immune cells (20-22).

The F protein plays a role in attachment of the virus particles to host cells, since variants of RSV that do not have G or SH proteins are still able to enter and infect cells *in vitro* (23). F has been shown to interact with many different cellular receptors, including intercellular adhesion molecule 1, epidermal growth factor receptor, and nucleolin (24-26). A study from 2011 demonstrated F binding to nucleolin and this interaction aiding in cellular attachment (26). Many other viruses are found to interact with nucleolin for cellular entry, such as parainfluenza virus 3, enterovirus 71, HIV-1, among others (27-29). In young children, cells of the alveoli in the lower respiratory tract are still growing and dividing, leading to higher nucleolin quantities on the cell surface. Nucleolin is also thought to interact with the G protein to promote infection. An increase in nucleolin on the cell surface can lead to a higher frequency of interactions between nucleolin and G. A recent study showed an induction of nucleolin expression upon interaction between G and CX3C chemokine receptor 1, indicating that G could be used for the facilitation of RSV attachment (30).

Upon attachment to the surface of a cell, the membrane of RSV and membrane of the host cell must fuse to allow the nucleoprotein-coated RSV genome into the cell cytoplasm (figure 1). It is thought that RSV may not only fuse at the surface of the cell with the plasma membrane but may also be able to fuse with endosomes after utilizing micropinocytosis pathways (31). Another report showed that the first several fusion steps may involve docking of the particles at cholesterol-rich domains in the plasma membrane, and the remaining fusion steps occur inside endocytic vesicles (32). In either case, the overall fusion steps remain the same, beginning first with a triggering event of F from its pre-fusion to an intermediate state, then to its post-fusion conformation. Prior to triggering and fusion, F exists as a metastable trimer on the surface of the virion. It is not entirely known what mechanism triggers F. One hypothesis is known as the ‘provocateur’ or ‘association model’, involving G triggering F by destabilization, after G has interacted with its cell surface receptor (33, 34). Another hypothesis is that there is a background of spontaneous conversion from pre-to-post fusion, leading to the triggering of F at the right place and time near the surface of a host cell. Since F is metastable and can convert to post-fusion spontaneously, it is possible that this type of triggering could

occur (35). During F triggering, heptad repeat A that contains the highly hydrophobic fusion peptide, extends out towards the host cell membrane (figure 1). The fusion peptide embeds itself into the lipid membrane of the cell, forming the intermediary structure of F. Heptad repeat B (HRB) then folds back onto heptad repeat A (HRA) and jackknifes around domains I and II to form a six-helix-bundle. Residues present within the heptad repeat motif allow for hydrophobic and charge-charge interactions leading to helix bundling. This bundling of motifs allows the membranes to come into close enough proximity that they can fuse together, leaving behind a fusion pore for the RSV genome to enter the cytoplasm of the cell (12, 36).

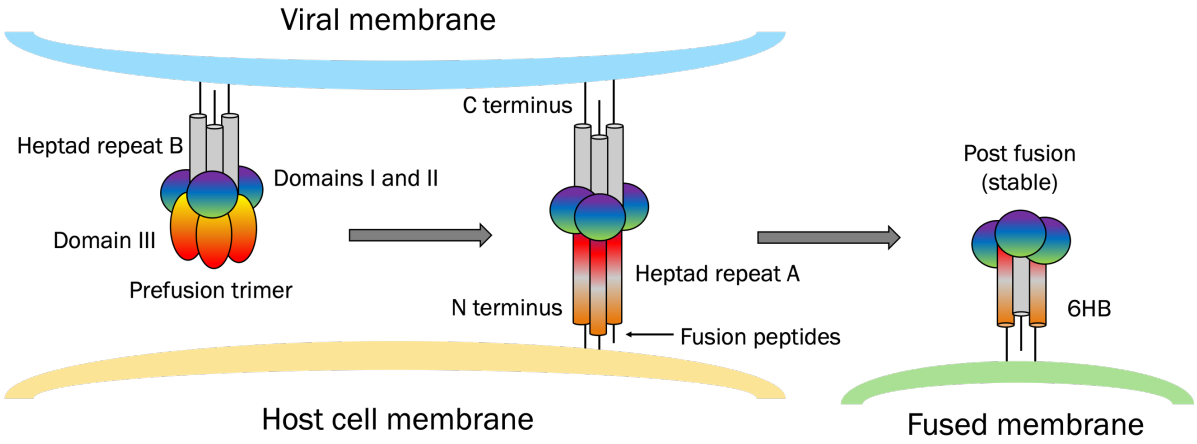

Figure 1: F protein mechanism of action. Pre-fusion F exists as a metastable trimer on the surface of the virion. Upon triggering, the fusion peptides on the N-terminal ends of the monomers are released from the core of the protein and embed themselves in the host cell membrane. HRA and HRB associate to form the stable 6-helix bundle to fuse the viral and host cell membranes together. Figure adapted from McLellan et al. 2011 (36).

After successful entry into the host cell cytoplasm, the RSV genome is utilized first as a template for transcribing mRNAs to be translated to viral proteins. These mRNAs are made using the virally encoded RNA-dependent RNA polymerase (RdRP) enzyme. Each mRNA is transcribed from an individual gene within the genome of RSV (37). RdRP binds the negative sense genome at the 3' end and transcribes the RNA into positive sense mRNAs in a gradient fashion. Genes that are closest to the 3' end are transcribed at a higher frequency than those genes closer to the 5' end, because the proteins that these genes encode are needed in much higher amounts for packaging new budding virions as well as downregulating host immune responses. The RdRP is also used for replicating the negative sense genome into

positive sense anti-genomes to be used by the RdRP again to yield more negative sense genomes to be packaged.

Clinical Significance of RSV Infection

Acute lower respiratory tract infections (ALRIs) are considered the leading cause of death for infants across the globe. One virus that greatly contributes to the disease burden of ALRI is RSV. RSV was first discovered and isolated in the 1950's. It is considered a common childhood infection, infecting approximately 98% of individuals by the age of three and it is the most common contributor to childhood ALRIs (38-40). Children who develop a more severe RSV infection at a young age are more likely to have asthma and wheezing later on in life, leading to potential health complications (41). Certain risk factors such as prematurity at birth, congenital heart disease, bronchopulmonary-related diseases, as well as other factors including crowded living conditions and malnutrition can all contribute to an infant being at higher risk of severe RSV infection (42). There are upwards of a million RSV cases per year worldwide including hundreds of thousands of deaths, and though RSV has been studied for over 50 years, there is no vaccine to prevent infection (43, 44). This can be attributed to many factors, including a lack of protection from natural RSV infection due to an induction of low-affinity neutralizing antibodies and a need for more knowledge surrounding this lack of protection among different populations including young children as well as the elderly (45, 46). The immature immune systems of infants under the age of 6 months may be a contributing factor for reduced immunity as well as maternal antibodies possibly playing a role in suppression of the immune response of the infant (39). In elderly populations, a process known as immune senescence is a confounding factor when designing and administering an RSV vaccine (47).

Over the years, many different avenues have been explored in the process of developing prophylactic options, vaccines, and therapeutics. In the 1960's, a formalin-inactivated subunit RSV vaccine was developed and administered to children. This vaccine caused enhanced respiratory disease upon infection by the induction of an incorrect T cell response leading to increased inflammation and

eosinophilia in the lungs (48, 49). After a re-evaluation of human sera from patients that received this vaccine, it was found that fusion inhibiting antibodies were not present. Instead, antibodies targeting non-neutralizing epitopes of F were found, which could have decreased the effectiveness of the vaccine, due to lack of neutralization by the antibodies (50).

During the next several decades, only RSV intravenous immunoglobulin (RSV-IVIG) and the monoclonal antibody (mAb) palivizumab (Synagis) developed in the 1990's have been licensed and administered to patients. Palivizumab is the only prophylactic option still used today but it has drawbacks and limitations: a high cost, a lack of broad protection for all infants, and the requirement for multiple intramuscular injections throughout the RSV season. Palivizumab is a humanized neutralizing antibody that targets the F protein to prevent membrane fusion in both RSV subtypes (51). This antibody was developed to eliminate the need for intravenous injection used with RSV-IVIG while better protecting infants and children with underlying cardiovascular diseases from severe infection from RSV. Subsequent studies showed that palivizumab greatly reduced hospitalizations related to RSV infection and was then approved by the FDA for at-risk children and infants and is still used today (52, 53).

Work across the globe is being performed to develop and test new vaccine, therapeutic, and prophylactic candidates. These include vaccines such as live-attenuated, vector-based, particle-based, and subunit vaccines as well as mAbs (46). One promising candidate is DS-Cav1, a subunit vaccine that aims to elicit an antibody response against pre-fusion F. DS-Cav1 was developed using structure-based design techniques, involving the stabilization of the F trimer using various mutations and stabilization domains to maintain antigenic site Ø for natural antibody production (54). Six different structures were designed with a stable antigenic site Ø and tested for eliciting neutralizing titers in mice and non-human primates, where the DS-Cav1 structure performed best (54). DS-Cav1 was then studied using human serum in 2019 to detect vaccine-induced neutralizing activity (55). In both RSV-A and RSV-B subtypes, neutralization was found to be robust, demonstrating the conservation between F across subtypes (55). A phase I clinical trial report released

in April of 2021 demonstrated that DS-Cav1 was tolerated well by adults and showed an increase in F specific antibodies in serum and neutralizing activity that was sustained for 44 weeks post injection (56).

Ideally, a vaccine candidate would be able to protect not just at-risk infants, but all infants and young children as well as older adults and keep person-to-person transmission minimal (57). There is also discussion about the immunization of pregnant mothers to protect their children from RSV infection after birth. Designing a vaccine to target all these demographic groups effectively is extremely difficult, and why it is essential that work continues to be performed in the laboratory setting.

RSV Therapeutics

The availability of therapeutics as well as vaccination or prophylactic options to protect individuals from RSV infection is important to consider. In some cases, antiviral drugs, therapeutic antibodies, or small molecule inhibitors may be utilized in conjunction with prophylactics to better control the onset of severe disease in certain individuals. Ribavirin was used as the first RSV therapeutic drug and remains the only FDA-approved therapy available for RSV infection. Ribavirin is a nucleoside analog that inhibits the activity of the highly conserved viral RdRP, and is administered as an aerosol that upon inhalation reaches the lower respiratory tract in infected individuals (58). This drug has shown activity against other RNA viruses as well, including Zika virus and hepatitis C virus (59, 60). Ribavirin has shown some clinical benefit in controlled studies, especially in adults, but has also been found to be potentially toxic for those administering the drug or others exposed to it during treatment (61, 62). Since 2006, use of ribavirin is not generally recommended due to lack of pediatric efficacy studies and potential toxicity, but is still used for patients that are immune compromised to try and prevent infection from reaching the lower respiratory tract (63-65). Thus, there is still a need for drugs that are more effective at treating RSV infections in children and adults with compromised immune systems as well as healthy children and older adults who suffer from severe disease.

Other RSV antiviral therapies come into play at multiple stages of the lifecycle of RSV, including viral attachment, during viral fusion and uncoating processes, and

mRNA synthesis as is the case for ribavirin (66). Several therapeutic antibody drug candidates in development include RI-001 and RI-002, REGN2222, ALX-0171, and the mAb 131-2G (66). All these antibodies, apart from RI-001 and RI-002, bind either the F or G protein to hinder attachment and fusion processes in an infected individual. RI-001 and RI-002 are polyclonal antibody pools containing high amounts of RSV-neutralizing antibodies. There are many other types of therapeutic candidates in the pipeline for clinical use, such as small molecules, nucleoprotein inhibitors and nucleoside analogs (66). Many of these candidates are still in need of further studies to prove antiviral activity and safety in their target population.

The D25 Monoclonal Antibody

The human antibody D25 targets pre-fusion specific F with high neutralizing capabilities (67, 68). This antibody was discovered through RSV specific memory B cells from a healthy donor. Memory B cells were transduced with genes aiding in proliferation and antibody production (Bcl-xL and Bcl-6). After two weeks of culturing the cells, the secreted monoclonal antibodies were harvested and subjected to microneutralization assays to test for resistance to neutralization. Four of the highest neutralizing monoclonal antibodies were then characterized as D25, AM14, AM16, and AM23 (67). In 2013, the D25 binding site was discovered and described in detail after its co-crystal structure was solved (69).

D25 binds antigenic site Ø of the pre-fusion F protein located on the apex of the protein furthest from the viral membrane (figure 2). In 2013, it was shown that D25 and other site Ø binding antibodies were able to block fusion when added after viral attachment (69). This site is not as conserved as other binding sites within the F protein, suggesting that it could contribute to subtype-specific immunity (70). Site Ø is only present on pre-fusion F and undergoes major conformational changes during F triggering (figure 2). It was then demonstrated that D25 bound to pre-fusion F stabilizes F in the pre-fusion state (69). Though there are few changes in the secondary structure of F between the pre-and-post fusion conformations, significant changes are found within the tertiary structure. The change in tertiary structure demonstrates D25's ability to bind pre-fusion F but not post-fusion F. It is thought that

because site Ø is located on the apex of the F trimer that antibodies can more easily access the site, possibly explaining why most naturally induced antibodies found in human sera are against pre-fusion F.

A derivative of D25 called MEDI-8897 (nirsevimab) is currently in later stages of clinical trials for prophylactic use in preventing RSV infection (71-73). MEDI-8897 was developed by mutating the complementarity-determining regions (CDR) of the D25 mAb until improved neutralization activity was demonstrated (71). In 2017, over 1500 mAb variants were tested until MEDI-8897 was selected and the co-crystal structure of MEDI-8897 bound to F was subsequently solved (PDB code 5UDC). MEDI-8897 had 5 amino acid substitutions in CDRs and 4 germline reversions within the heavy chain sequence. MEDI-8897 was shown to be 4 times more potent at neutralizing RSV than D25 based on microneutralization assays. It is suspected that the difference in potency between D25 and MEDI-8897 involves amino acid interactions of the antibodies with the F2 subunit of the F trimer since both D25 and MEDI-8897 interact with F residues at sites 200, 201, 208, and 209 (71). Many of the altered residues in MEDI-8897 are in or near CDRH1 and CDRH3, leading to an increase in the negative charge of the CDRH1 (71). This CDRH1 is near the positively charged lysine of site 68 in F2, promoting charge-charge interactions. A mutation in the CDRH3 again creates a negative charge that participates in a salt bridge with a lysine at site 65 in the F2 subunit (71).

To extend the half-life of the antibody, 3 amino acid mutations were made in the fragment crystallizable (F_c) region of the antibody allowing for 2-4-fold increase in the half-life of the mAb in healthy adults and cynomolgus monkeys (74). Due to similarities in binding between MEDI-8897 and D25, it is important to study potential escape mutations in D25 that could also escape MEDI-8897. Characterizing variants that show significant escape from D25 could lead to improvements in the design of MEDI-8897 to better protect individuals from severe disease.

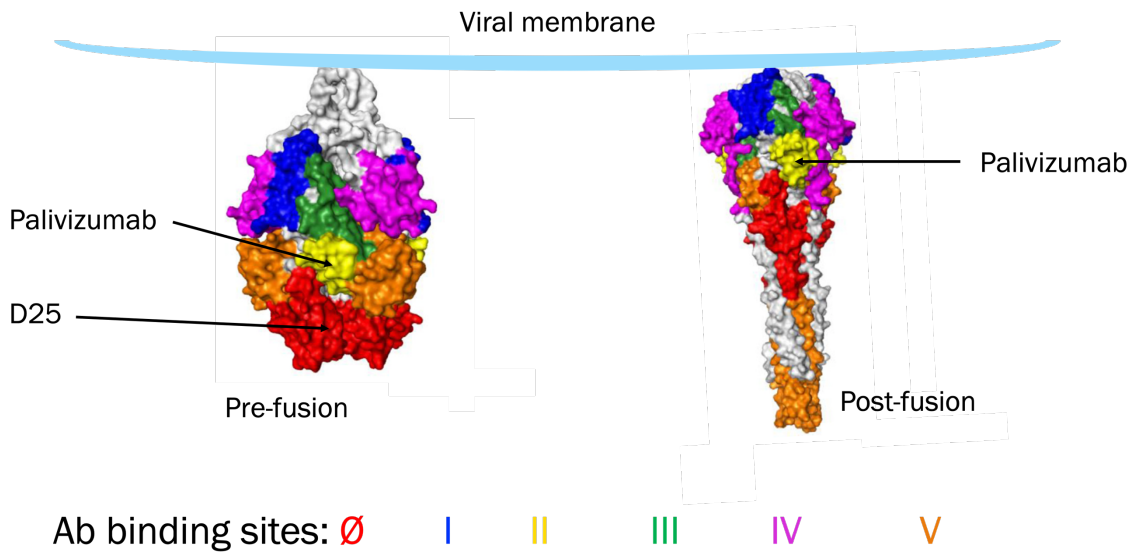

Figure 2: Pre-and post-fusion forms of F and corresponding antibody binding sites coloring the space-filling diagrams. Palivizumab binds site II of pre-and post-fusion F, while D25 and MEDI-8897 bind site Ø. Site Ø is a pre-fusion specific antibody binding site, meaning that it is present on pre-fusion F only. Image adapted from Rossey et al. 2017 (75).

Use of Monoclonal Antibodies

Monoclonal antibodies are becoming increasingly more common as either a therapeutic or a prophylactic for treating or preventing viral infections, respectively (76-78). There are many mAbs in development and clinical trials currently underway for several viruses, including RSV, Ebola virus, influenza virus, human HIV-1 and more (79-83). MAbs can bind antigens potently and specifically, and there are many ways to generate mAbs for various kinds of viruses. These include CHO-S cell-based antibody expression, single-memory B cells, and antibody secreting plasma B cells (84). Freestyle™ CHO-S® (Gibco) cell-based antibody expression has been used in the Miura lab to generate anti-F antibodies such as D25 and 101-F. CHO-S cells are transfected with heavy and light chain antibody plasmids to generate the heavy and light chain proteins. The heavy and light chains then associate to form the mature antibody and are secreted from the cells where they can be harvested and purified.

MAbs are often initially made by humans who were naturally infected with a virus and those antibodies are further optimized to improve stability and half-life (78). These mAbs can potentially be used for prevention or treatment in the incredibly young, the elderly, and immune compromised who are unable to receive vaccines. A

major drawback to using mAbs is the potential for the phenomenon known as antibody escape, discussed in more detail in the next section. Antibody escape can render the antibody therapy or prophylactic ineffective due to mutations in the antibody binding site. This can lead to the neutralization of the virus by sterically hindering viral-host cell protein interactions that typically lead to fusion and subsequent uncoating of the virus genome.

In the context of RSV, the use of antibodies as both a prophylactic and treatment option began in the mid 1980's. Researchers at this time discovered that the administration of IVIG, containing a high titer of anti-RSV antibodies, greatly decreased recovery time after infection with RSV in one infant. IVIG was also found to reduce viral replication in both a cotton rat and non-human primate model when used as a therapeutic, and when given prophylactically prevented the virus from causing lung pathology in the cotton rats (85-87). The development of a more specific and potent neutralizing antibody to RSV was thought to be the next best way to improve upon the use of IVIG. These neutralizing monoclonal antibodies would then be developed, leading to several prophylactic and therapeutic mAb developments over the next several decades (51, 72, 83, 88-93).

MAbs are developed to target the F protein of RSV, which makes an excellent target for mAbs mainly because antibodies found to clear RSV during natural infection are primarily anti-F antibodies (94, 95). F also maintains a highly conserved protein sequence between the two different subtypes of the virus, A and B, roughly 95% (88, 96-99). It is also a promising target because of its primary function of mediating viral membrane fusion with host cell lipid bilayers and is essential for the first steps of viral infection (69, 100). The binding of mAbs to F can prevent membrane fusion and cell-to-cell spread via syncytia formation, thus neutralizing the virus. As mentioned in the clinical significance section, palivizumab is the only mAb for the prevention of RSV infection (46). Palivizumab is a humanized mAb given to at-risk infants and young children via intramuscular injection several times during the typical cold and flu season as a prophylactic to prevent the onset of RSV infection. The mAb functions by targeting antigenic site II of the F protein (figure 2), preventing genome entry by inhibiting conformational changes required to induce fusion during

infection (101, 102). As mentioned previously, palivizumab has been shown to be somewhat effective as a prophylactic but is not the most cost-effective option and is only approved for at-risk infants with underlying conditions especially affecting the heart and lungs (91, 103). Another antibody called motavizumab (MEDI-524), is an affinity-optimized mAb that also binds site II of the F protein as it is derived from palivizumab. Motavizumab was developed by evaluating different affinity-optimized variants from palivizumab in cotton rats for their inhibition of RSV replication as a prophylactic (104). The most potent antibody, later named motavizumab, initially showed promising results in studies focused on its potency for neutralization and binding specificity to F *in vitro*, neutralizing F 20-fold better than palivizumab and a binding improvement of 70-fold (104). Though initially promising, motavizumab was turned down because it did not demonstrate enough improved efficacy over palivizumab in phase II and III clinical trials. Clinical trial results from 2010 however, demonstrate that motavizumab as a prophylactic for high-risk children yielded approximately the same rates of hospitalizations as children given palivizumab, and motavizumab decreased medically attended RSV lower tract infections by 50% (105). These reasons, among others, is why it is imperative to continue exploring other more protective, potent, and cost-efficient immunoprophylaxis options that protect a broad group of individuals (106).

As mentioned previously, a more recent mAb of interest for the prevention of RSV infection is MEDI-8897 or nirsevimab, that has a longer half-life in serum than D25 due to modifications in its F_c region (82). Nirsevimab would only need to be administered to patients once at the beginning of their first cold and flu season and would be a more broad-reaching mAb for most infants and children instead of only at-risk groups. This mAb is currently in phase III of clinical trials after showing success in earlier phases (107). It has been shown to neutralize several RSV A and B strains at a higher potency than that of palivizumab and reduces viral load in the lungs of cotton rats more effectively than palivizumab (72, 82).

Antibody Escape

The phenomenon known as antibody escape is an extremely important caveat to consider when designing mAbs that target viruses (108, 109). This is especially true for RNA viruses, that have a high genomic mutation rate. The use of mAbs that bind a specific epitope on a viral protein can create a selective pressure that drives the evolution of escape variants in the population (110-112). The presence of clinical escape variants can render mAbs ineffective as a treatment or prophylactic, therefore a greater understanding of all the possible escape mutations within virus systems is crucial. A greater understanding of possible escape mutations can assist in the process of optimizing clinically used mAbs for a broader protection against escaping viruses. Antibody escape is typically studied by first allowing the wild-type virus of interest to replicate in cell culture in the presence of neutralizing antibody. This generates antibody-resistant mutants in the population that can be further isolated. Once these mutants have been isolated and sequenced, they can then be used in several different assays to analyze neutralization by antibodies, viral growth kinetics, and antibody binding. Antibody neutralization assays can involve a $TCID_{50}$ assay (tissue culture infectious dose 50) to first quantify infectious virus, then determine how much antibody is required to effectively neutralize the infecting virus *in vitro* (113). $TCID_{50}$ assay materials and methods can be found on page 54. There are multiple other ways to assess antibody neutralization, including serum virus neutralization assays (SVN) and pseudotyped virus-based assays (114-116). SVN assays use serially diluted serum that contains neutralizing antibodies and virus that is added to the serum to test for neutralization. Cells are then added to the serum and virus mixture and assessed for cytopathic effect. A pseudotyped virus-based neutralization assay was developed in 2020 to quantify SARS-CoV-2 neutralizing antibody. In this study, the researchers used VSV-G pseudotyped virus packaging system with a luciferase reporter gene and the spike protein from SARS-CoV-2 (116). When neutralizing antibodies are present, the amount of chemiluminescence activity is diminished and subsequently detected.

The gold standard method to approach neutralization assays, however, are plaque reduction neutralization tests (PRNTs) (117). The basis of this assay is to mix

virus with antibody, allowing any neutralization to occur. The virus is then added to cells *in vitro* and the wells are overlayed with a viscous media. Plaque formation, or regions of viral replication leading to the destruction of cells, is then detected by dyeing the wells with a vital dye such as crystal violet. If there are plaques present within the well, that indicates that the virus is not being neutralized by the antibody. Few or no plaques in the well indicates that the antibody is neutralizing the virus. This type of assay can involve the screening of different viral mutants but can also be somewhat labor intensive and low throughput. This aspect of PRNTs can make it difficult to screen large variant libraries for resistance to neutralization by antibodies (118). It should also be noted that not all viruses form plaques, making this assay difficult for assessing neutralization using those viruses (119).

Viral growth kinetics are also analyzed to determine if the escape mutants replicate as effectively as the wild-type virus *in vitro*. Viral titers can be determined by use of $TCID_{50}$ or plaque assay and compared between different viral variants (120, 121). Many studies also incorporate a competitive replication assay, involving the infection of cells with wild-type virus and escape mutants simultaneously, sequencing the released virus to determine the variants present, then measuring the relative amounts of virus using qRT-PCR. Sequence analysis can then be used on the wild-type and escape mutant-containing viruses to distinguish between variants. This method yields relative replication rates of the different variants as well as the reference wild-type virus within the same culture (122). Antibody binding kinetics are typically analyzed in these studies because it is important to know that the relationship between antibody binding and susceptibility to neutralization is positively linear. As neutralization susceptibility increases, antibody binding also increases, indicating that viral variants that are less susceptible also bind antibody at a lower strength (121). These kinds of experiments help indicate that the variants of interest are indeed escaping antibody neutralization.

This traditional workflow of studying antibody escape is somewhat incomplete. The selection steps that initially establish variants within the population in the presence of antibody also create a strong bias that can lead to overwhelming the population with only those prevalent escape variants. This results in only a small

fraction of the potential escape mutations being identified and further studied; thus, these experiments are not as completely thorough as they could be (109).

Antibody escape has been well-studied using many virus models, including RSV, rabies virus, influenza virus, Ebola virus, dengue virus, and Zika virus among others (113, 123-130). Even more recently, antibody escape has been studied in the context of the current SARS-CoV-2 pandemic (131, 132). Studying antibody escape in the context of RSV is important when creating a watchlist of potential escape mutations that could become prevalent clinically. Antibody escape studies can help researchers better design prophylactics or treatment options for infected individuals before antibody-resistant variants arise.

With palivizumab being used clinically for the prevention of RSV infection in at-risk infants and children since 1998, studies began to focus on potential clinical palivizumab escape mutations that could be a cause for concern in RSV-infected patients. Before palivizumab was introduced clinically, research groups were already studying anti-F antibody escape. The murine parent of palivizumab, mAb 1129, was being studied along with other mAbs to find antigenic sites on F to elucidate antibody escape variants at certain neutralizing epitopes. The escape mutants of interest in this study were not neutralized by any of the mAbs in antigenic site A, where mAb 1129 binds (99). An amino acid change at position 275 from a serine to phenylalanine was found in F due to selection with mAb 1129, indicating that this antibody escape mutation arose *in vitro* in a critical antibody binding and fusion-mediating region of F (133). A research group in 2004, led by Xiadong Zhao, showed resistance to palivizumab in RSV mutants using *in vitro* as well as *in vivo* methodologies. In cell culture, RSV strain A1 was propagated in the presence of palivizumab for several passages. The researchers picked viral plaques and performed nucleotide sequencing. Several mutations were found within the F gene, including a change from alanine to threonine at amino acid site 828 as well as a change at site 272 from lysine to methionine (134). In 2008, nasal wash samples from infants infected with RSV and developed lower respiratory tract infections (LRTI) who were also given palivizumab showed a mutation in F at amino acid 272. The amino acid change at this site was from a lysine (K) to a glutamate (E) (135). These

data sparked an interest in many research groups to identify potential escape variants in RSV. A research group from MedImmune in 2011 generated several palivizumab and motavizumab escape mutants *in vitro* and obtained clinical samples from a phase three clinical trial to study the resistance to antibody in these mutants. It was found that the *in vitro* selected RSV variants were mutated at the same 272 amino acid site that was observed in the 2008 study. The wild-type lysine was found to have mutated to several other amino acids including glutamate. This K272E mutant, among others at this position as well as position 275, was also observed in the patient samples analyzed by the research group. Further experimentation demonstrated that all the mutants were palivizumab resistant but only K272E was also motavizumab-resistant (136). The Miura lab has also recently demonstrated motavizumab resistance in RSV, and evolutionary experiments have also shown the K272E mutant sweeping through the viral population. Further experimentation assessing binding kinetics by surface plasmon resonance (SPR) have been performed comparing wild-type F binding to motavizumab to several F protein mutants, including K272E. In cell-ELISA experiments have also shown differences in binding to motavizumab across several mutants. Overall, much work has been done studying antibody escape in F over the last several decades (137-141).

Recent research published in 2018 found nirsevimab escape variants at site N208 and N67 in RSV subtype A and at sites N208, N201 and K68 in RSV subtype B (121). The escape variants found at each of these sites in subtype A and B are located at the same position. The subtype A variants on their own showed some resistance to nirsevimab neutralization, but not nearly as significant as the variants in subtype B. When N208Y and N67I were present together, the neutralizing concentration increased dramatically. Based on the crystal structure of F, the researchers cannot find an obvious explanation as to why the changes in these amino acid sites cause disruptions in antibody binding. Asparagine being a polar residue could be involved in hydrogen bonding interactions with other polar residues in site Ø of F. It is unclear why this change on its own causes such a dramatic difference in binding in RSV subtype B but not RSV subtype A without the secondary mutation at site N67.

Deep Mutational Scanning

Traditional methods of studying the function of specific amino acid residues within a mutational library framework typically include the use of methodologies such as site directed mutagenesis, alanine scanning, scanning saturation mutagenesis, and iterative saturation mutagenesis (142-147). These methods provide some information regarding important residues within a protein but are limited in their ability to explore each individual amino acid change or multiple amino acid changes at once. Alanine-scanning, for example, replaces amino acids of interest with the small, non-polar alanine residue. This technique only permits the study of a small sample of possible escape mutations. This method takes a certain number of amino acids in a viral protein and mutates those amino acids individually to alanine using SDM and determines the phenotypic outcome (142). For certain experimental designs, changing a few amino acids to alanine to better understand the impact of those residues is acceptable when working with a few amino acid sites. When projects expand beyond evaluation of just a few residues, methods such as alanine scanning do not give the coverage needed for assessing every amino acid site within a protein. It can also be difficult using methods such as PCR-based site-directed mutagenesis (SDM) to generate all mutants of interest due to the length of time it takes to generate all mutants and a potential bias towards the sites being targeted for mutagenesis (148). In some cases, researchers may be interested in studying all amino acid mutations within a specific protein site in an unbiased manner. Techniques such as SDM and alanine scanning fall short in their ability to provide such comprehensive sets of data in a relatively short amount of time.

Within the last decade, researchers have developed high-throughput assays that allow the expression and screening of large variant libraries. One of the first technologies developed was termed deep mutational scanning (DMS), which has been successfully used to study the effects of mutations at all or nearly all sites within a protein of interest (149-151). Many research groups have utilized DMS to study antibody escape in the context of several different viruses, including Zika virus, influenza virus, and HIV (129, 152, 153). Before using a technology like DMS, large variant libraries must first be generated. These libraries can be developed in several

ways, including error-prone PCR, Kunkel mutagenesis, EMPIRIC (extremely methodical and parallel investigation of randomized individual codons), POPCode, or commercially available mutagenesis by gene synthesis (151, 154-157). These methodologies have been reviewed elsewhere (158).

After generating the library, the next step is selecting an expression approach. There are several ways that can be used to express a mutational library, including viral gene delivery and expression systems, yeast display, and phage display (150, 152, 159-162). Other assays can be used to express a library of variants such as phage or yeast displays. These types of assays can be used to study protein variants of interest by displaying the protein on the surface of a phage or yeast cell that contains the corresponding gene (158). Another technique, called the landing pad system, may also be used to express mutational libraries *in vitro* (163-167). This system site-specific recombinase enzymes, where a landing pad vector containing a recombination site along with a selectable marker is integrated into the genome. A recombinase enzyme that matches the site can then recombine the gene of interest into that specific site (163). In studies using viral expression systems, the goal is to individually express hundreds or sometimes thousands of variants of interest from the library so each can be individually assessed for expression or antibody binding without an excess of time and materials. Retroviral gene expression systems can be utilized for optimal expression and analysis of mutational libraries. An expression system using a murine leukemia virus (MLV) packaging backbone for example, allows for the expression of variants in cell culture by utilizing the reverse transcription and integration activity of these viruses. Genes of interest that are packaged into a retroviral particle can then be recombined into the genomes of cells, where they are subsequently expressed.

Selection or screening the expressed variants from the library is the final portion of DMS studies. As with the expression portion of this pipeline, there are multiple ways to screen library variants. Depending on the model used to scan the protein of interest, selection can take place using ligand binding, growth rate, or small molecule binding among other methods (168). For example, a study from 2012 involving influenza inhibitors used yeast display selection by expressing their

hemagglutinin libraries of interest on the surface of yeast, and selected beneficial mutations based on binding to HA1-2 (169). A study from 2011 used the abundance or growth rate of heat shock protein 90 (Hsp90) mutants displayed in yeast to screen their libraries. Deep sequencing was used to analyze the abundance of the Hsp90 mutants (151). A technique that is often used for selection and assessment of variants from a mutational library expressed on the surface of cells is fluorescence activated cell sorting, or FACS (164, 170-172). This type of method can sort protein-expressing cells based on their binding to fluorescently labeled antibodies of interest. FACS can be used as an initial screening to assess binding differences across library variants in a relatively short amount of time. Since this technique involves cell sorting, it leads right into the process of DNA extraction and generation of amplicons for deep sequencing.

Overall, DMS coupled with an effective selection and sequencing technique can provide a powerful pipeline, allowing the assessment and characterization of large variant libraries as compared to more traditional methods. The ways in which libraries are generated, expressed, and screened are continually evolving and are flexible enough to provide researchers with a unique tool to suit the needs of their protein library studies.

CHAPTER 2: BUILDING A D25 MUTATIONAL LIBRARY FOR HIGH-THROUGHPUT SCREENING OF ANTIBODY ESCAPE

Introduction

Building the D25 Mutational Library

The F protein of RSV undergoes dramatic evolutionary pressures to maintain fitness over the course of its lifecycle. It is important to elucidate amino acid residues of interest that when mutated, disrupt antibody binding in the context of antibody escape (109, 121, 129, 173). *In silico* approaches to model D25 - F interactions can be used for the identification of residues that are involved in intermolecular interactions between the proteins. Once these residues have been identified, mutations can be made at the selected amino acid sites to further identify specific variants that affect binding interactions. For this study, F residues within 5 angstroms of D25 antibody residues were chosen to build the D25 mutational library. Thirty sites were selected for this library, and to assess mutational changes at each of these sites, all 19 amino acid mutations were made at each of the 30 sites. This resulted in 570 total variants in the library that we aim to assess using well-established high-throughput techniques: DMS and FACS. We ultimately aim to compare our results from the DMS-based library screen to molecular modeling predictions to validate our *in silico* estimation capabilities.

DMS as a High-Throughput Method for Studying Antibody Escape

There are many ways to study the effect that amino acid substitution mutations have on a protein's ability to be expressed and function properly. DMS, as described in chapter 1, has been used successfully in demonstrating the ability to assess thousands of mutations within a protein in a relatively short period of time (129, 152, 168, 174-176). Traditionally, when studying protein genotype-to-phenotype relationships, there are limitations to the number of mutants that researchers can study. Being able to evaluate every possible mutation at every single site within a protein, as with DMS, can provide valuable information that may lead to discovery of unique intermolecular interactions between residues as well as fitness effects (177).

Our objective is to elucidate amino acid residues in F that when mutated alter interactions with the D25 mAb, leading to antibody escape. Using DMS as a tool to assist in our assessment of ~570 variants, we aim to effectively screen our D25 library for antibody escape variants in a high-throughput manner. A DMS-based approach has been coupled with a Murine Leukemia Virus (MLV) based gene expression system and FACS to sort and screen F variants for antibody escape. It is predicted that this pipeline will allow us to successfully identify potential escape variants by evaluating the enrichment of mutants in different sorted populations. We can then assess those variants that are potentially escaping D25 binding on an individual basis to characterize them further. DMS has proved successful in past studies assessing libraries containing thousands of variants, and thus we predict that this workflow will be effective. The developed pipeline in this project will allow us to potentially screen the D25 library variants in a relatively straightforward and efficient manner and allow us to compare these empirical results to D25 escape mutants predicted by molecular modeling.

Moloney Murine Leukemia Virus (MLV) Gene Expression System to Screen for Potential Antibody Escape Mutations

Different virus systems can be used to express genes of interest *in vitro* with relative ease using compatible plasmids and simple transfection procedures. Several different systems may be used to best suit an experimental design, such as retroviruses, adenoviruses, or lentiviruses (160, 162, 178). Retroviruses are often used so that a gene of interest is incorporated into the genome of a given cell in cell culture. Once inserted into the genome, that gene expresses the protein of interest, and can be detected in downstream applications (159). In the context of this project, the F variants from the D25 library are cloned into the expression plasmid and transfected into cells along with a gag-pol encoding packaging plasmid and a vesicular stomatitis virus glycoprotein (VSV-G) envelope plasmid. VSV-G is commonly used to extend cellular tropism of these expression systems in cell culture (161). After transfection, the virus particles used to package the individual F-variant expression plasmids (pLPCX-F) are harvested from the spent media. These particles

can then be added to cells for transduction, where VSV-G mediates fusion of the particle with a host cell, and a pLPCX-F variant plasmid is released into the cytoplasm. The F variant gene is then translocated to the nucleus where it is incorporated into the genome of the cell, where the variant can be expressed upon activation of the CMV promoter within the expression system. Using this kind of system allows us to analyze variants in a high-throughput manner without having to perform individual transfections with all 570 variants in the library. We are also able to control the number of integrations into the genome of the host by testing several different volumes of virus and measuring median fluorescence intensity (MFI), correlating that to the percent of cells transduced. This way, we can make sure there is only one variant gene from the library being incorporated into a host cell genome.

Overall, the goals of this chapter are to establish a D25 library based on *in silico* molecular modeling approaches, utilize an expression system to express F variants on the surface of cells in a high-throughput manner, and to screen the D25 mutational library for potential escape mutations. To do this, we used an MLV-based expression system to express F, and FACS to screen the variants and sort them into different populations in preparation for deep sequencing. We aim to establish a pipeline using these techniques that can be used to screen this D25 library as well as other large variant libraries of interest. Our hope is that this pipeline can be used in the future to identify D25 antibody escape variants and the results may be compared to molecular modeling predictions for validation of the modeling.

Materials and Methods

Design of the F Protein D25 Library using Molecular Modeling

The F protein D25 library was designed in collaboration with the University of Idaho's Institute for Modeling Collaboration and Innovation (IMCI) and by Dr. Jagdish Patel. Modeling studies paired with molecular dynamics simulations aimed to identify potential interacting amino acids between F and the D25 mAb. To address these interactions, the modelers used the F – D25 co-crystal structure (PDB code 4JHW) to identify residues of F that came within 5 angstroms of the D25 mAb, indicating interaction sites (69). These residues, when mutated, were estimated to disrupt amino acid interactions. These amino acid residues within site Ø of F are highlighted in red in figure 3 below. The chosen sites for the library were S62, N63, I64, K65, K66, N67, K68, C69, G71, T72, D73, A74, L83, N197, Y198, I199, D200, K201, Q202, L203, L204, P205, I206, V207, N208, K209, Q210, S211, C212, N216 (figure 3). Figure 7 shows the linear F gene and the location of all 30 sites in red.

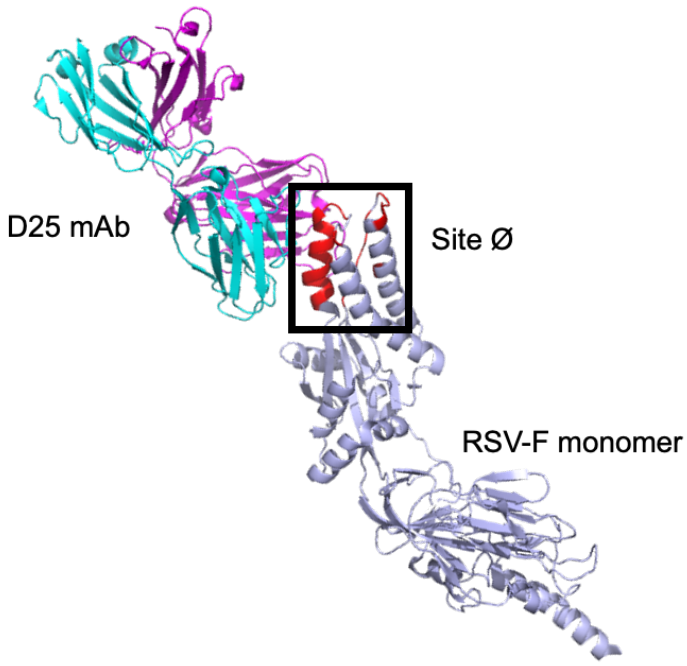

Figure 3: D25-F co-crystal structure (D25-cyan and magenta) interacting with residues within the site Ø epitope on F (gray monomer). Red highlighted residues indicate those residues of F that come within 5 angstroms of D25).

Cloning Linear F Variants into Expression Vectors

The F protein D25 library was designed by Dr. Tanya Miura and Dr. Paul Rowley, and subsequently purchased through Twist Biosciences™ as linear F-gene variants pooled by amino acid site. Thirty sites within the D25 epitope on F were used to construct the library, where every amino acid was mutated to all other amino acids. The library was based upon a plasmid called pHRSVFoptA2, which is codon-optimized for expression in mammalian cells. The F gene in this system does not contain any cryptic splice sites or polyadenylation sites and includes restriction sites for ease of mutagenesis studies (141, 179, 180). We maintained the use of the optimized codons when designing the mutant library to include only one codon per amino acid residue. Each linear segment of DNA was designed to be flanked by recombination sites, *attB1* and *attB2* which are compatible with the Gateway Cloning™ system (181). The pooled F gene segments for each site were first cloned into the pDONR-221 entry vector using the following reaction:

25 ng F DNA
150 ng pDONR-221
4.5 µL TE buffer
2 µL of BP Clonase II enzyme
Room temperature incubation, overnight

One µL of proteinase K was added to the reaction and incubated for 10 minutes at 37°C. Once cloned into pDONR-221, variants were transformed into transformation-competent Top 10 or 10ß *E. coli* and used for cloning reactions into either the MLV compatible transfer plasmid pLPCX-dest or the mammalian expression vector pcDNA3.1-GW using the following reaction:

100 ng pDONR-221 DNA
100 ng pcDNA3.1-GW or pLPCX-dest DNA
1 µL of TE buffer
0.5 µL LR clonase II enzyme
Room temperature incubation, overnight

After incubation at room temperature overnight, 0.25 µL of proteinase K was added to the reaction for an incubation at 37°C for 10 minutes. These clones were

then transformed into *E coli* as described above. Variants were stored at -80°C by site as a pool by making glycerol stocks in Top10 *E. coli* and referred to as pLPCX-F or pcDNA3.1-F variants. To generate the MLV-based library vector delivery particles, each glycerol stock of the pLPCX-F variants was used to inoculate 5 mL of lysogeny broth (LB) containing ampicillin for selection. Each culture was incubated at 37°C while shaking overnight (~18 hours). DNA was then extracted from the cultured *E. coli* using a Zymo Research™ plasmid DNA mini-prep kit. After determining the concentration of each plasmid pool, equal amounts based on plasmid concentration were added to one large, pooled prep to ideally represent all variants present within the D25 library at each site. This procedure was performed twice for technical replicates, and each large library pool was then used during HEK-293T transfections as the transfer plasmid (figure 4).

Producing MLV Expression System Particles

After the transfer plasmid pools were made, we transfected HEK-293T cells in 100 mm dishes to generate the MLV particles using Lipofectamine3000 reagents and protocol from Thermo Fisher Scientific™. Packaging and envelope plasmids pMD-gagpol and pMD-VSVG, respectively, along with MLV production protocol optimizations were generously shared with us by Dr. Lee Fortunato at the University of Idaho. Equal amounts (0.4 µg) of pLPCX-F, pMD-gagpol, and pMD-VSVG were used for this transfection. The plasmid-lipofectamine complex was gently dripped onto the cells for even distribution, and the dish was incubated at 37°C for 24 hours (figure 4). At 24 hours post-transfection, the spent media was syringe-filtered using a 0.45 µm filter and aliquoted into cryovials for flash freezing and storage in -80°C. Six mL of fresh Dulbecco's Modified Eagle's Media (DMEM) was gently added to the cells and the plate was further incubated in 37°C for another 24 hours. At the 48-hour timepoint, the media was again syringe-filtered, aliquoted into cryovials and flash frozen for -80ºC storage. Three different MLV stocks were generated, including a wild-type control (MLV-WTF) and two library stocks (MLV-Lib 1 and MLV-Lib 2).

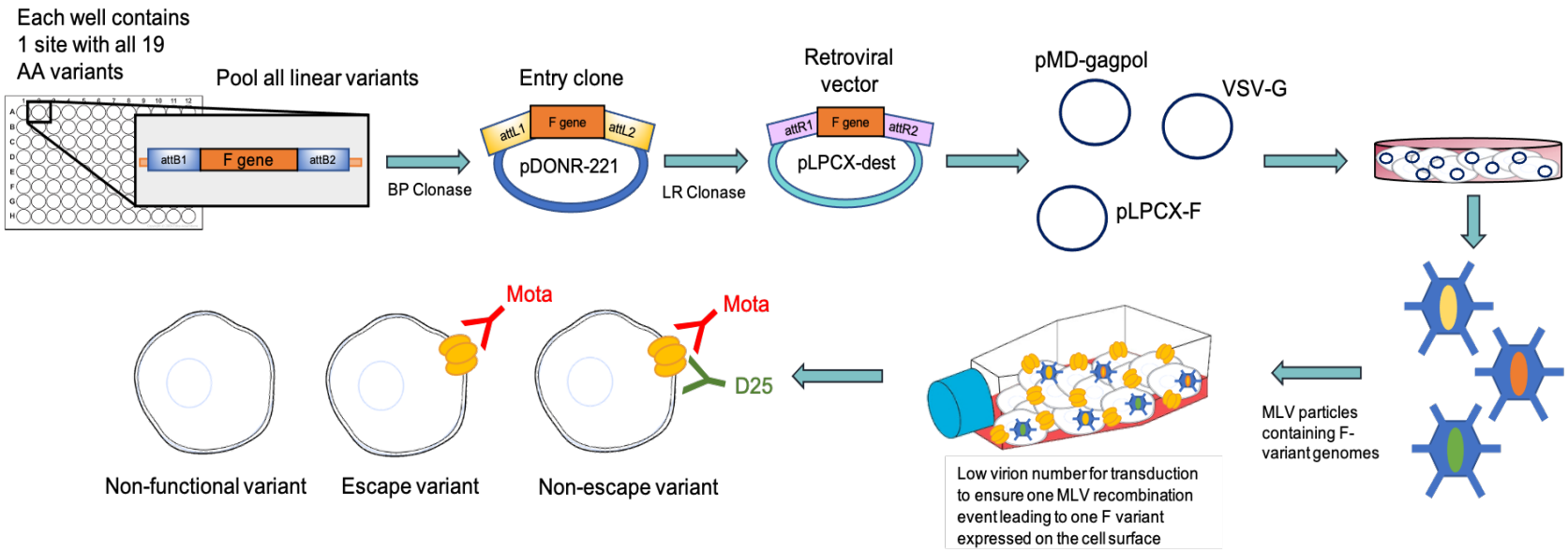

Figure 4: F protein variants are recombined into the MLV transfer plasmid (pLPCX-dest), then co-transfected with a VSV-G and packaging plasmid into HEK-293T cells to make MLV particles. The HEK-293T cells are transduced with the MLV virus stock, and subsequently the F gene is recombined into the genome of the cell. Cells are stained with fluorescently conjugated D25 and motavizumab, then subjected to fluorescence activated cell sorting (FACS). Deep sequencing is then performed to screen for potential escape variants (F mutants that bind motavizumab only).

Flow Cytometry Optimization for Transduced Cell Sorting

HEK-293A cells were first seeded at $1.5x10^5$ cells/well in a 12 well plate and left to adhere overnight at 37°C. To transduce the wells, different volumes of MLV virus stocks were added to their respective wells with 8 µL/mL of polybrene in a final volume of 3 mL. The volumes of virus included 1 mL, 500 µL, 250 µL, and 125 µL. The cells were incubated with virus for 48 hours at 37°C, until prepared for flow cytometry. Cells were first lifted with accutase, counted, and aliquoted into a round bottom 96 well plate (~$3x10^5$ cells/sample). The cells were then blocked in 10% fetal bovine serum (FBS) in FACS buffer (FCSB) for 30 minutes. An Alexa Flour™ 594 antibody labeling kit from Invitrogen was used to conjugate motavizumab (used as an expression control). Motavizumab-594 was then incubated with the cells for 30 minutes in the dark at final a concentration of 2 µg/mL. Cells were fixed in 1% formaldehyde, resuspended in FCSB, and brought to the CytoFlex™ flow cytometer for analysis. Un-transduced cells were used as a negative control to assist in the gating strategy on motavizumab positive versus negative cells.

MLV D25 Library Transductions, Cell Sorting, and DNA Extractions

MLV transductions were performed using HEK-293A cells that were seeded in 100 mm dishes. MLV-Lib 1 and MLV-Lib 2 were gently added (3.33 mL) to their respective dishes while swirling along with 6 µL of polybrene and 3.7 mL of DMEM for a final volume of ~6 mL. The dishes were then incubated at 37°C for 48 hours, for F to be expressed on the surface of the cells. Previous optimization experiments were performed to determine the volume of virus needed when transducing cells in the dishes to prevent multiple different F variants on the surface of individual cells. The prevention of superinfection at this step is critical for elucidating potential escape variants during the cell sorting screen. At 48 hours post-transduction, the cells were prepared for FACS performed at Washington State University in Pullman, WA with the assistance of Melissa Oatley using a Sony Biotechnology SY3200 FACS machine. The cells were first gently washed with pre-warmed PBS and then lifted with accutase. The plate was incubated for approximately 1 minute at 37°C to assist in detaching the cells from the plate. Pre-warmed PBS (0.5 mL) was then added to

the plate and the cells were mixed with a serological pipette. The cells were counted (~$1x10^6$ cells/mL) and aliquoted into samples needed for sorting. This experiment included an HIV-Ace2 transduced negative control as well as wild-type MLV-F as a positive control. Cells transduced with MLV-library were dual stained with motavizumab and D25 directly conjugated to Alexa-Fluor 594 and Alexa-Fluor 488, respectively. Motavizumab was used as an expression control, since all D25 variants should be detected by motavizumab but not D25 in the case of potential escape. Motavizumab-594 was used at a final concentration of 1 µg/mL and D25-488 was used at a final concentration of 10 µg/mL. After staining, the cells were then strained using a 40 µm mini cell strainer to remove clumps of cells. Cell populations stained with motavizumab or D25 only were used as controls to set up appropriate gating for the sorted populations (figures 5 and 13, B). Cells were first sorted on their motavizumab positivity, then those motavizumab positive cells were sorted based on differences in D25 intensity. Post-sort confirmation of the four different sorted populations (figure 6) was performed by running sorted cells back through the sorter to confirm that they had been sorted into the proper bins (figure 13, C). After sorting and running post-sort confirmations, the cells were taken back to the University of Idaho, where DNA extractions were performed using a Qiagen™ DNeasy Blood and Tissue kit. The DNA was successfully extracted, and the concentrations for each sorted sample were determined using the University of Idaho Qubit2.0 in the University of Idaho IBEST Genomics Resources Core.

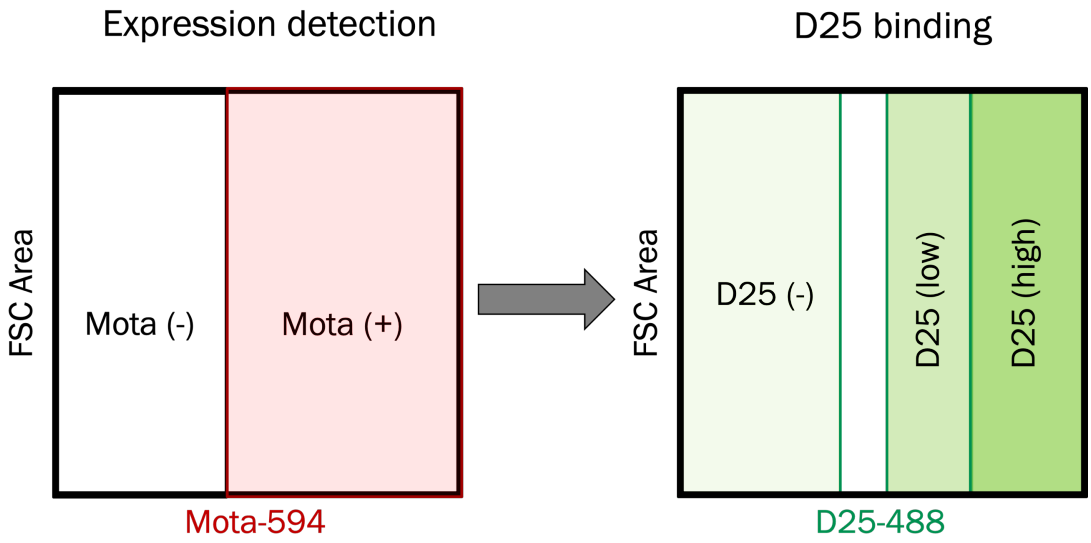

Figure 5: FACS gating scheme to sort on motavizumab positive cells. Motavizumab-594 used as an expression control to distinguish F-expressing cells versus non-expressing cells. Mota-594 positive cells were then gated on D25-488 dot plots gated with three bins: D25 (-), D25 (low), and D25 (high).

Sequencing PCR Optimization and Pipeline

We aimed to sequence the sorted cells from FACS as well as the MLV-library stocks used to transduce the cells and the pLPCX library plasmid pools packaged into the MLV-library particles (figure 6, top panel). The generation of amplicons for deep sequencing follows the pipeline shown in figure 6, bottom panel. After quantification of the DNA, the first round of PCR was performed to isolate and amplify the region of F we are interested in for deep sequencing. Figure 7 shows the forward and reverse primer set locations on the F gene in orange and blue, respectively. This figure also shows the location of all 30 amino acid sites in red that make up the D25 library. These sites correspond to the red highlighted sites in figure 3. The primers used for this first round included 7 forward and 7 reverse primers pooled together based on the primers shown in figure 7 below. The tagged primer sequences are found in table 1 where the tags are highlighted in red. These primer sets were pooled together and the universal CS1 and CS2 tags were added to the amplified products. These universal tags were designed with spacer sequences and used for recognition and binding by the primers used in the second round of PCR.

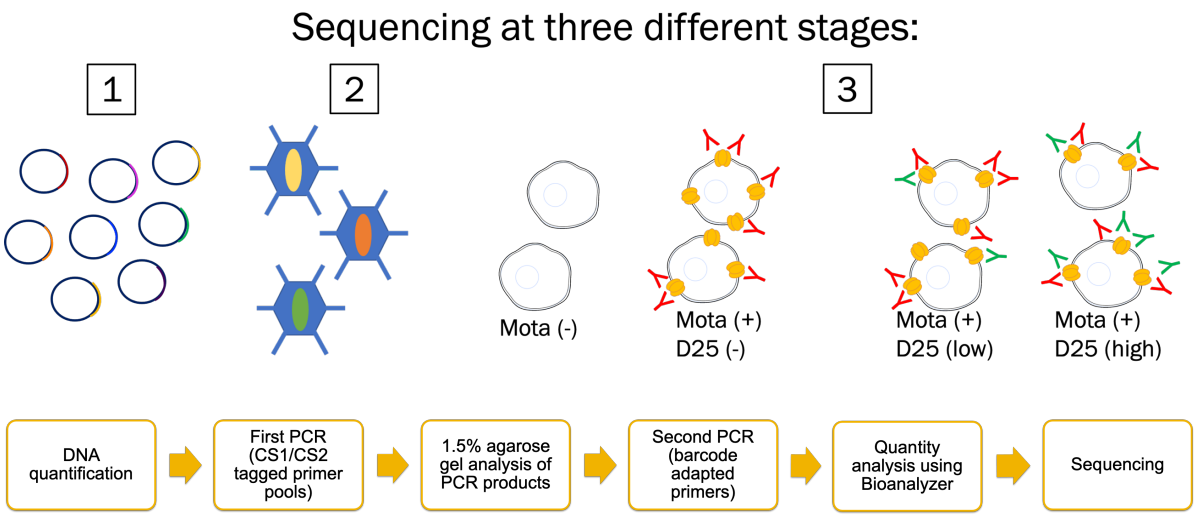

Figure 6: Amplicon generation for pLPCX-F library plasmid pools, RNA converted to cDNA from MLV library stocks, and FACS sorted cells using motavizumab and D25 antibodies. Amplicon generation pipeline describing the necessary steps for preparing samples for deep sequencing.

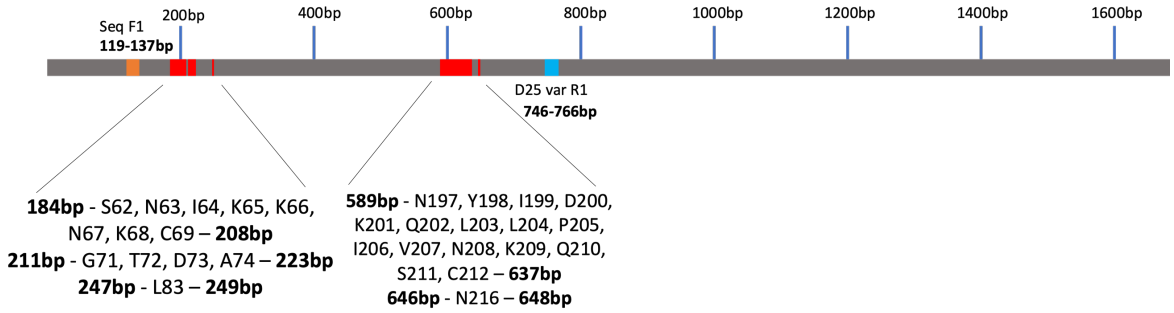

Figure 7: Visual representation of the F gene (gray) and the D25 library sites highlighted in red. The D25 library sites along with their location in base pairs on the F map are listed below the figure. The D25 variant primer (blue) was used previously for confirmation of mutants using Sanger sequencing. The orange block illustrates the sequencing primer designed specifically for deep sequencing of the library-infected sorted cells.

Phusion polymerase from New England Biosciences was used for these PCR reactions. The thermocycling conditions used for the first round of PCR are listed below along with the non-CS-tagged primer sequences and CS-tagged primer sequences (table 1) for the first round PCR optimization to amplify the F region of interest.

1. 98ºC	30 sec	
2. 98ºC	10 sec	30 cycles
3. 65ºC	30 sec	
4. 72ºC	10 sec	
5. 72ºC	10 min	
6. 4ºC	HOLD	

Seq F1 sequence: 5' – TGAGCAAGGGCTACCTGAG – 3'
D25 var R1 sequence: 5' – CGCTGTTGGTCAGCATGTAGG – 3'

Table 1: CS-tagged primers used to amplify region of F of interest for deep sequencing

Forward Name	F Sequence (including CS-tag in red)
CS1-D25DMS_Primer1-for	ACACTGACGACATGGTTCTACATGAGCAAGGGCTACCTGAG
CS1-D25DMS_Primer2-for	ACACTGACGACATGGTTCTACACTGAGCAAGGGCTACCTGAG
CS1-D25DMS_Primer3-for	ACACTGACGACATGGTTCTACAGCTGAGCAAGGGCTACCTGAG
CS1-D25DMS_Primer4-for	ACACTGACGACATGGTTCTACAAGCTGAGCAAGGGCTACCTGAG
CS1-D25DMS_Primer5-for	ACACTGACGACATGGTTCTACATAGCTGAGCAAGGGCTACCTGAG
CS1-D25DMS_Primer6-for	ACACTGACGACATGGTTCTACACTAGCTGAGCAAGGGCTACCTGAG
CS1-D25DMS_Primer7-for	ACACTGACGACATGGTTCTACAGCTAGCTGAGCAAGGGCTACCTGAG
Reverse Name	R Sequence (including CS-tag in red)
CS2-D25DMS_Primer1-rev	TACGGTAGCAGAGACTTGGTCTCGCTGTTGGTCAGCATGTAGG
CS2-D25DMS_Primer2-rev	TACGGTAGCAGAGACTTGGTCTCCGCTGTTGGTCAGCATGTAGG
CS2-D25DMS_Primer3-rev	TACGGTAGCAGAGACTTGGTCTTCCGCTGTTGGTCAGCATGTAGG
CS2-D25DMS_Primer4-rev	TACGGTAGCAGAGACTTGGTCTATCCGCTGTTGGTCAGCATGTAGG
CS2-D25DMS_Primer5-rev	TACGGTAGCAGAGACTTGGTCTGATCCGCTGTTGGTCAGCATGTAGG
CS2-D25DMS_Primer6-rev	TACGGTAGCAGAGACTTGGTCTCGATCCGCTGTTGGTCAGCATGTAGG
CS2-D25DMS_Primer7-rev	TACGGTAGCAGAGACTTGGTCTTCGATCCGCTGTTGGTCAGCATGTAGG

After this first round PCR, the products were run on a 1.5% agarose gel for analysis to confirm correct amplification size. These tagged products were then used in a second round of PCR to add unique barcode sequences to each of the tagged products to be identifiable during deep sequencing. The barcodes were added by using barcode-adapted primers in a second PCR reaction that added the unique barcode sequence onto the ends of the CS1 or CS2 tags on the amplified products from PCR 1. Taq polymerase from NEB was used for the second round PCR, adding the barcode-flanked adaptor sequences to the ends of the products from PCR 1. See the thermocycling conditions below for the PCR 2 reaction.

1. 95ºC	1 min	
2. 95ºC	30 sec	20 cycles
3. 60ºC	30 sec	
4. 68ºC	1 min	
5. 68ºC	5 min	
6. 10ºC	HOLD	

A bioanalyzer system was then used to assess the quality of the samples and size-based beads were used to clean up the PCR products in preparation for sequencing. The last step of this pipeline involves the actual sequencing of the amplicons by Illumina NGS (next generation sequencing), where the sequencing reads are then analyzed for determination of the enrichment of variants within the different populations of interest (figure 6).

Results

Twist Library Breadth of Coverage

We assessed the D25 library for variant coverage to determine whether this pipeline for library generation is an efficient method or not. D25 sites were cloned into the donor plasmid pDONR-221 and subsequently into the expression plasmid pcDNA3.1-GW using Gateway Cloning™ technology as described in the methods section. Upon receiving the library, Twist Biosciences provided an excel file containing sequencing data for each pool. For example, site N208 had a total variant read count of 4355 compared to that of most other sites that averaged around 5000 total read counts. This total variant read count is a pooling of all the individual mutations for each site and their overall proportions within each pool. To separate out individual variants, we plated 75 µL of transformed *E. coli* onto an agar LB ampicillin plate. After a 24-hour incubation at 37°C, either 48 or 96 individual colonies were picked and plated onto a gridded LB ampicillin plate and grown up overnight at 37°C. These colonies were then transferred to a deep well 96 well plate containing 1 mL of LB ampicillin broth. Cultures were grown overnight at 37°C shaking, then put through a Promega™ 96 well Wizard Purification System to extract plasmid DNA from all colonies. The plasmid DNA was then sequenced to determine which variants were successfully isolated using this procedure. Sixteen of the 48 colonies screened from site N208 were wild-type and the remaining were other variants of interest or contained a failed sequence. Several variants that we isolated from site N208 were predicted by Twist to have an exceptionally low occurrence in the pool. This is demonstrated by figure 8 below, where expected proportions for variants at sites 208 or 201 are shown in purple and what we observed for the actual proportion for those variants are shown in blue. This was found to be a typical occurrence when compared to other library sites, except for site I206 (data not shown). This site had 50 wild-type sequences out of 96 total screened colonies, but even though over half of the isolated variants were wild-type, we were still able to separate out 11 of the 19 variants for this site. Q202 isolated variants (data not shown) had a large breadth of coverage, where only 4 of the 19 variants were missing after assessing the variant

pool, and of those only 9 were wild-type sequence. Overall, we predict that there will be varied efficiencies when isolating variants from different sites within our D25 library.

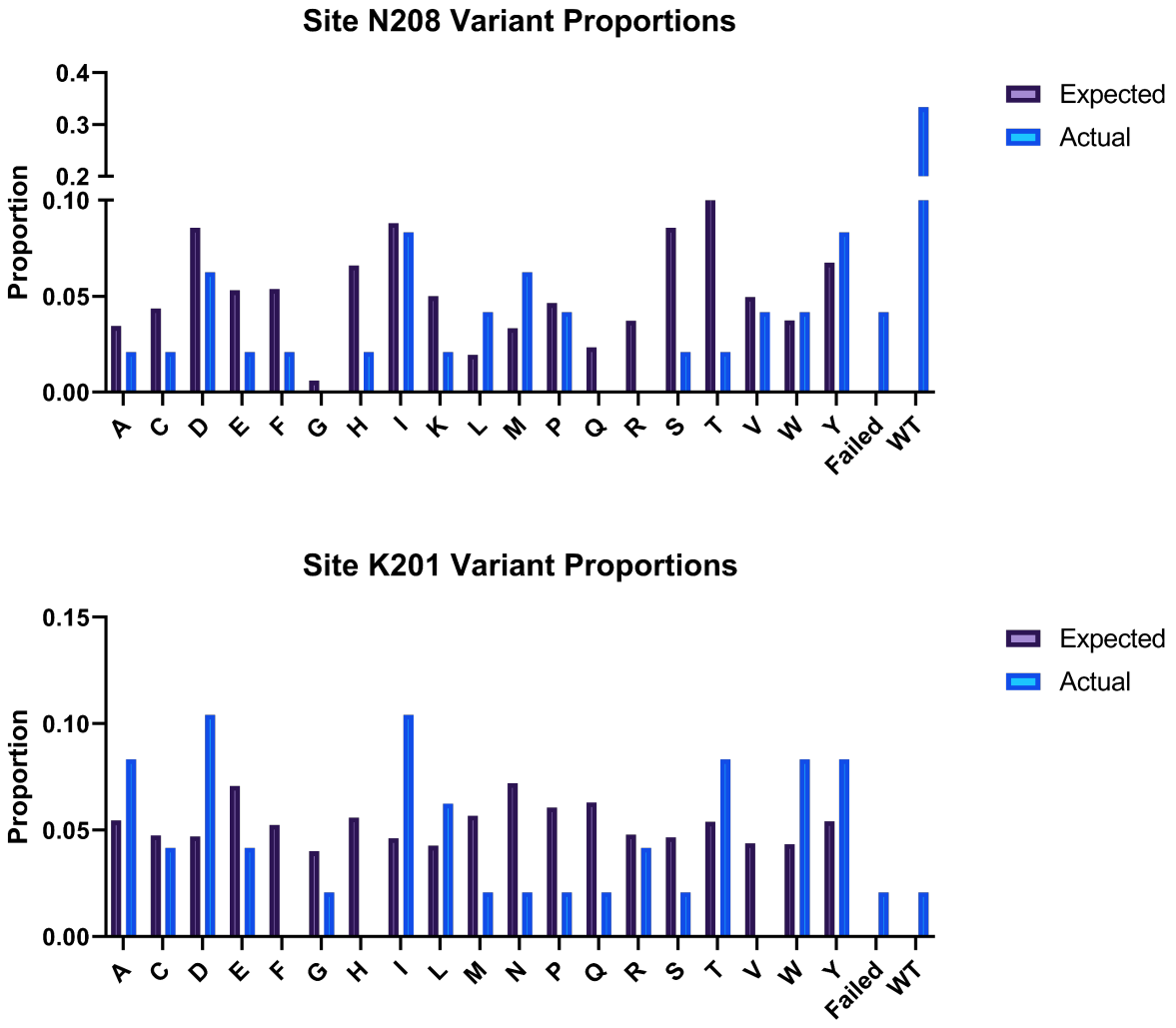

Figure 8: Representative sites N208 and K201 with their expected versus actual proportion of amino acid variants from the Twist D25 library. Expected proportions were provided by Twist via read counts for each mutant within the pool for each site. Actual proportions were calculated based upon the results from isolating individual mutants from sites N208 and K201 variant pools.

Optimizing MLV Expression System Transduction Efficiencies

We first optimized antibody staining procedures for detection of F by flow cytometry by determining the amount of virus particles that would yield enough F expression to detect, but not superinfect the cells. A key element of the design of this experiment was to express one unique F variant on the surface of each cell. The addition of too much virus could potentially result in multiple variant integration events into the cellular genome. This could result in the expression of multiple F variants on the surface of the cell, leading to confounding results when assessing antibody binding and sorting cells based on the interaction between different mutants and D25. To ensure expression of only one variant per cell, we tested several different volumes of virus on HEK-293A cells to analyze the change in percent positive cells along with the MFI of those positive stained cells. We were trying to identify a volume that gave us enough positive cells to effectively sort but also maintain a steady MFI to indicate the prevention of multiple integration events. Several volumes of wild-type, library-1, and library-2 MLV expression stocks were tested, from 125 µL per well of a 6 well plate to 1 mL (figures 9 and 10). Figure 9 shows the motavizumab (ECD) percent positive for the wild-type, library-1 and library-2 MLV-transduced cells on motavizumab positive histograms in red compared to un-transduced cells in gray. Figure 10 plots the data from figure 9 as volume of virus stock vs MFI for the wild-type, library-1, and library-2 MLV stocks along with the same percent positive values found in figure 9. Based on these data, we decided to use 500 µL of virus stock, due to the relatively high positivity rate (~32-42%) as well as the plateau of MFI shown by all three virus stocks tested. The increase from 500 µL to 1 mL of virus stock demonstrated an increase in MFI, suggesting multiple integration events of F variants.

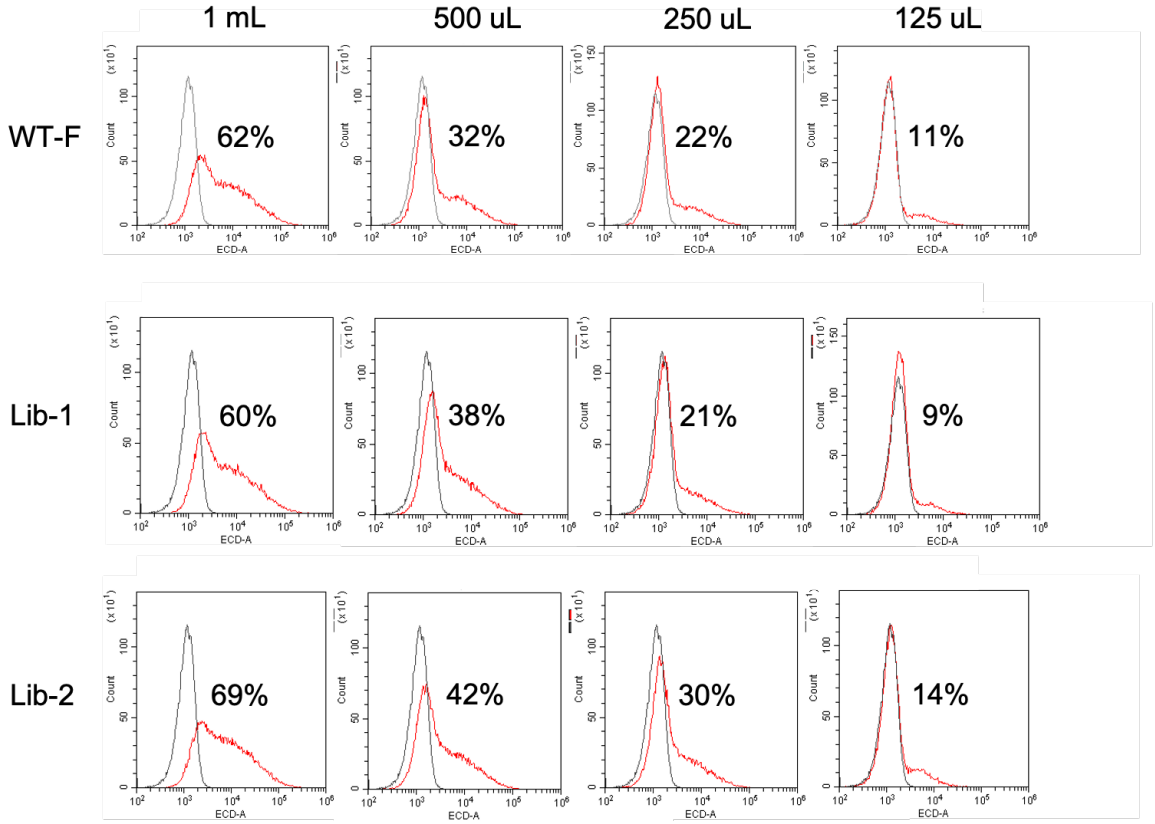

Figure 9: Optimization of the volume of virus to use for library sorting experiments using wild-type F and two individually prepped libraries. ECD-A vs count plots indicating the intensities of cells that are motavizumab positive. Gray indicates un-transduced cells while red indicates transduced cells, both stained with mota-594. The percentage shown on each plot is the percent motavizumab (ECD) positive cells in the transduced cells.

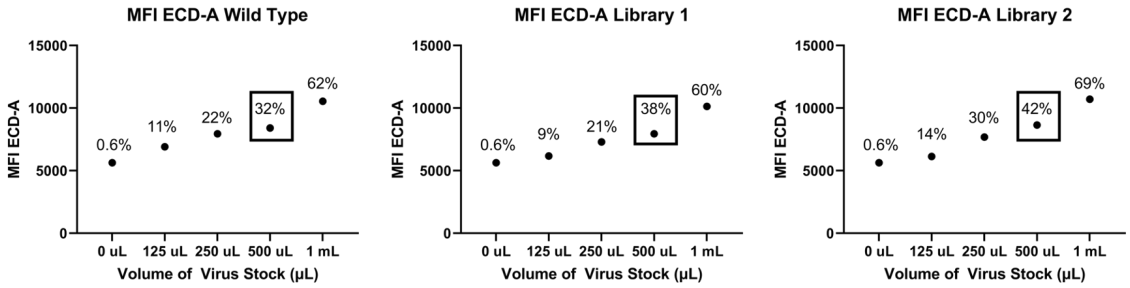

Figure 10: Median fluorescent intensity of ECD-A channel (motavizumab-594) of wild-type, library-1, and library-2 transduced cells for each volume of virus stock used. As the volume of virus stock increased, the percentage of motavizumab (ECD) positive cells also increased as well as the median ECD-A as indicated by the percentages above the points on the graphs. An increase in the MFI of the ECD-A channel suggests multiple F integration events. The squares surrounding the percentages on each graph indicate the chosen volume (500 µL) of MLV stock for later experiments.

Flow Cytometry Sorting Optimization Experiments

After the appropriate virus volume was determined, we moved forward with the library transductions in HEK-293A cells in preparation for cell sorting and DNA extraction. We wanted to first dual stain cells that had been transduced with the MLV-library and wild-type stocks as well as an HIV-Ace 2 transduced population as a negative control. The HIV-Ace 2 transduced cells did not express F but had undergone a similar treatment in terms of the transduction procedure. The left-hand panel of figure 11 shows HEK-293A cells transduced by the HIV-Ace 2 control, MLV wild-type, or MLV-library and their corresponding percent motavizumab or D25 positive. Using the MLV wild-type and HIV-Ace 2 controls, we were able to draw gates to indicate where the positive and negative populations were on the graphs. These gates were carried over to the MLV library transduced samples to identify percent positivity. For the HIV-Ace 2 transduced cells, we do not expect to see any positivity for either D25 or motavizumab, and that is what we observe. In the wild-type transduced population, we do expect to see both motavizumab and D25 positivity at approximately the same percentage. In the wild-type sample, we see similar percentages, 23% positive for D25 and 33% positive for motavizumab. This could be partially attributed to D25's pre-fusion F specific binding, causing a slight decrease in percent positivity compared to motavizumab's pre- and post-fusion binding specificity. In the library samples, the motavizumab positive percentages should be approximately equal to that of wild-type, roughly 33%. We see this pattern for both library-transduced samples, although library 1 had a slightly lowered percentage than that of library 2, at about 24%. One encouraging observation we made about these data is that the D25 percentage in the library populations decreased compared to that of wild-type, from 23% to 13% and 17% for libraries 1 and 2, respectively (figure 11). This is expected because there should be potential D25 escape variants within those populations. We then analyzed the percentage of motavizumab positive cells that were also D25 positive in the wild-type and library – transduced cells. To do this, we plotted the motavizumab (ECD) positive populations on their corresponding D25 (FITC) dot plots. In the wild-type population, we expect to see approximately 100% of cells that are positive for motavizumab are also positive for D25 binding indicative of

no escape. Our results show ~71% of motavizumab positive cells are also D25 positive, which is slightly lower than we had anticipated, but reflects the reduced binding of D25 to wild-type F-expressing cells (figure 11). For the library samples the percentage dropped even further, which can be expected since many of the variants that are motavizumab positive may indeed not be D25 positive, indicating antibody escape. These results were very consistent between the two MLV library – transduced populations.

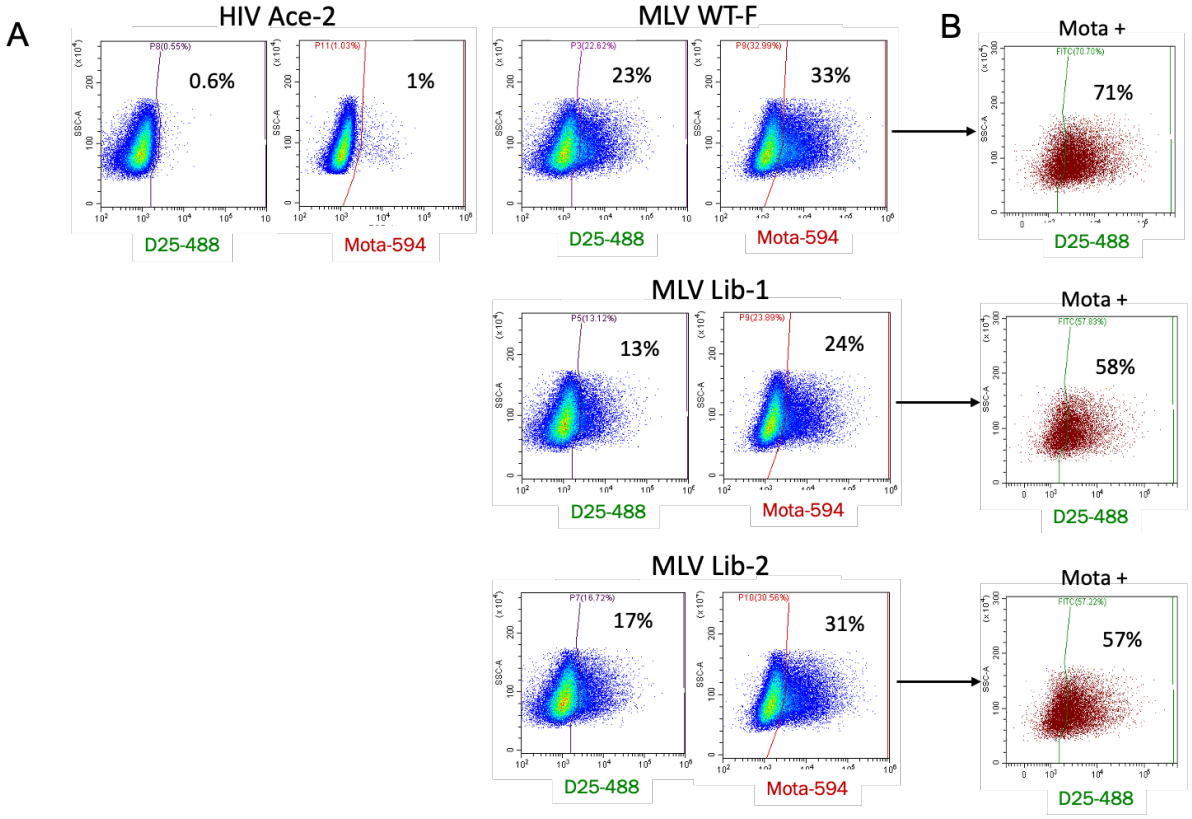

Figure 11: D25 and motavizumab binding percentages as shown by flow cytometry density dot plots. FITC and ECD gating was set by using MLV WT-F as a positive control and HIV Ace-2 as a negative control. Motavizumab was used as an expression control for this experiment (A). Dot plots in red are motavizumab positive cells gated on D25 (FITC) dot plots (B).

After performing these experiments, we observed slight differences in D25 (FITC) intensity along the x-axis of the plots shown in figure 11. We could see that the number of cells that were farther to the right on the D25 dot plots, corresponding to high FITC intensity, differed between the wild-type and the library samples. Due to the differences in FITC intensity, we decided to break the population up into four smaller bins and analyze any differences in percentage across the bins. The results shown for this analysis are in figure 12, demonstrating the grouping of different populations across the D25 dot plots. This type of approach would ideally be mirrored during the actual sorting of these cells, collecting samples that differ in their D25 intensity but are all motavizumab positive. Overall, there are fewer cells in the high D25 bin (P4) for the library populations compared to wild-type, as well as more D25 negative cells (figure 12). Table 2 summarizes the percentages found in each bin for wild-type, libraries 1 and 2, and the Ace-2 control. This experiment helped plan for setting gate thresholds when performing the actual sorting experiment at WSU.

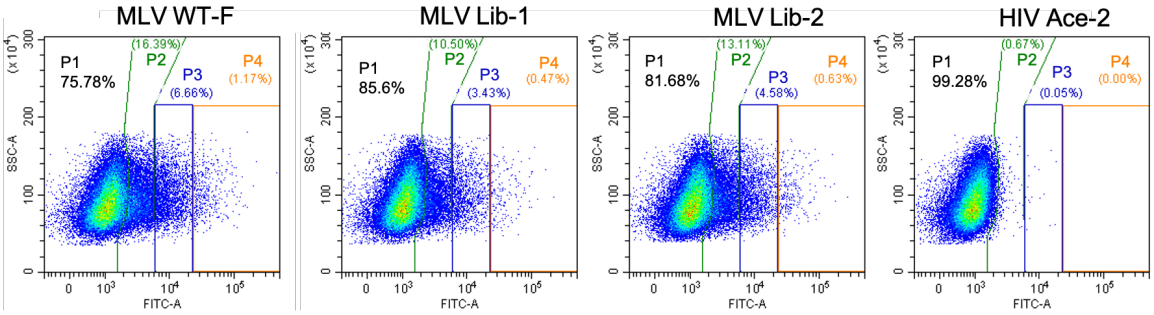

Figure 12: Plots from 11 were grouped into corresponding bins according to their FITC intensity. Cells were dual-stained with mota-594 and D25-488. Populations from left to right indicate cells that are D25 negative (P1), D25 low binding (P2), D25 medium binding (P3), and D25 high binding (P4). These bins were used as a guide for future cell sorting gate set-up.

Table 2: Summary of percentages in each bin from figure 8 above

	MLV WT-F	MLV Lib-1	MLV Lib-2	HIV Ace-2
P1	75.78%	85.6%	81.68%	99.28%
P2	16.39%	10.5%	13.11%	0.67%
P3	6.66%	3.43%	4.58%	0.05%
P4	1.17%	0.47%	0.63%	0.00%

MLV Library – Transduced Cell Sorting Using FACS

Library-transduced HEK-293A cells were subjected to screening by flow cytometry to sort cells into separate populations based on differences in D25 binding. Gates were drawn to capture the varying D25 (FITC) intensity of cells that were all motavizumab (ECD) positive, as described previously with optimization experiments. A representative set of plots is shown in figure 13 below for the first set of sorted cells that had been transduced with MLV library 1. Figure 13, A shows unstained HEK-293A cells as a negative control. As expected, there are no D25 or motavizumab positive cells in this sample. Figure 13, B shows a D25 negative sample versus D25 positive sample, and a motavizumab negative sample versus a motavizumab positive sample. Motavizumab positive cells were then grouped according to D25 intensity, and the different bins can be shown in A-C. After sorting the cells into their respective bins, some of the samples were run through the sorter again to confirm their location within the correct bin. This data is shown in the top panel of figure 13, C, where the motavizumab negative cells are not present on the D25 dot plot as expected. Motavizumab positive cells that had a low D25 intensity are shown in middle panel of figure 13, C, and these cells are found in the correct bin. Motavizumab positive and D25 negative cells are shown in the bottom panel of figure 13, C, appearing in the left-most bin as predicted. Motavizumab positive and D25 high cells are not shown, as data was not collected for these samples due to a low number of cells being sorted into that population.

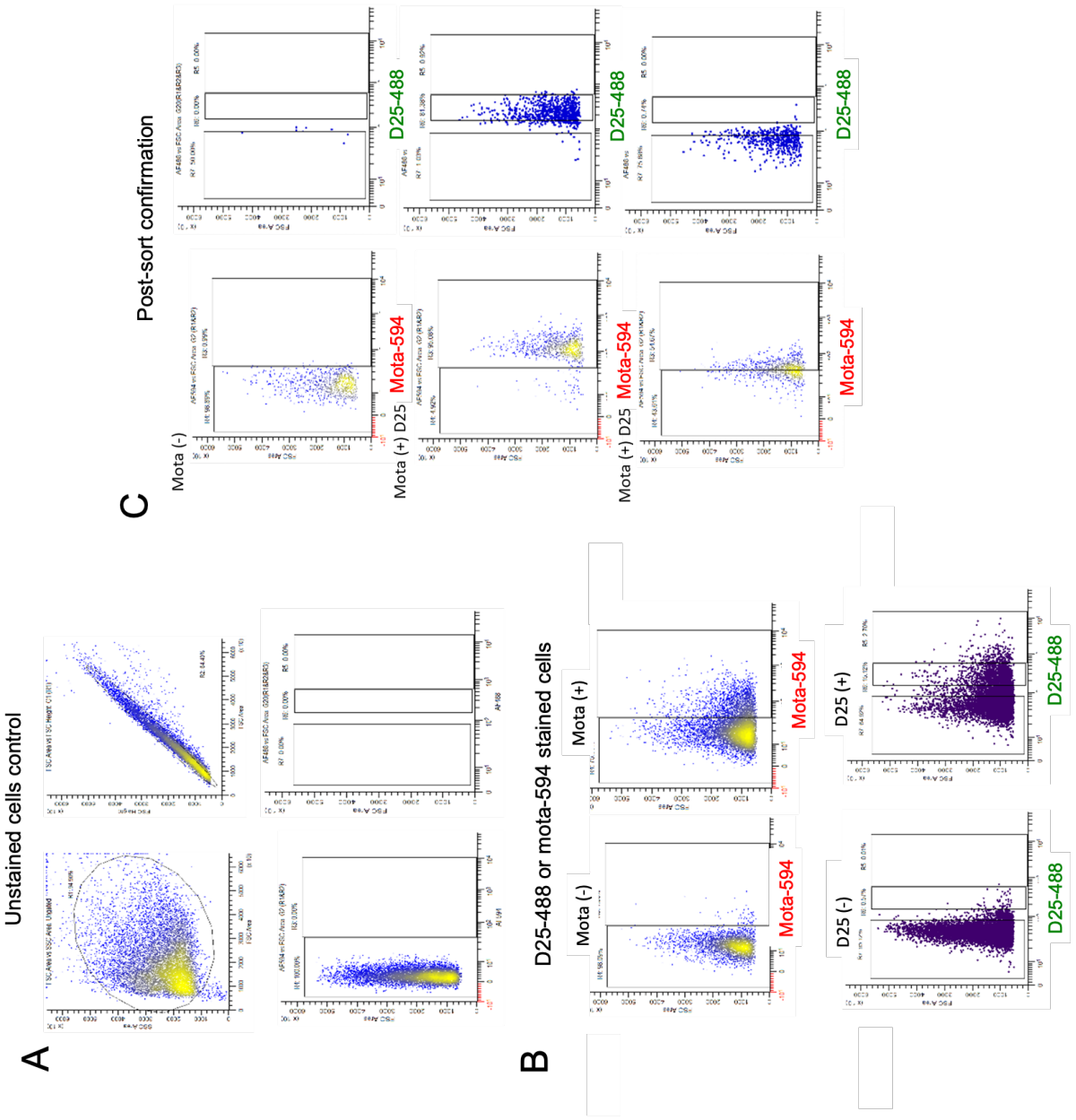

Figure 13: Representative data collection for sorted cells on the first of two runs with D25 library 1 – transduced cells. A demonstrates an unstained control (HEK-293A cells only), B shows single stained controls to help set up location of sorting bins, and C is a set of plots confirming correctly sorted cells post-sort.

DNA Extractions and PCR Optimizations for Illumina Sequencing

Sorted cells were brought back to the University of Idaho and DNA extractions were performed to isolate the DNA from the cells for generating amplicons for deep sequencing. For optimizations, DNA from MLV wild-type F – transduced cells were used as a positive control along with DNA from un-transduced cells as a negative control. Once the DNA was extracted, the samples were taken to the University of Idaho IBEST Genomics Resources core for Qubit quantification (table 3). Samples named A and B refer to the first and second replicates sorted from libraries 1 and 2, respectively. The sample names listed in the sorted bins column correspond to the P1-P4 populations (left to right in each graph) from figure 12.

Table 3: MLV library 1 and 2 extracted DNA concentrations post-cell sorting

Virus	Replicate	Sorted Bin	Amount of DNA (μg)
Lib-1	A	Mota (-)	1.1
Lib-1	A	Mota (+) D25 (-)	0.44
Lib-1	A	Mota (+) D25 (low)	0.48
Lib-1	A	Mota (+) D25 (high)	0.098
Lib-2	A	Mota (-)	4.94
Lib-2	A	Mota (+) D25 (-)	1.23
Lib-2	A	Mota (+) D25 (low)	0.612
Lib-2	A	Mota (+) D25 (high)	0.086
Lib-1	B	Mota (-)	5.1
Lib-1	B	Mota (+) D25 (-)	1.1
Lib-1	B	Mota (+) D25 (low)	0.375
Lib-1	B	Mota (+) D25 (high)	0.052
Lib-2	B	Mota (-)	5.4
Lib-2	B	Mota (+) D25 (-)	0.143
Lib-2	B	Mota (+) D25 (low)	0.586
Lib-2	B	Mota (+) D25 (high)	0.097

Concentrations were not exceptionally high for any of the sorted samples but after amplification using PCR, the 1:64 dilutions of the wild-type template amplified to show a visible band on an agarose gel (figure 14, lanes 10-17). Several different combinations of primers were used when testing the wild-type DNA for amplification in preparation for sequencing. The primer combination seen in wells 8, 17, and 26

gave bands that amplified the sequence of the F gene we wanted without any extra bands indicating non-specific interactions. This combination also did not give a band in the negative control well (number 26) using un-transfected cellular DNA extracts as the template. This primer set was then tagged with CS1/CS2 universal tags to generate amplicons for sequencing. To test these tagged primers, a master mix of all 7 forward primers and all 7 reverse primers from table 1 were made and used in the PCR reaction set up.

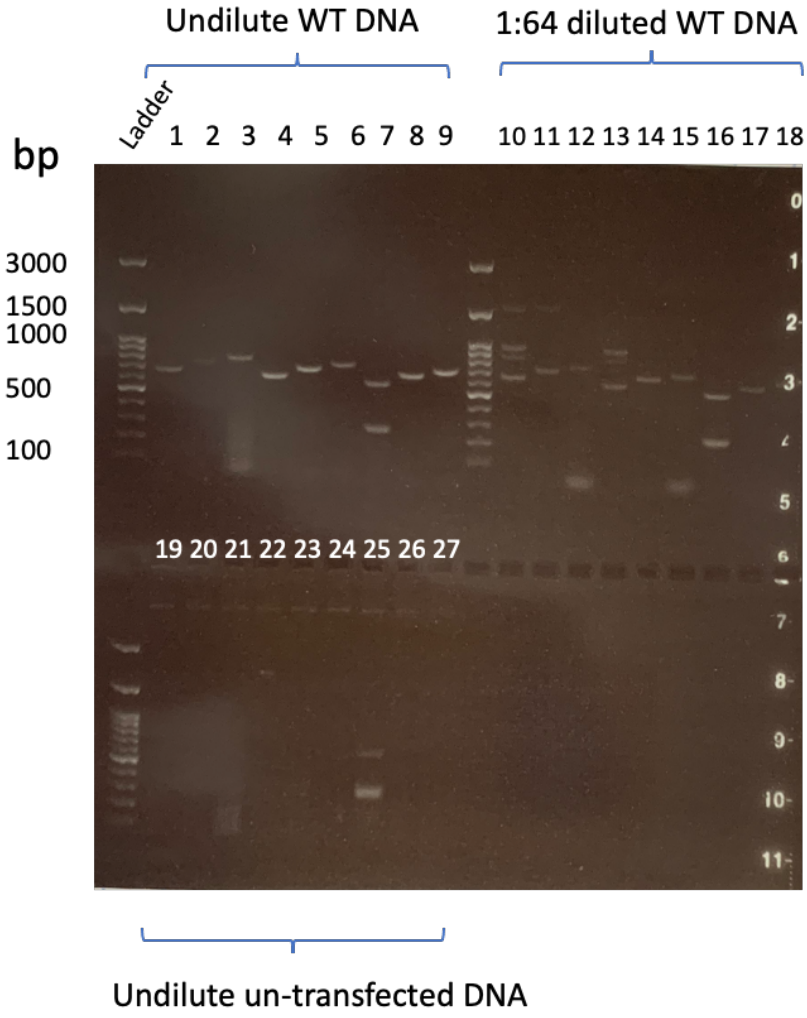

Figure 14: Sequencing PCR optimization using different combinations of primer sets (D25seqF1/R1, D25varF1/R1, LentiFF1/R1). The combination we chose based on these results was D25seqF1 and D25varR1, shown in sample wells 8, 17, and 26 and gives expected band size of 648 bp.

After the tagged primer PCR conditions were optimized, we set up PCR reactions with all the library sorted samples from all three replicates and ran the products on a 1.5% agarose gel. The results of the first round PCR are shown in figure 15, A and B below, where all but two samples showed a band at the proper size. Bands were displayed at different intensities presumably because there are differing amounts of F extracted from the different populations. Cell populations that were not detected by motavizumab or D25 most likely do not express F protein at all or high enough quantities to be detected, so those populations may be expected to have low yield. We are not only interested in the mutants that are sorted from the FACS experiments, but also in the pLPCX transfer plasmid pools that went into making the MLV library stocks for transduction as well as the MLV library stocks themselves. Sequencing the pLPCX plasmid pools as well as the MLV library stocks would yield information about the cloning efficiency of the D25 library into pLPCX as well as the efficiency of pLPCX getting successfully packaged into the MLV particles. Figure 15, C and D highlights the amplified PCR products from running the pLPCX library pools using this PCR set up as well as cDNA made from RNA extracts of the MLV library stocks. As expected, the pLPCX library pools yield bands and the expected size as well as the MLV RNA – derived cDNA. Reactions where no reverse transcriptase enzyme was added (No RT) were included as controls to confirm that the visualized bands were indeed from the extracted RNA. No bands are present in the no RT control samples, indicating that we successfully extracted the RNA from the MLV library stocks and converted that to cDNA.

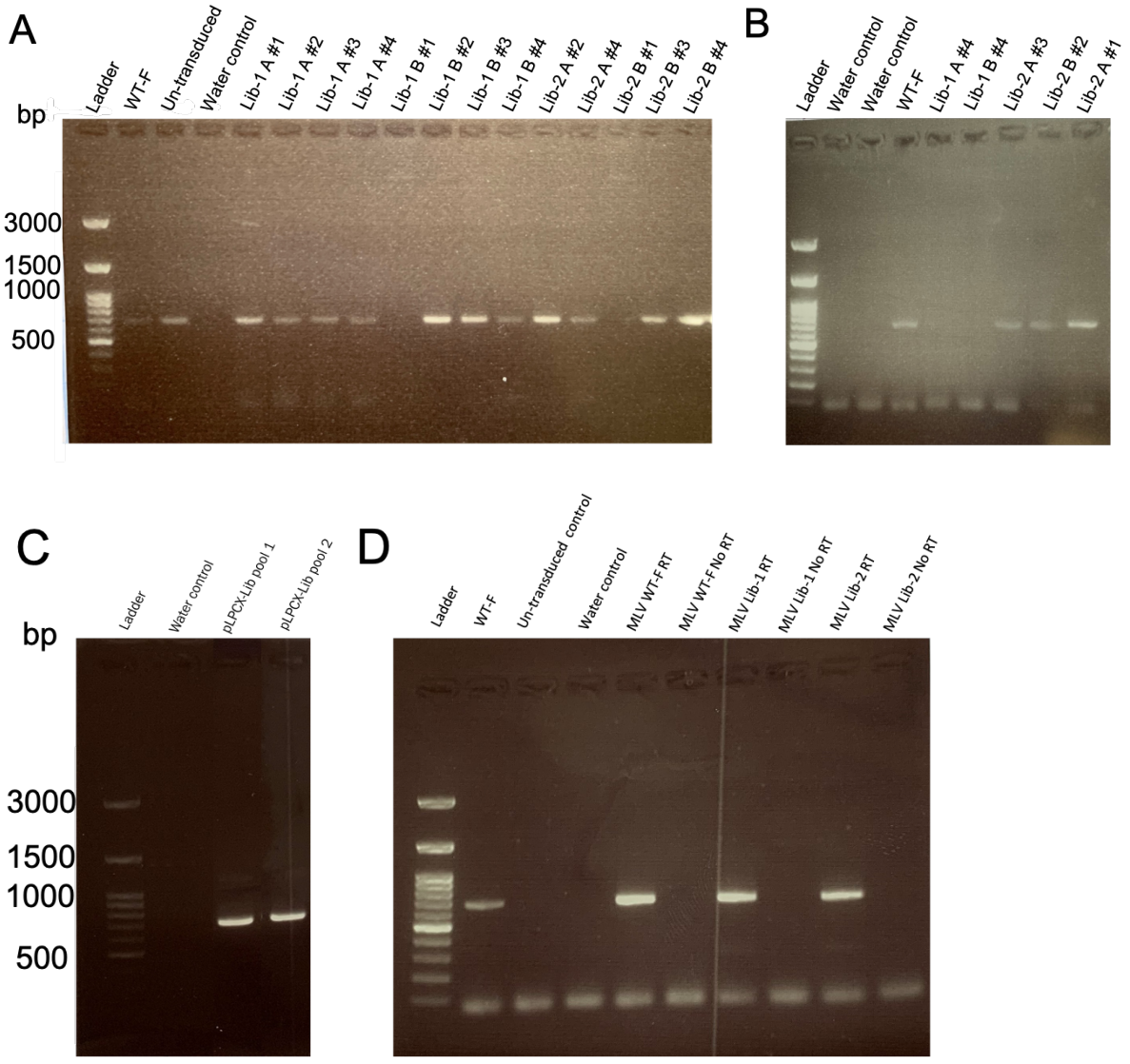

Figure 15: A and B show library sorted samples run on a 1.5% agarose gel using the CS1/CS2 primer mix. All but two library samples amplified enough to show a band at the proper size (~675 bp). Diluted (1:500) pLPCX library pool dilutions using the tagged primer mix (15, C). PCR products from the cDNA template made from RNA extracts of the MLV library stocks using SuperScript IV VILO reverse transcriptase kit (15, D).

PCR products from the first round of amplification using CS1/CS2 tagged primers were run in a second round of PCR to add unique barcode adaptors to the products. Figure 16 shows the library sorted samples, pLPCX pools 1 and 2, and MLV library stocks 1 and 2 second round PCR amplifications on a 1.5% agarose gel. The numbers below the samples indicate the samples' ranking based on band intensity. To pool approximately the same amount of DNA from each sample, the

bands were assigned these ranks to compensate for the relative amount of DNA for each product (positive and negative pool key, figure 16). A higher rank indicates a smaller volume in µL added when pooling all samples together for sequencing, and a lower rank indicates a larger volume added. Samples without a visible band were pooled separately into the negative pool (see table to the right of figure 16).

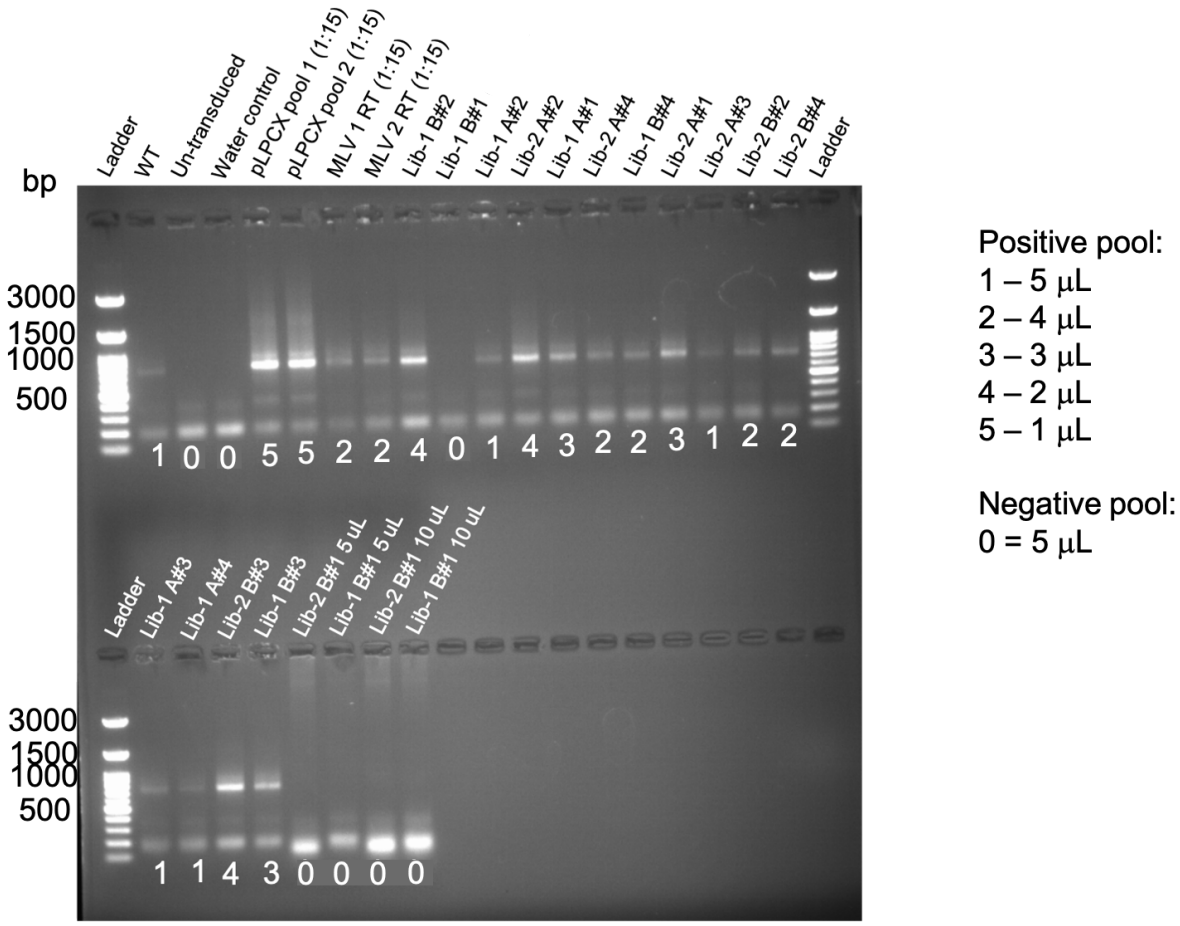

Figure 16: Second round PCR 1.5% agarose gel with all library sorted samples, pLPCX pools, and MLV library cDNA stocks with *proper product length (~795 bp). Samples with bands were ranked 1-5 depending on band intensity and aliquoted into the* positive *pool based on the chart above, and 5 µL of samples without bands were aliquoted into the* negative *pool for deep sequencing.*

Discussion and Future Directions

The use of retroviral gene expression systems can assist in the throughput of screening mutational libraries without increasing time and materials. This was demonstrated by our use of the MLV expression system, where we incorporated D25 library variants into the genomes of HEK-293A cells by relatively simple transfection and transduction procedures. Using individual plasmid-based transfections to screen hundreds of mutants in a mutational library is not feasible, which is why systems are needed that can introduce the library into downstream expression systems all in one go. We chose a retroviral vector system to utilize the genomic recombination machinery that is already a part of the MLV system. By trading out the MLV genome for our library variants when making the viral particles, the variants could be recombined into the genome of the host cell and expressed without induction.

Based on the rationale of the project, there are other types of viral vector delivery methods available for expressing mutation libraries into cells. Adeno-associated viruses (AAV) and HIV-1 are examples of other viral vectors that can be used to deliver genes into cells. In both systems, the viral genome is delivered into the cells of the host as with the MLV system (182, 183). AAV vectors have also been used for treatment of disease by replacement of downregulated or deleted genes in humans (184, 185). Including the pLPCX library plasmid pools as well as the MLV library stock cDNA in the deep sequencing as control populations will allow us to determine the efficiency of this type of method. We will be able to evaluate how many variants were successfully cloned into the pLPCX vector, and if there was any bias during the packaging of those vectors into the MLV-based particles. This information will be valuable moving forward when this kind of pipeline is repeated.

Optimization experiments from this chapter demonstrate unequal binding of motavizumab and D25 antibodies to wild-type F- expressing cells. When HEK-293A cells were transfected with wild-type pcDNA3.1-F, 33% of the cells were motavizumab positive while only 23% percent were D25 positive. This is a 10% decrease in percent positivity from motavizumab to D25, when only wild-type is being expressed on the surface of the cells. Since F is thought to spontaneously trigger to

post-fusion F, enhanced by the use of formaldehyde for fixing, this could explain why we see the decrease in percent positivity (186). As previously discussed, D25 only binds pre-fusion F, thus is there is a decrease in pre-fusion F on the cell surface, there will be a subsequent decrease in D25 binding. Though we observed a consistent decrease in D25 binding using flow cytometry, we were still able to detect trends in binding differences between the wild-type MLV-transduced cells and the library MLV-transduced cells.

Studies using DMS to evaluate antibody escape have shown great promise for use as an effective scan of large mutant libraries. As mentioned in chapter 1, a study in 2019 used DMS to study how mutations in the envelope protein of Zika virus affect antibody escape (129). This study was able to first confirm structure-function relationships in the E protein based on the different mutational tolerance levels of amino acids. They were able to validate antibody escape mutants from their DMS screen by performing neutralization assays on selected mutants. Using DMS, these researchers were able to ultimately develop a sequence-function map that introduces novel information about mutationally-tolerant and intolerant amino acids as well as characterize mutations that may lead to antibody escape. Two other papers published by the same laboratory in early 2021 demonstrate a similar pipeline for studying antibody escape in the context of SARS-CoV-2 (131, 132). One study focused primarily on residues within the spike receptor-binding domain and used 10 mAbs, some individually and some in a cocktail, to screen for potential escape mutations. Interestingly, they found that antibodies that bind the same epitope tend to have different escape mutations (131). The second study identified a single amino acid mutation that escaped the antibody cocktail REGN10933 and REGN10987, E406W. This mutation was found to escape both antibodies in neutralization assays (132).

Data from this current study will ultimately be used to compare to the molecular modeling results, to verify that predicting escape mutations using *in silico* methods are valid or lead to the discussion of changes that could be made to improve the modeling predictions. We are currently waiting on the deep sequencing analysis of these samples to be completed. Once the deep sequencing analysis has been

performed, the IBEST GRC will then analyze the F variants and determine the population they came from based on their unique barcode identifier sequence that was added during PCR 2. After we know which variants are present in which populations, we can then determine escape versus non-escape variants and how molecular modeling predictions compare to our findings. With this type of experimental design, we do not expect to see only binary responses from the sequencing data. It would not be surprising to observe the same variant in the D25 low population and the D25 high population within the same dataset. There may also be variants present that are D25 – as well as D25 low at the same time. The gating strategy used for sorting these populations of cells is somewhat ambiguous, where cells that are just to the right or left of a gate may be sorted to either bin. For this reason, further analysis of these mutants must follow these experiments and use individual binding assays. Overall, this DMS-based approach will assist in validation and/or refinement of the molecular modeling prediction pipeline for the future.

Figure 17: Flowchart describing necessary steps for analysis of deep sequencing results. When the F variants are sequenced, they will then be analyzed by the IBEST GRC and sorted based upon their unique barcode sequences to determine which population they initially came from. These results will then be compared to molecular modeling predictions.

CHAPTER 3: AN INDIVIDUALIZED APPROACH TO ANALYZE BINDING DIFFERENCES AMONG MODELED RESIDUES WITHIN THE D25 EPITOPE OF F

Introduction

Overview of Studying Viral Escape

Studying viral escape in the presence of antibody *in vitro* is commonly used for many viral systems, including RSV. Typically, these studies consist of infection with a virus in the presence of an antibody that when resistant mutations in the virus occur randomly, the antibody applies a pressure that selects for resistant variants in the population. Ideally, the amount of antibody used is at a concentration that allows for evolutionary selection to occur without abolishing virus or ending the experiment with the dominant viral phenotype being wild-type. After preliminary studies confirm the amount of virus to be used for cultivating escape mutations, researchers will infect cells and monitor them for cytopathic effect, indicating adequate infection. The virus is then harvested and can be used to re-infect a new flask of cells. These studies will often include sequencing at each re-infection (passaging) step to identify when specific escape variants showed up in the population over time. Passaging the virus will continue for several passages, where the media harvests from each passage will be sequenced for escape variants. Deep sequencing, as opposed to Sanger sequencing, shows not only the predominant mutants present at the end of the experiment but also identifies mutations with smaller frequencies that are still relevant within the viral population. Once these variants are identified, studies will then typically assess these variants on a more individualized basis in terms of their growth kinetics, antibody binding, and antibody neutralization (121, 134). We aim to compare results of previously performed viral escape experiments identifying predominant RSV escape variants in the presence of D25 to individual mutants selected for D25 binding analysis based on molecular modeling estimations. Individual binding analysis of mutants will allow us to validate not only the molecular modeling used to build the D25 library, but also variants that screened positive for antibody escape in the DMS-based approach in chapter 2.

Dot Blot, Flow Cytometry, and In-cell ELISA to Assess D25 Binding

Techniques such as biolayer interferometry (BLI) or surface plasmon resonance (SPR) are important assays to consider when assessing ligand binding, especially when attempting to identify small changes in binding across between protein variants (187-191). These types of techniques are not ideal for the assessment of many protein variants, however, due to the labor-intensive steps required to purify and analyze samples (192). Purified protein or virus particles are also necessary to gather binding data using these methods and this can prove to be a time-consuming and difficult process to optimize (193, 194). That is where techniques such as western or dot blotting, flow cytometry, or in-cell ELISA's are useful when assessing mutants of interest in a relatively short amount of time and are techniques that we utilized within this chapter. Dot blotting may be used to determine the expression levels of a protein of interest and this expression can be compared across different mutants using densitometry analysis (195). Dot blotting has been used by the Miura lab as a more high-throughput version of western blotting, where as many as 96 mutants may be blotted onto a nitrocellulose membrane at once without running SDS-PAGE prior to blotting. Primary antibodies used for the detection of the protein of interest do not always bind efficiently, resulting in a lack of signal on the membrane. This is what we observed in the case of the D25 mAb (figure 26). This can make assessment of mutants difficult or impossible when using certain antibodies.

Flow cytometry is another method that can be used for assessing antibody binding to protein variants. This technique may utilize a primary and secondary antibody combination or a fluor-conjugated primary antibody only and can detect changes in antibody binding based upon the fluorescent signal captured by the flow cytometer. Flow cytometry, like dot blotting, can assess many variants in a 96 well plate format, making it relatively high throughput (196, 197). The Miura lab has demonstrated the use of flow cytometry to detect changes in antibody binding based upon the percent positivity and the MFI of each sample that gives information about the intensity of the signal for the samples. Some antibodies such as D25 and motavizumab do not bind surface proteins equally based on conformation, therefore

challenges may arise when using multiple different antibodies to detect expression and escape when antibodies only bind conformation-specific epitopes.

In-cell ELISA's may be used to express protein variants of interest on the surface of cells in a 96 well plate format and detect binding using antibodies. The secondary antibody used for our purposes is conjugated with a horseradish peroxidase (HRP) enzyme that reacts with 3,3',5,5'-Tetramethylbenzidine (TMB) substrate that is put into the wells after incubation with secondary antibody. This reaction turns the wells from clear to colored due to the chromogen formed during the enzymatic reaction with the substrate. Cells can be transfected with protein-encoding plasmid variants to express those variants on the cell surface. HEK-293A cells used for our experiments express protein robustly but do not adhere well to the surface of the plate, causing cell lifting during incubation and washing steps. We have found that using formaldehyde for adhering the cells to the wells can cause conformational changes to surface proteins and antibodies that are conformation-specific can no longer bind.

Taking each of the drawbacks into consideration when performing these assays, we predict that the flow cytometry and in-cell ELISA approaches will allow us to assess individual potential escape mutations for their differences in D25 binding, while using motavizumab as an expression control antibody. Using these approaches will allow us to validate the DMS screen and molecular modeling by testing mutants that are both predicted to escape and not escape D25 binding. We also predict that we will observe escape using flow cytometry or in-cell ELISA for those mutants that escaped D25 in the evolution experiments performed by Frankie Scholz. Validating those escape variants from the evolution experiments will be important for demonstrating the effectiveness of the assays used for an individual approach to evaluate D25 binding differences.

Materials and Methods

Previous Viral Evolution Studies

Frankie Scholz performed these evolution experiments using an RSV infectious clone system developed by Dr. Martin Moore at Emory University (198). The infectious clone system was used in the Miura lab following this reverse genetics system by transfecting cells with a BAC vector containing the A2line19F RSV genome (pSynk) along with several helper plasmids to help build the rest of the virion (198). pSynk also contains a fluorescent marker monomeric Katushka 2 (mKate2), that fluoresces red to indicate infection in cell culture and can be visualized with fluorescence microscopy. The RSV infectious clone was first passaged in HEp-2 cells to assist the virus with obtaining background variation before beginning the passages in the presence of D25 mAb. This pre-passaged infectious clone was then added to fresh HEp-2 cells in the presence of D25 at a concentration of 0.16 µg/mL (low). This passaging scheme was continued every 3-5 days based on visualization of red cells (mKate2 expression indicating RSV infection) over the course of 5 passages at the low D25 concentration. Once the 5 passages were complete, the D25 concentration was increased to 2.5 µg/mL (high) for 5 subsequent passages. This protocol was replicated three times, although one replicate was not able to survive the high concentration of D25 during those passages. RNA was then extracted from the released rRSV particles in the harvested supernatant media from each passage and converted to cDNA using reverse transcription-PCR (RT-PCR) in preparation for deep sequencing as well as Sanger sequencing. Deep sequencing was used to target the F gene to identify the variants present in each passage and at what frequencies those variants were present.

Dominant Escape Variants Assessed for Differences in Growth and Antibody Neutralization

Upon completion of Frankie's F protein evolution experiments, we wanted to characterize the mutants from those experiments in terms of their growth kinetics and sensitivity to D25 neutralization compared to wild-type virus. These experiments were performed by Kevin Hutchison at the University of Idaho. Site-directed mutagenesis

(SDM) was first used to make the mutations in F within a vector called pBlueScript KS(+) (pBKST). The mutants were then excised by restriction digest and subsequently cloned into pSynk to be compatible with the infectious clone system. Mutagenesis in pSynk is not possible due to its large size (~16000 bp), so pBSKT is used as an intermediary plasmid for SDM. After the mutants are cloned into pSynk, a transfection into BSR-T7/5 cells was performed using pSynk and four helper plasmids. This transfection generates the infectious clone containing the mutants of interest from the evolution experiments. The pSynk RSV system has been utilized successfully for making other mutant RSV infectious clones for testing antibody binding and comparing growth kinetics across different mutants in the motavizumab binding site.

Growth Kinetics and Neutralization Assays Performed on Variants Identified from Evolution Experiments

Growth kinetics experiments using $TCID_{50}$ assays were first performed to compare growth rates between the mutants identified during the evolution experiments performed by Frankie Scholz. HEp-2 cells were seeded at $7.5x10^4$ cells/well in a 24 well plate. Virus was put onto cells (150 µL) using an MOI of 0.1 $TCID_{50}$/cell and incubated with cells while rocking for 1 hour. The virus was then aspirated, and the cells were washed 3 times, the first wash was kept for a zero-hour timepoint. Media was then added back onto wells and incubated for timepoints. Media was collected at each timepoint, centrifuged, and the supernatant media was collected and flash frozen. After all samples were collected, $TCID_{50}$ assays were performed using the previously collected supernatant on freshly seeded HEp-2 cells.

Neutralization assays were performed to determine the D25 neutralizing concentration for each mutant and if those values had any correlation with their overall fitness. HEp-2 cells were seeded at $5x10^4$ cells/well the day before infection in a 96 well plate. The RSV infectious clone was diluted in minimal essential media (MEM) according to $TCID_{50}$/mL values in table 5 below. A multiplicity of infection (MOI) of 2 was used for all mutants. Viral dilutions were incubated with D25 at varying concentrations from 10 µg/mL serially diluted to 0.15625 µg/mL for 1 hour at

37°C with 5% CO_2. One hundred µL of virus plus antibody mixture was then added to the wells and incubated at 37°C with 5% CO_2 for 18 hours. The wells were fixed in 1% formaldehyde and flow cytometry was performed on the samples.

Table 4: $TCID_{50}$ values for each mutant used in growth kinetics and neutralization assays

rRSV Mutant	Titer ($TCID_{50}$/mL)
Q202R	$1.78x10^6$
N208Y	$5.62x10^6$
Q202R/N208Y	$3.16x10^6$

Predicting D25 Escape Mutations for Individual Analysis

As discussed in chapter 2, molecular modeling was used to predict mutations in the D25 binding site of F that reduce or abolish D25 binding. Previous work by Dr. Craig Miller and colleagues at the University of Idaho demonstrated the use of molecular modeling software to predict amino acid residues that when mutated may cause antibody binding disruption but still allow proper protein folding. The groundwork laid by Miller set ΔΔG boundaries for protein folding and antibody binding using bacteriophage capsid subunit interactions, and the same boundaries were used in work with the Ebola virus envelope glycoprotein (EBOV-GP) and its binding with the mAb KZ52 (124, 199). These boundaries are described as ΔΔG > 2.0 kcal/mol for a disruption in antibody binding, and ΔΔG folding between -2.5 and 2.5 kcal/mol. To create a watchlist of mutations, each possible amino acid making up the EBOV-GP was used to predict sites that disrupt binding to KZ52 but allow proper folding and trimerization of GP. This same pipeline was utilized when calculating ΔΔG values of folding and binding for this RSV project, where 100 ns molecular dynamics simulations were performed on the F monomer crystal structure to extract snapshots to be fed into the FoldX algorithm. FoldX was used to calculate ΔΔG of

folding (stability) for all possible 19 amino acid variants at each site. The 100 ns snapshots were averaged for each individual variants at each site. To address binding disruptions, the modelers then used the F-D25 co-crystal structure to run 100 ns molecular dynamics simulations similar to the methods described above. The FoldX algorithm then calculated ΔΔG values of binding for all possible mutations in F to predict changes in D25 binding. Results for ΔΔG of folding and binding values of variants for all library sites are found in the top panel of figure 18 below. The bottom panel of figure 18 shows ΔΔG values for all D25 library variants in grey and highlights variants from sites N208 and K201 in red and purple, respectively.

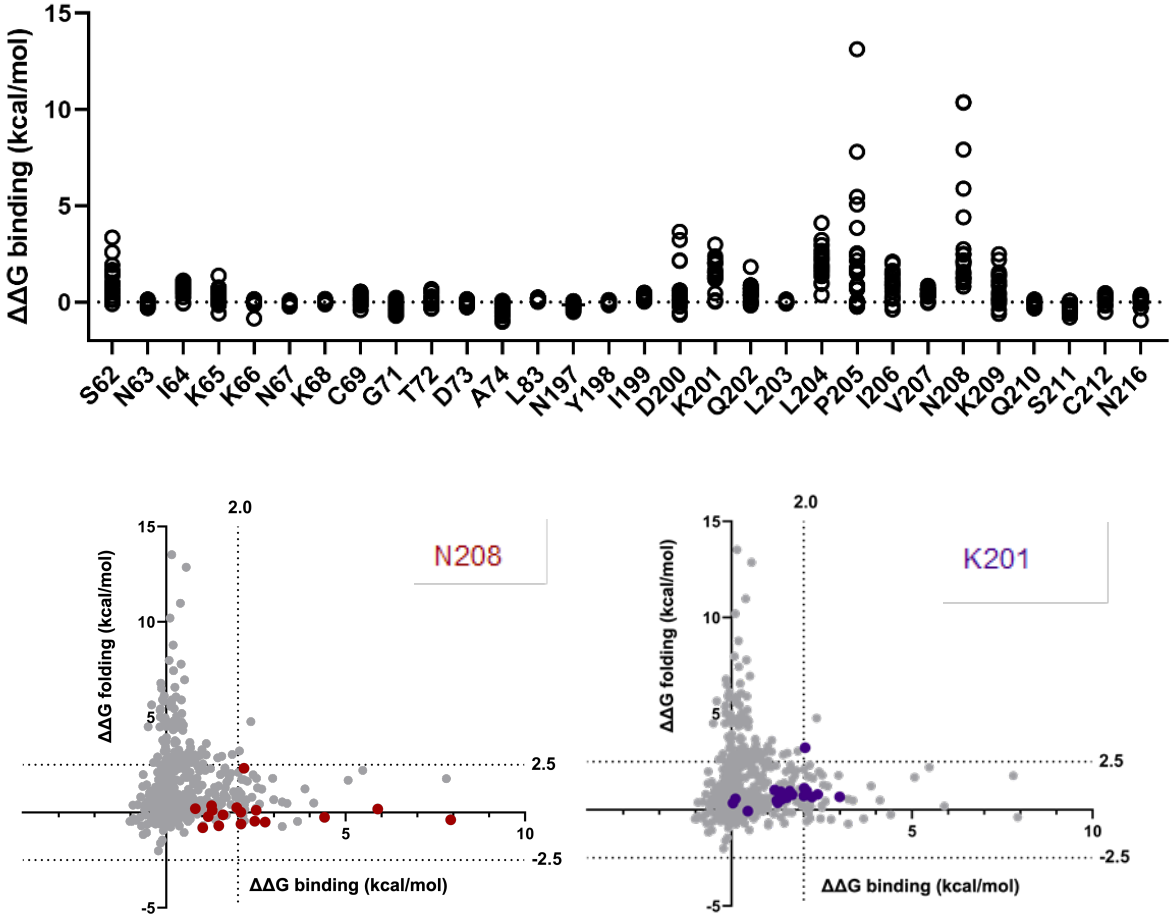

Figure 18: ΔΔG values of folding and binding for all variants at each amino acid site within the D25 epitope of F (open circles, top panel and gray dots, bottom panel). Open circles with higher ΔΔG of binding values are estimated to disrupt D25 binding. Red and purple dots on the bottom panel plots correspond to variants from site N208 and K201, respectively. Dotted lines indicate previously determined cut-off values for predicting a disruption in folding or binding (ΔΔG binding > 2.0 kcal/mol, ΔΔG folding between -2.5 and 2.5 kcal/mol).

Dot Blot to Analyze Mutant Expression

HEK-293T cells were seeded at $7.5x10^4$ cells/well in a 96 well plate and incubated overnight at 37°C. Cells were transfected with pcDNA3.1 variant plasmids using Lipofectamine 3000™ reagents. Wild-type plasmid was used in this assay to test for D25 binding compared to the 101F antibody. Twenty-four hours after transfection, media was gently aspirated from the wells and 100 µL of pre-warmed PBS was added to each well to lift cells from plate. Cells were then transferred to a 96 well U-bottom plate and pelleted by centrifugation at 600xg for 2 minutes. Cells were resuspended in 10% FBS in PBS and incubated on ice for 15 minutes. Cells were pelleted again as previously described, then samples were run through the dot blotter. Nitrocellulose membranes were first soaked in 1X TBS for 10 minutes and the dot blotter was assembled. Cell samples were added at 100 µL per well to each well of the dot blotter and vacuum was applied to run samples through the apparatus, leaving protein-expressing cells behind on the membranes. The membranes were then allowed to dry and blocked in 5% milk in TBST at room temperature for 1 hour. The membranes were then incubated overnight at 4°C with 50 ug/mL D25 or 101F in 100 µL After the overnight incubation with primary antibody, the membranes were then rinsed 3-5X with 1X TBST and subsequently incubated with 1:1000 diluted secondary antibody (GαHu or GαMu HRP) for 1 hour at room temperature. The membranes were rinsed 3-5X with 1X TBST and used ThermoFisher Pierce™ ECL Western Blotting Substrate kit to visualize the dots using a chemiluminescent imager.

In-cell ELISA

HEK-293A cells were seeded at a density of $3.25x10^5$ cells/well in a 96 well plate. Cells were left to adhere and incubate at 37°C for approximately 24 hours. Cells were transfected with pcDNA3.1-F plasmid variants using Lipofectamine 3000™ reagent. Forty-eight hours post-transfection, cells were fixed in 4% formaldehyde for 15 minutes in preparation for blocking and antibody incubation steps. The plate was then washed 3X with PBS and stored in PBS at 4°C. The following steps were adapted from an Abcam™ in-cell ELISA protocol. Cells were blocked in a 0.5% BSA in PBS solution for 2 hours at room temperature while

rocking. Diluted D25 or motavizumab was then added to the wells (10 µg/mL D25 and 5 µg/mL motavizumab) and was incubated at 4°C overnight. The plate was then washed with 250 µL of wash buffer (0.05% tween in PBS) 3X, then incubated with diluted goat anti-human IgG conjugated with horseradish peroxidase (GαHu-HRP) secondary antibody for 2 hours at room temperature while rocking. After the secondary antibody incubation, wells were washed 4X with wash buffer to eliminate background binding and TMB substrate solution was added. Adding the TMB substrate solution to the wells with an abundance of D25 or motavizumab binding with GαHu-HRP secondary antibody binding resulted in a blue color in the well, while wells without sufficient binding maintained a clear color. Hydrochloric acid (HCl) was added to stop the reaction and the blue color turned yellow. The plate was then read by our plate reader, giving absorbance values at ~450 nm. Un-transfected cells that were not treated with either primary or secondary were used as a background for the reading, while pcDNA3.1-GW transfected cells that were stained with secondary only were used as a negative control.

Results

Previous Evolution Experiments

Evolution experiments were replicated 3 times and 2 of the 3 experiments were successful in allowing D25 resistant F variants to become present in the viral population. These experiments first used neutralization assays to compare resistance to D25 neutralization over the different passages from all three replicates (figure 19, A). In the first line, we see an increase in resistance to D25 neutralization to roughly 20 μg/mL within the first 5 passages of 0.16 μg/mL D25 as shown by the red line. After 5 passages in the higher concentration of D25 (2.5 μg/mL), we see an even greater increase in resistance to D25 neutralization, at nearly 80 μg/mL. The second replicate from this study only continued through high passage one, and we do not see any resistance to D25 neutralization within the first 5 low passages of D25. The final replicate shows resistance to D25 neutralization only during the passages with 2.5 μg/mL of D25, not during the early passages with low D25. This resistance is approximately 20 μg/mL and is shown by the purple line (figure 19, A).

After RT-PCR was used to generate cDNA from the viral RNA extracts from each of the passages, Sanger sequencing was used initially to identify the dominant mutants within the population after passages with low and high concentrations of D25. To further identify mutations that occurred at lower frequencies, deep sequencing was used on the harvested virus stocks (low frequency mutations not shown). Several unique mutations were identified, some of which were predicted by our modeling team. In the first replicate, N208Y appeared after only a few passages in the low concentration of D25 followed by a secondary mutation, Q202R. Site N208 was predicted to be a potential escape site due to its high ΔΔG of binding value with multiple variants at this site (figure 18, top panel). Figure 19, B shows the results from the deep sequencing for all 3 lines. The N208Y/Q202R mutant maintained a frequency of 100% after passage ~7. As stated previously, the second replicate for this experiment was only studied through the first high concentration of D25, beyond that passage no virus continued to replicate. Deep sequencing was still able to identify mutations that were present in the population, including N208Y (~8%

frequency) as well as K226R (~0.2% frequency). The final replicate identified another unique mutation at site 208, however instead of an asparagine to a tryptophan the mutant found encoded a lysine (N208K). This mutation, like the first replicate was the predominant mutation (figure 19, B).

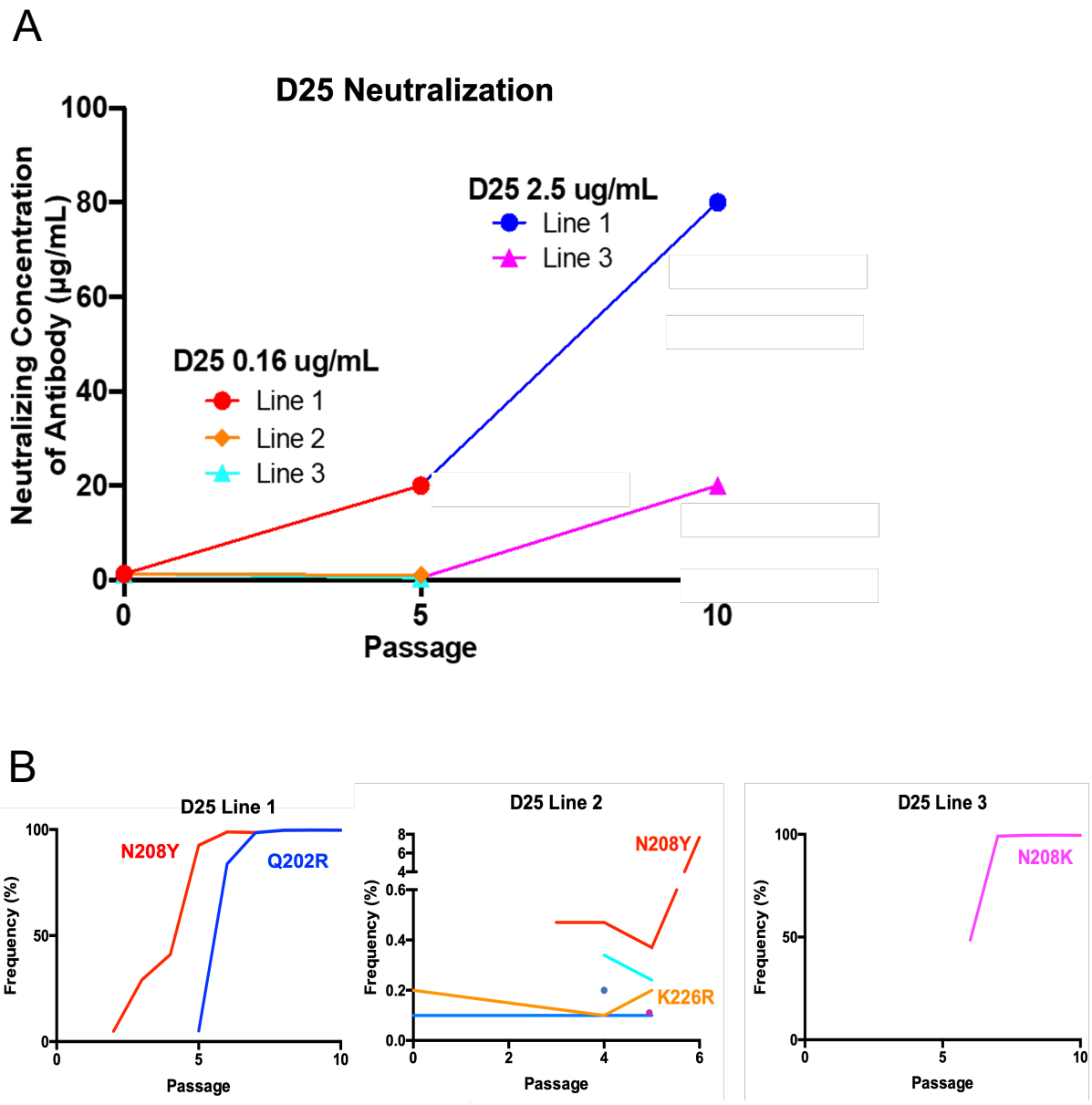

Figure 19: Lines 1 and 3 show resistance to D25 neutralization. There is an increase in resistance in line 1 after the first 5 passages in 0.16 µg/mL and continued to increase in resistance through the 5 passages in 2.5 µg/mL D25. Line 3 only showed resistance to D25 neutralization after passages in 2.5 µg/mL D25 (A). Deep sequencing elucidates dominant mutations that are providing resistance to neutralization by D25. A double mutant arose in line one, N208Y/Q202R, and another mutation at site N208 (N208K) arose in line three (B). These dominant mutations were also identified by Sanger sequencing.

Growth Kinetics of Three Unique Mutants Identified by Evolution Experiments do not Show Significant Differences

Growth curves performed on N208Y, Q202R, and N208Y/Q202R double mutants that were present in high frequencies during evolution experiments showed slight differences between them over time, but not significantly different according to multiple unpaired t tests (figure 20). Though not significant, it appears that all three mutants had slightly slower growth compared to wild-type rRSV. The growth of N208Y appeared to be the most impacted at early timepoints, especially within the first 24 hours. Of all the mutants tested, Q202R had growth kinetics similar to wild-type especially early during the time course. The double mutant seemed to be somewhere in between N208Y and Q202R, suggesting that the Q202R mutation might provide some benefit for growth that the N208Y mutation does not provide.

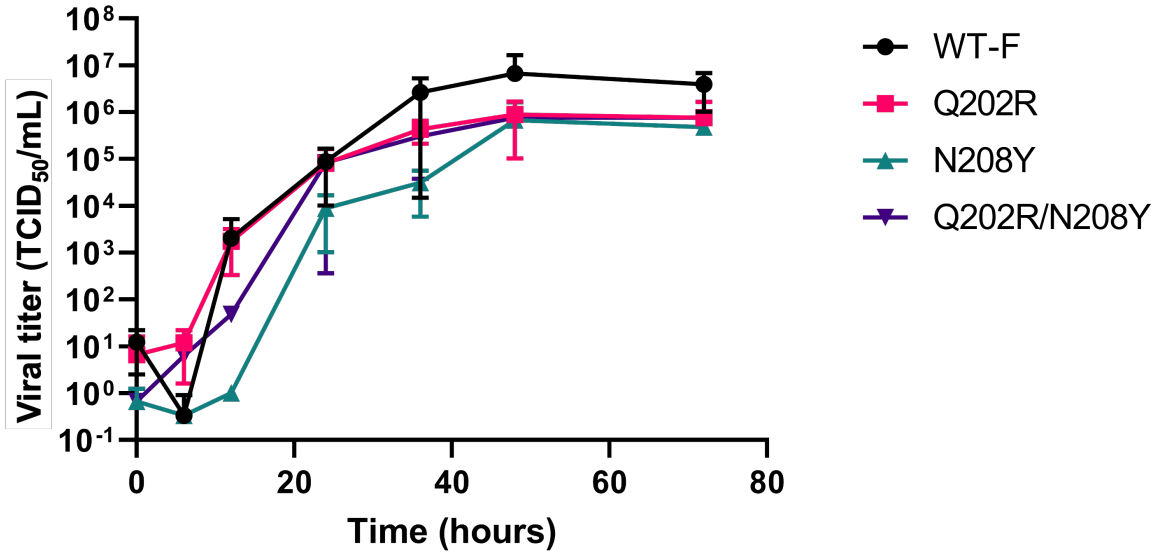

Figure 20: Growth curves of N208Y, Q202R, and N208Y/Q202R mutants using a $TCID_{50}$ assay. $TCID_{50}$ values were calculated for each mutant at 12-, 18-, 24-, 36- and 72-hours post-infection in HEp-2 cells.

Resistance to Neutralization by D25

Along with gaining information about the growth profiles of each of these mutants, we were also interested in their resistance to D25 neutralization using the infectious clone system. The results of these experiments show that there is significant resistance to D25 neutralization in the N208Y and double mutant, but not

in Q202R mutant alone (figure 21). There is a significant difference in resistance to neutralization for the N208Y mutant for all D25 concentrations except for the lowest concentration (0.156 µg/mL) and the highest concentration (10 µg/mL). The N208Y/Q202R double mutant also showed significant differences in resistance to neutralization every concentration except for the lowest concentration (0.156 µg/mL). These data provide validation that both the N208Y and the double mutant are resistant to D25 neutralization, with the N208Y single mutant showing greater resistance. From previous evolution experiment data, we would have expected the double mutant to have the greatest resistance to D25 neutralization, but we do not see this. Previous data demonstrated that upon the addition of the Q202R mutation to the N208Y mutation, there was an increase in resistance to neutralization by D25 surpassing the single N208Y mutant. Previous neutralization experiments were not performed on clonal variants, which could impact the results as compared to the neutralization data using isolated variants. A potential hypothesis is that there could be a trade-off occurring, resulting in the double mutant being able to grow well with the addition of the Q202R mutation as indicated by figure 20 but does not prevent neutralization by D25 as well as the single mutant.

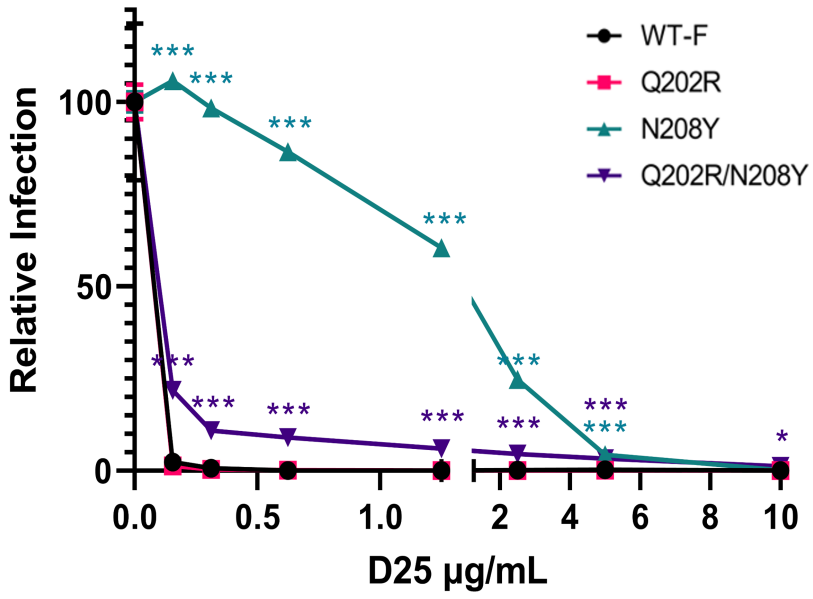

*Figure 21: N208Y, Q202R, and N208Y/Q202R mutants subjected to D25 neutralization assay showed differences in sensitivity to neutralization. Flow cytometry was used to quantify the relative infection percentage based on mKate positive cells at differing concentrations of D25 for each of the mutants of interest. Statistical analysis was performed using multiple unpaired t tests using GraphPad Prism. *, p <0.033; **, p<0.002; ***, p<0.001.*

Consequences of N208 and Q202 Amino Acid Mutations by Molecular Modeling

Figure 22 below visualizes N208Y and Q202R mutants in the context of the F-D25 co-crystal structure. The analysis of this mutagenesis was performed by Dr. Jagdish Patel, where it was determined that a change from asparagine (N) to a tyrosine (Y) at site 208 would prevent access to a small hydrophobic pocket in F by steric hindrance since Y maintains such a large and aromatic side chain. The change from glutamine (Q) to an arginine (R) at site 202 on F would abolish three hydrogen bonds between the D25 mAb and site Q202. Based on the molecular modeling data, we might expect the Q202R mutant on its own to provide more resistance to D25 neutralization due to the abolishing of hydrogen bonds between that site and D25, but this is not what we observe (figure 22). It could be that the blocking of the hydrophobic pocket by N208Y may be more influential for D25 binding than the abolishing of hydrogen bonds at site Q202. This is something that could be tested in the future to determine whether hydrogen bonding at site Q202 is more important for D25 binding or if blocking the hydrophobic pocket at site N208 is more important.

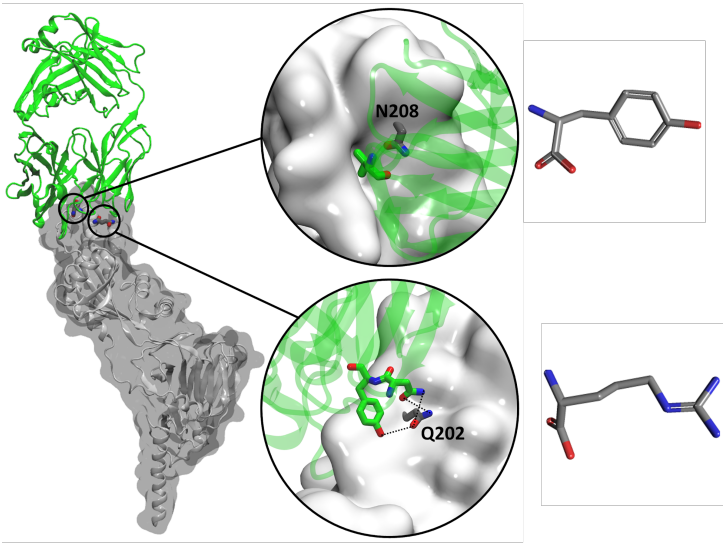

Figure 22: F-D25 co-crystal structure with N208Y and Q202R variants using VMD software. The change from asparagine (N) to tyrosine (Y) at site 208 prevents access to hydrophobic pocket on F due to steric hindrance. Changing glutamine (Q) to an arginine (R) abolishes hydrogen bonds between the Q202 residue and the D25 mAb.

Flow Cytometry on Individual Mutants Show Slight Differences in D25 Binding

Several D25 mutants were transfected into cells and expressed on the cell surface for individual assessment of D25 binding differences using flow cytometry. Motavizumab was used as an expression control antibody to detect adequate expression of the mutants to confirm that a decrease in D25 signal was due to possible antibody escape. In the wild-type F – transfected cells, we can see a ~2:1 binding efficiency in motavizumab and D25, respectively. Since D25 is conformation specific, some of the F proteins that are present on the surface of the cells may be triggered to its post-fusion conformation before or during the cell-preparation protocol. To help prevent F triggering, we fixed the cells with 1% formaldehyde after staining with D25 since it has been shown that formaldehyde fixing triggers F to post-fusion (186). The data presented in figure 23, B has been normalized to the percent of cells positive in the wild-type F-expressing population. We can then compare the differences in D25 or motavizumab binding across the mutants tested.

These results show that there is a decrease in D25 binding for one of the mutants tested, N208E. The wild-type F – transfected cells showed approximately 44% of cells positive for D25 binding, while the N208E mutant had 21% of cells positive for D25 binding (figure 23 A, B). This result makes sense in terms of the high ΔΔG of binding value for N208E, 4.41 kcal/mol (figure 23, B). Along with testing D25 sites, we also tested one known motavizumab escape variant (K272E) and a proposed escape mutation found from work performed by Sierra Beach in the Miura lab (S275R). We included these mutants in this experiment to verify antibody binding by observing a decrease in motavizumab binding and a consistent D25 binding percentage. For these mutants, we used D25 as the expression control antibody and motavizumab to assess escape. From these results, we can see there was a decrease in motavizumab binding while the D25 signal stayed approximately at the level of wild-type.

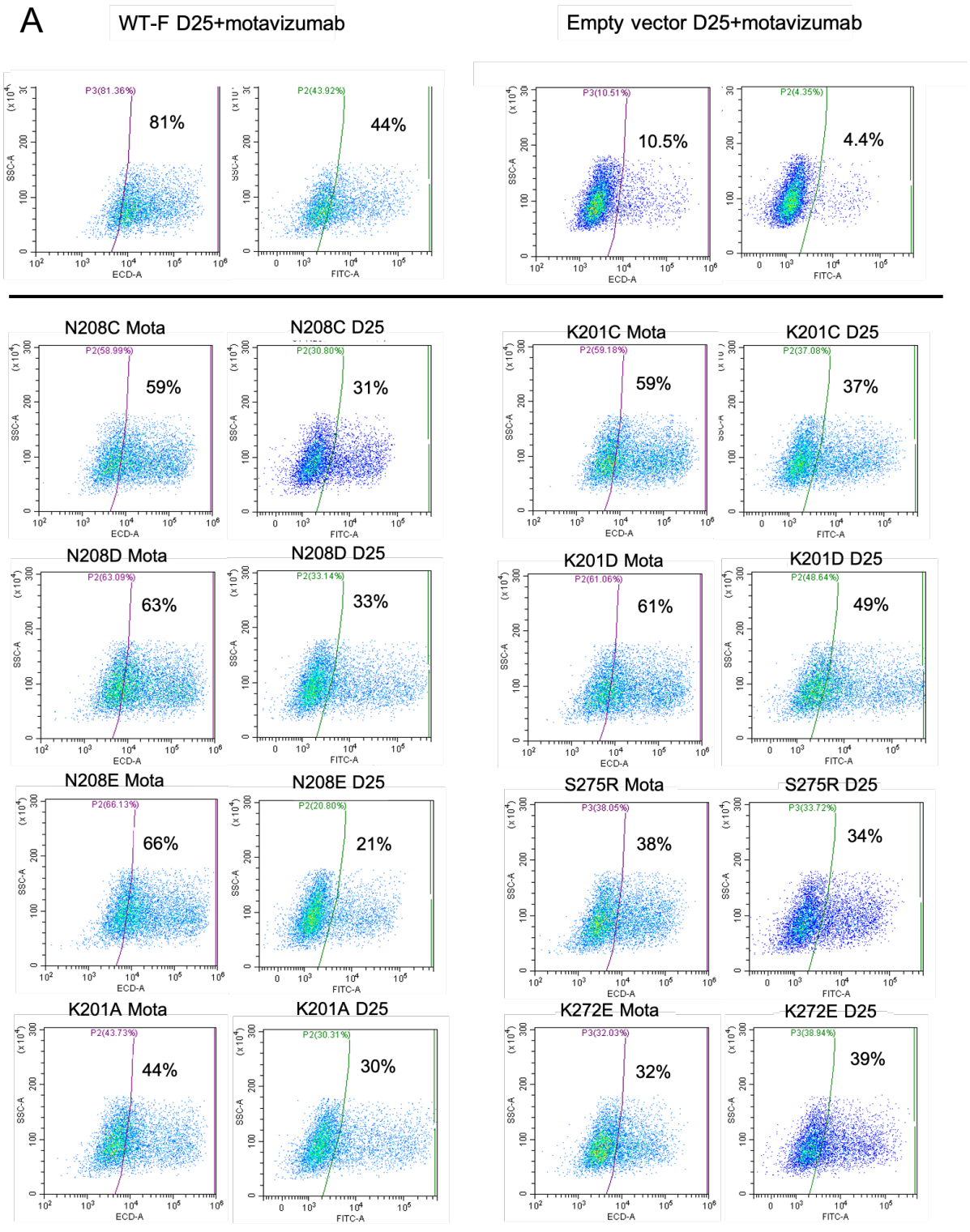
A
WT-F D25+motavizumab
Empty vector D25+motavizumab
81%
44%
10.5%
4.4%
N208C Mota
N208C D25
59%
31%
K201C Mota
K201C D25
59%
37%
N208D Mota
N208D D25
63%
33%
K201D Mota
K201D D25
61%
49%
N208E Mota
N208E D25
66%
21%
S275R Mota
S275R D25
38%
34%
K201A Mota
K201A D25
44%
30%
K272E Mota
K272E D25
32%
39%
SSC-A
ECD-A
FITC-A

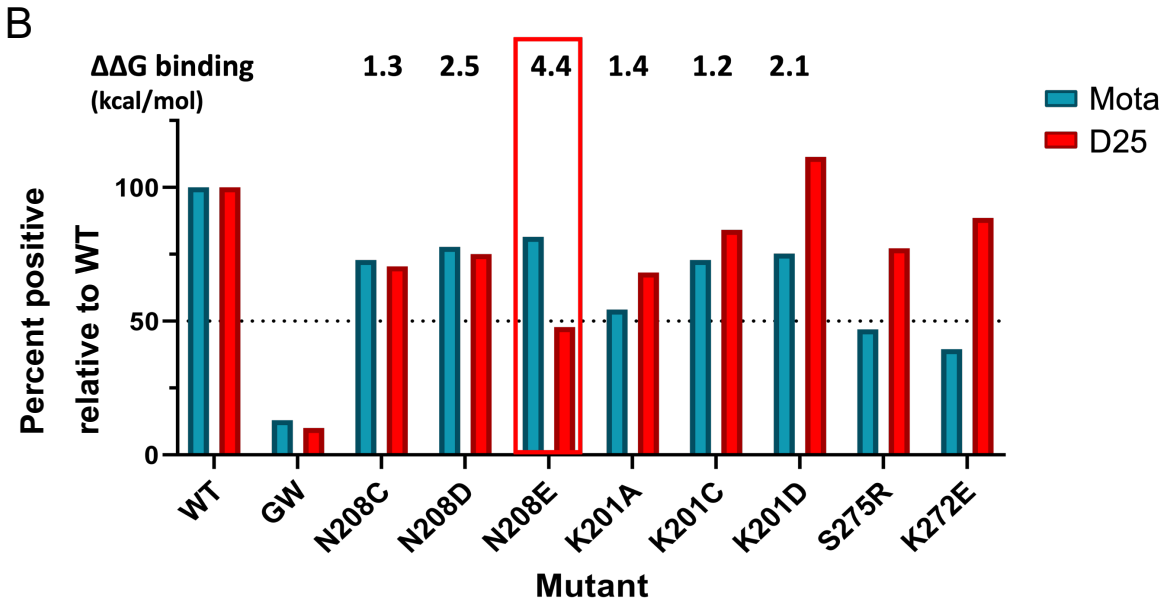

Figure 23: Flow cytometry binding assay used to evaluate differences in binding across six different D25 mutants and two motavizumab escape mutants (S275R and K272E). FITC and ECD channels were used to identify D25 and motavizumab percent of wild-type positivity, respectively (A). A summary of the results in figure 23, A displayed as a bar chart, comparing motavizumab and D25 expression normalized to the percent of wild-type F-expressing cells that are positive for antibody binding (B).

In-cell ELISA

This assay was optimized for use in this project to assess binding differences in individual mutants in another way that utilized transfected cells expressing F. To determine the concentrations of antibody to be used for this assay, we first fixed wild-type F expressing cells with 4% formaldehyde and incubated the cells with different primary and secondary antibody concentrations. From these data, we decided to use 10 µg/mL D25 antibody, 5 µg/mL motavizumab, and 1:250 dilution of the secondary antibody GαHu HRP (figure 24). This combination gave us enough detection of F while keeping the background minimal on un-transfected cells. As described previously with the flow cytometry binding assay, motavizumab was used as an expression control antibody to make sure a decrease in signal was due to potential antibody escape. Motavizumab could be utilized in this assay because it binds site II on F, a distinct site from the D25 binding site Ø.

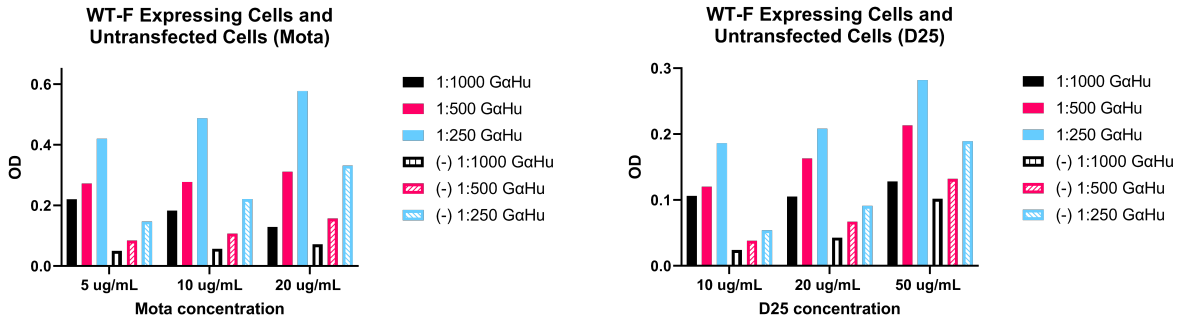

Figure 24: Primary and secondary antibody concentration optimization experiments for in-cell ELISA. A range of 10 µg/mL to 50 µg/mL of D25 and 5 µg/mL to 20 µg/mL of motavizumab was used on wild-type F transfected cells (filled bars) as well as un-transfected cells (-) to assess background (lined bars). Dilutions of secondary antibody at 1:250, 1:500, and 1:1000 were used on transfected and un-transfected cells as well.

The in-cell ELISA was then tested on the same panel of mutants as in the flow cytometry binding assay for comparison and includes N208Y, N208K, N208W, and N208V due to their interest from molecular modeling and appearance of N208Y and N208K in the evolution experiments. pcDNA3.1-GW (empty vector) – transfected cells were used as a negative control for this experiment. This experiment demonstrates effective measurement of mutant expression based on the motavizumab binding and changes in D25 binding depending on the mutant. Comparing these results to the predicted ΔΔG values as with the flow cytometry binding assay, we can observe some correlations (table 6). N208E was predicted to be disruptive to D25 binding and that is reflected in the ELISA data as it was with the flow cytometry binding assay. There is a trend towards a decrease in D25 binding compared to that of wild-type, while motavizumab expression signal remains consistent. K201D interestingly shows a higher percentage of D25 binding than motavizumab in the flow cytometry experiment, but a decrease in D25 binding compared to motavizumab binding in the ELISA is observed.

Other mutants that were not predicted to escape D25 binding as estimated by molecular modeling still showed trends toward antibody escape. K201A for example, demonstrated a trend towards D25 escape in the in-cell ELISA context, even though the ΔΔG of binding value for this mutant is lower than 2.0 kcal/mol (figure 25, table 6). The K201 mutation along with other mutants can be seen below in figure 25, relating the amino acid mutations back to F structure and D25 binding (table 6). A

similar conclusion can be drawn for several other mutants tested in this assay, including N208C, N208D, and K201C. In the context of the flow cytometry binding assay, none of these mutants showed any trends towards a decrease in D25 binding. Both N208Y and N208W have the highest ΔΔG of binding values in the entire library and show some trends towards a decrease in D25 binding (table 6). The overall expression for these mutants is decreased, so further work will need to be performed to increase their expression to more effectively assess D25 escape.

Figure 27 models several mutants of interest including N208Y, N208E, K201A, and Q202R. N208E and K201A were both identified as potential escape mutations by either flow cytometry or in-cell ELISA (figures 23 and 25). The F monomer is represented by the light purple ribbon structure while the cyan and magenta ribbon structures represent the heavy and light chains of the D25 antibody. Red discs represent clashes with nearby structures upon mutating the wild-type amino acid to the indicated variant. The change from N208 to N208Y shows a drastic increase in clashing with nearby amino acids, further validating the disruptive properties of the tyrosine at site 208. The change from N208 to N208E shows a bit of clashing, but not to the extent of the N208Y mutant. The change from Q202 to Q202R does not show any clashing at all, validating our findings related to a lack of neutralization resistance activity with the Q202R mutant on its own. The K201A mutant interestingly shows clashing with nearby structures, even though it was not predicted by molecular modeling to disrupt antibody binding. K201A was found to be a possible escape mutant by in-cell ELISA and mutating to an alanine at this residue seems to cause structural disruption (figure 27).

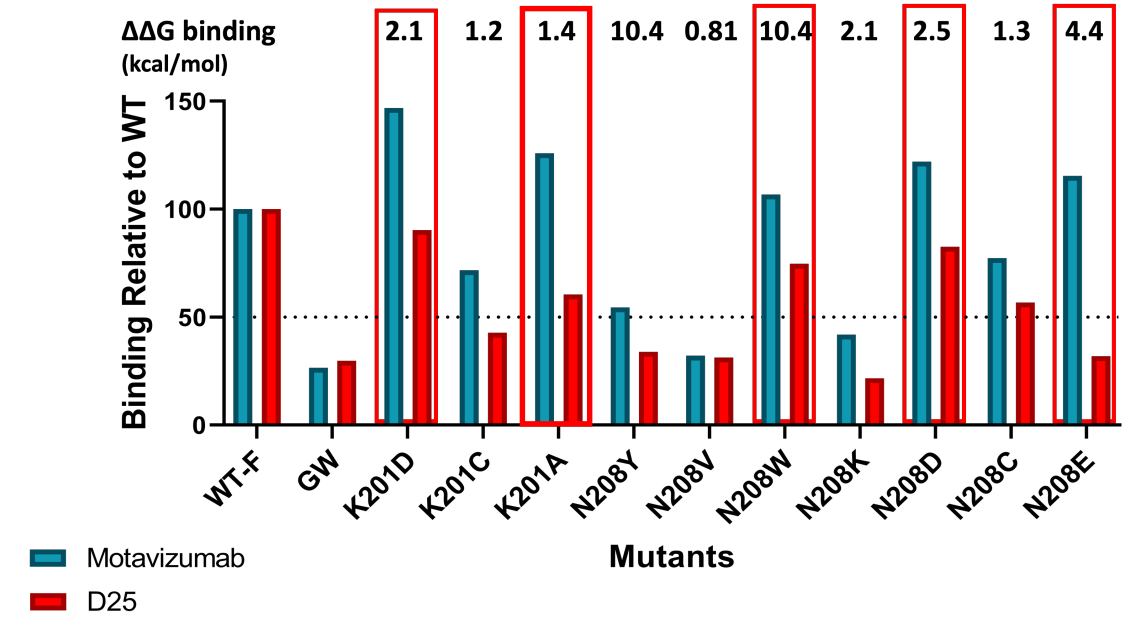

Figure 25: Panel of mutants tested are the same as the flow cytometry binding assay plus more site N208 mutants of interest. Binding is relative to wild-type for both D25 and motavizumab and this experiment was performed in technical triplicate.

Table 5: Summary of predicted versus observed escape in N208 and K201 variants tested by flow cytometry and in-cell ELISA

Mutation	ΔΔG binding (kcal/mol)	Predicted	Observed (Flow)	Observed (ELISA)
N208Y	10.4	Escape	N/A	Low expression
N208K	2.1	Escape	N/A	Low expression
N208E	4.4	Escape	Escape	Escape
N208D	2.5	Escape	No escape	Escape
N208C	1.3	No escape	No escape	No escape
N208W	10.4	Escape	N/A	Escape
N208V	0.81	No escape	N/A	Low expression
K201A	1.4	No escape	No escape	Escape
K201C	1.2	No escape	No escape	No escape
K201D	2.1	Escape	No escape	Escape

Dot Blot with 101F and D25 mAbs Using Whole Cells Expressing F

As shown by figure 26 below, the 101F antibody worked very well for detecting wild-type F expression in this dot blot assay. The empty vector control, pcDNA3.1-GW did not show expression on this blot as expected. D25 did not show any expression of wild-type F using this method. Since this assay did not work in the context of wild-type F, we did not proceed further with assessing mutants using this assay. F was most likely being triggered to post-fusion during one or more steps of the dot blotting procedure, resulting in D25 not being able to detect F.

Figure 26: Two nitrocellulose membranes blotted with wild-type pcDNA3.1-F using a dot blotting apparatus. Each membrane was blocked and stained with either 101F or D25 and corresponding HRP-conjugated secondaries were used after primary antibody incubation. Chemiluminescent exposure revealed detection by 101F but not D25.

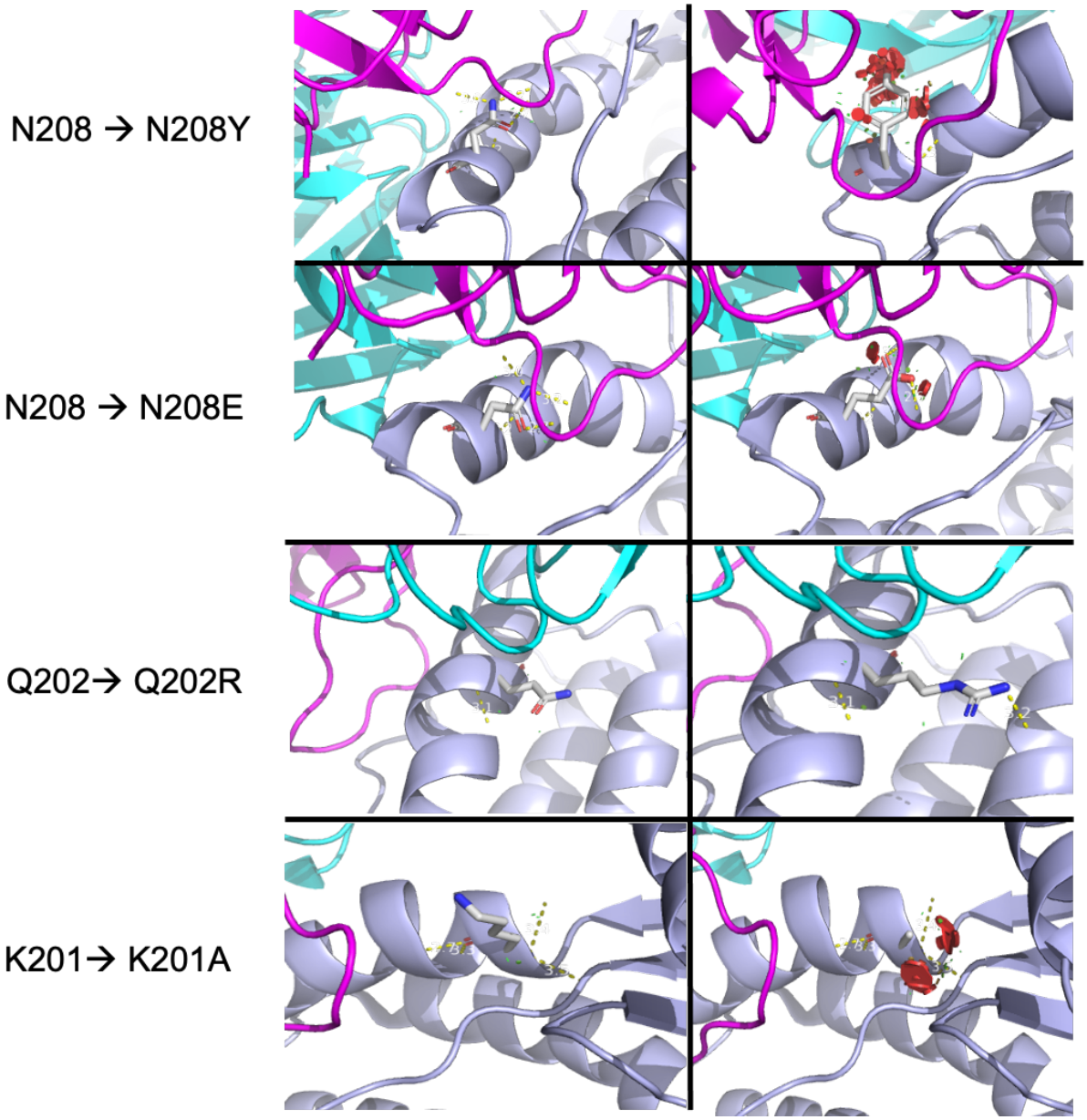

Figure 27: PyMOL images demonstrating the wild-type amino acid and a variant from individual analysis at sites 201, 202, and 208. Cyan and magenta indicate the heavy and light chains of the D25 mAb and light purple represents the F monomer. The wild-type amino acid is shown in the left-hand column and the variant (N208Y, N208E, Q202R, and K201A) is shown in the right-hand column of the figure. Clashes with the structure upon changes in amino acid are represented by red discs.

Discussion and Future Directions

Testing individual variants for differences in D25 binding became a somewhat difficult task. Due to the conformation specificity of D25 binding, this posed some challenges for the design of binding assays that could detect enough binding in the wild-type -transfected samples to effectively compare to selected variants. In the context of both binding assays, we saw different results for the panel of mutants tested. The flow cytometry assay and in-cell ELISA assays both demonstrating differences in antibody binding but showed slightly different results. During flow cytometry preparation, the cells are subjected to fewer steps and manipulations before being analyzed on the cytometer. We are also measuring percent positive cells for this assay and using those percentages to compare variants. Using percent positivity makes this assay more binary in terms of whether a cell is positive or not for FITC or ECD. Compared to the ELISA, there is a broader range of positivity or negativity based on the amount of antibody binding and thus the color change measured in each well. One other difference between this assay and the in-cell ELISA is that each cell is analyzed individually and plotted using flow cytometry compared to the ELISA that is measuring the bulk sample in each well of the 96 well plate. In flow cytometry preparation, cells are fixed in 1% formaldehyde as the last step before analysis, allowing for as much pre-fusion specific F to be present for D25 to bind. Compared to the ELISA, the cells undergo slightly harsher conditions with more rigorous washing and longer incubation steps at colder temperatures. We also must fix the cells as the first step of the assay to prevent cells from sloughing off the bottom of the wells (186). This could decrease the amount of pre-fusion F available for D25 to bind, contributing to inconsistent results.

Other studies have had success in using D25 to detect F expression in the context of dot blotting. In a study from 2016, researchers wanted to better understand the effect of formalin and heat inactivation on the conformation of F (186). This study utilized dot blotting with motavizumab, AM14, D25, and 5C4 antibodies to detect both pre- and post-fusion F conformations. The DS-Cav1 construct was used in this study to provide the pre-fusion stable conformation of F to allow those pre-fusion specific antibodies (AM14, D25, and 5C4) to bind efficiently (186). Experiments where we

clone D25 library mutations in the DS-Cav1 construct could assist with the pre-fusion F conformation problems we have run into with dot blotting and our other binding assays. One study from 2012 successfully utilized in-cell ELISAs for the detection of different RSV proteins from infected cells (200). Our experiments did not use infected cells for our ELISAs, but this could be something to test in the future with mutants cloned into the RSV infectious clone system. Overall, preliminary data suggests that we can use molecular modeling to predict individual antibody escape variants in the D25 epitope of F. More repeats of these experiments are needed to better distinguish between true antibody escape and experimental background to elucidate if the modeling predictions are accurate.

Summary and Conclusions

The second chapter of this project was able to successfully develop a high-throughput pipeline for screening D25 library mutants for antibody escape using molecular modeling, an MLV-based gene delivery system, FACS, and deep sequencing. Through our optimization studies, we were able to observe differences in D25 percent positivity between the wild-type MLV and library MLV – transduced cells by flow cytometry. These trends gave us confidence to proceed with establishing sorting bins for different populations of F-expressing cells to screen for potential D25 escape mutants. Upon cell sorting, we were then able to successfully extract DNA from the different populations and generate amplicons for deep sequencing using two distinct rounds of PCR reactions. When analyzing the sequencing reads for the sorted populations, we expect to find our escape mutants in the motavizumab positive, D25 negative or low populations. These mutants should also be present in the MLV library and pLPCX-F plasmid pools. Though the libraries 1 and 2 were prepared separately, we would expect to see redundancy in the sorted mutants. Once the amplicons have been sequenced and analyzed, we would want to assess the variants found in each sorted population and compare that to molecular modeling predictions in terms of ΔΔG values of folding and binding. It would be important to Identify mutants that screened positive for antibody escape that were also predicted by molecular modeling to escape D25 for validation of the modeling. We could also identify mutants that did not express well on the surface of cells, based on their presence in the MLV library stocks and sorted into the motavizumab negative population. This information could be used to assist in the building of logo plots to summarize mutational tolerance at different sites within the D25 epitope of the F protein. Tolerance to mutations at different sites within F would be an important takeaway from this study to further understand sites of interest that could become prevalent clinically, in terms of escape.

Chapter 3 first examined previous viral evolution experiments using D25 to select for escape mutations *in vitro.* These experiments resulted in three major variants that reached nearly 100% frequency: N208Y, N208Y/Q202R, and N208K. Neutralization experiments demonstrated an increase in resistance to neutralization

by D25 for each of these mutants, especially the double N208Y/Q202R mutant. To address how these mutations affected viral growth, N208Y, Q202R, and the double mutant were recombined into the pSynk vector as part of the RSV infectious clone system. The mutant viruses were then assessed for growth, and these data demonstrated that there was no significant difference between any of the three variants. Neutralization data with these three mutants then showed some interesting results. The N208Y mutant was significantly more resistant to neutralization than wild-type RSV, as well as the N208Y/Q202R double mutant. The double mutant, however, was not nearly as resistant as the N208Y mutant on its own. Q202R did not show any significant difference in its resistance to neutralization by D25 compared to wild-type. We can hypothesize that the Q202R mutation provides some stability for better growth but maybe does not provide as much for the virus in terms of resistance to D25 neutralization. Further studies to examine this in more detail are needed in the future.

We also wanted to assess several mutants for D25 binding in the context of a flow cytometry and ELISA binding assay and compare the results to molecular modeling predictions. Several variants were chosen for these assays from sites N208 and K201. Both sites had variants predicted to escape D25 binding and predicted not to escape D25 binding to be used as a control. The flow cytometry binding assay showed a decrease D25 binding and consistent motavizumab binding for the mutant N208E. This mutant was predicted to escape D25 binding by molecular modeling. N208E was also shown to have decreased D25 binding in the ELISA format, along with other mutants such as N208C, N208D, and K201A. The flow cytometry and ELISA binding assays give slightly different results but could be used to confirm escape variants identified in the DMS pipeline from the second chapter. In the future after receiving deep sequencing results, we would like to run those possible escape mutations through these individual binding assays to confirm that they escape D25 binding. It would also be interesting to recombine some of our variants of interest into the DS-Cav1 construct to be able to better assess D25 binding in this context. Using techniques such as biolayer interferometry (BLI) or surface plasmon resonance

(SPR) could be other techniques that would be useful in better understanding the binding kinetics of the proposed escape mutations found in the DMS screen.

Overall, this project has laid the groundwork necessary for assessing large variant libraries that yield valuable information regarding antibody escape and F mutant expression. This pipeline can be used in future projects with different antibodies of interest for F where hundreds of variants can be assessed in a relatively high-throughput manner. We have also tested many variations of flow cytometry and ELISA binding assays that can be further optimized and used for assessing more D25 variants or variants from different antibody libraries. There are more data to gather in the future related to this project in terms of possible escape mutations as well as answering questions about the use of molecular modeling to predict escape mutations in F.

Literature Cited

1. Rose EB, Wheatley A, Langley G, Gerber S, Haynes A. Respiratory Syncytial Virus Seasonality - United States, 2014-2017. MMWR Morb Mortal Wkly Rep. 2018;67(2):71-6. Epub 2018/01/19. doi: 10.15585/mmwr.mm6702a4. PubMed PMID: 29346336; PMCID: PMC5772804.

2. Melero JA, Moore ML. Influence of Respiratory Syncytial Virus Strain Differences on Pathogenesis and Immunity. Springer Berlin Heidelberg; 2013. p. 59-82.

3. Laham FR, Mansbach JM, Piedra PA, Hasegawa K, Sullivan AF, Espinola JA, Camargo CA. Clinical Profiles of Respiratory Syncytial Virus Subtypes A AND B Among Children Hospitalized with Bronchiolitis. Pediatric Infectious Disease Journal. 2017;36(8):808-10. doi: 10.1097/inf.0000000000001596.

4. Walsh EE, McConnochie KM, Long CE, Hall CB. Severity of Respiratory Syncytial Virus Infection Is Related to Virus Strain. The Journal of Infectious Diseases. 1997;175(4):814-20. Epub 1997/04/01. doi: 10.1086/513976. PubMed PMID: 9086135.

5. Asenjo A, Villanueva N. Phosphorylation of the human respiratory syncytial virus P protein mediates M2-2 regulation of viral RNA synthesis, a process that involves two P proteins. Virus Res. 2016;211:117-25. Epub 2015/10/18. doi: 10.1016/j.virusres.2015.10.011. PubMed PMID: 26474524.

6. Cao D, Gao Y, Roesler C, Rice S, D'Cunha P, Zhuang L, Slack J, Domke M, Antonova A, Romanelli S, Keating S, Forero G, Juneja P, Liang B. Cryo-EM structure of the respiratory syncytial virus RNA polymerase. Nature Communications. 2020;11(1). doi: 10.1038/s41467-019-14246-3.

7. Förster A, Maertens GN, Farrell PJ, Bajorek M. Dimerization of Matrix Protein Is Required for Budding of Respiratory Syncytial Virus. Journal of Virology. 2015;89(8):4624-35. doi: 10.1128/jvi.03500-14.

8. Meshram CD, Baviskar PS, Ognibene CM, Oomens AGP. The Respiratory Syncytial Virus Phosphoprotein, Matrix Protein, and Fusion Protein Carboxy-Terminal Domain Drive Efficient Filamentous Virus-Like Particle Formation. Journal of Virology. 2016;90(23):10612-28. doi: 10.1128/jvi.01193-16.

9. Ghildyal R, Baulch-Brown C, Mills J, Meanger J. The matrix protein of Human respiratory syncytial virus localises to the nucleus of infected cells and inhibits

transcription. Arch Virol. 2003;148(7):1419-29. Epub 2003/06/27. doi: 10.1007/s00705-003-0112-y. PubMed PMID: 12827470.

10. Gan S-W, Tan E, Lin X, Yu D, Wang J, Tan GM-Y, Vararattanavech A, Yeo CY, Soon CH, Soong TW, Pervushin K, Torres J. The Small Hydrophobic Protein of the Human Respiratory Syncytial Virus Forms Pentameric Ion Channels*. Journal of Biological Chemistry. 2012;287(29):24671-89. doi: 10.1074/jbc.m111.332791.

11. Fuentes S, Tran KC, Luthra P, Teng MN, He B. Function of the Respiratory Syncytial Virus Small Hydrophobic Protein. Journal of Virology. 2007;81(15):8361-6. doi: 10.1128/jvi.02717-06.

12. McLellan JS, Ray WC, Peeples ME. Structure and Function of RSV Surface Glycoproteins. Curr Top Microbiol Immunol. 2013;372:83-104. Epub 2013/12/24. doi: 10.1007/978-3-642-38919-1_4. PubMed PMID: 24362685; PMCID: PMC4211642.

13. Battles MB, McLellan JS. Respiratory syncytial virus entry and how to block it. Nat Rev Microbiol. 2019;17(4):233-45. doi: 10.1038/s41579-019-0149-x. PubMed PMID: 30723301; PMCID: PMC7096974.

14. Bukreyev A, Yang L, Fricke J, Cheng L, Ward JM, Murphy BR, Collins PL. The Secreted Form of Respiratory Syncytial Virus G Glycoprotein Helps the Virus Evade Antibody-Mediated Restriction of Replication by Acting as an Antigen Decoy and through Effects on Fc Receptor-Bearing Leukocytes. J Virol. 2008;82(24):12191-204. Epub 2008/10/10. doi: 10.1128/jvi.01604-08. PubMed PMID: 18842713; PMCID: PMC2593351.

15. Walsh EE, Hruska J. Monoclonal antibodies to respiratory syncytial virus proteins: identification of the fusion protein. J Virol. 1983;47(1):171-7. Epub 1983/07/01. doi: 10.1128/JVI.47.1.171-177.1983. PubMed PMID: 6345804; PMCID: PMC255221.

16. Zhang L, Peeples ME, Boucher RC, Collins PL, Pickles RJ. Respiratory Syncytial Virus Infection of Human Airway Epithelial Cells Is Polarized, Specific to Ciliated Cells, and without Obvious Cytopathology. Journal of Virology. 2002;76(11):5654-66. doi: 10.1128/jvi.76.11.5654-5666.2002.

17. Escribano-Romero E, Rawling J, Garcia-Barreno B, Melero JA. The soluble form of human respiratory syncytial virus attachment protein differs from the membrane-bound form in its oligomeric state but is still capable of binding to cell surface proteoglycans J Virol. 2004;78(7):3524-32. Epub 2004/03/16. doi: 10.1128/jvi.78.7.3524-3532.2004. PubMed PMID: 15016875; PMCID: PMC371076.

18. Krusat T, Streckert HJ. Heparin-dependent attachment of respiratory syncytial virus (RSV) to host cells. Arch Virol. 1997;142(6):1247-54. Epub 1997/01/01. doi: 10.1007/s007050050156. PubMed PMID: 9229012.

19. Zhang L, Bukreyev A, Thompson CI, Watson B, Peeples ME, Collins PL, Pickles RJ. Infection of ciliated cells by human parainfluenza virus type 3 in an in vitro model of human airway epithelium. J Virol. 2005;79(2):1113-24. Epub 2004/12/23. doi: 10.1128/JVI.79.2.1113-1124.2005. PubMed PMID: 15613339; PMCID: PMC538579.

20. Chirkova T, Lin S, Oomens AGP, Gaston KA, Boyoglu-Barnum S, Meng J, Stobart CC, Cotton CU, Hartert TV, Moore ML, Ziady AG, Anderson LJ. CX3CR1 is an important surface molecule for respiratory syncytial virus infection in human airway epithelial cells. J Gen Virol. 2015;96(9):2543-56. Epub 2015/08/25. doi: 10.1099/vir.0.000218. PubMed PMID: 26297201; PMCID: PMC4635495.

21. Johnson SM, McNally BA, Ioannidis I, Flano E, Teng MN, Oomens AG, Walsh EE, Peeples ME. Respiratory Syncytial Virus Uses CX3CR1 as a Receptor on Primary Human Airway Epithelial Cultures. PLOS Pathogens. 2015;11(12):e1005318. Epub 2015/12/15. doi: 10.1371/journal.ppat.1005318. PubMed PMID: 26658574; PMCID: PMC4676609.

22. Jeong KI, Piepenhagen PA, Kishko M, DiNapoli JM, Groppo RP, Zhang L, Almond J, Kleanthous H, Delagrave S, Parrington M. CX3CR1 Is Expressed in Differentiated Human Ciliated Airway Cells and Co-Localizes with Respiratory Syncytial Virus on Cilia in a G Protein-Dependent Manner. PLoS One. 2015;10(6):e0130517. Epub 2015/06/25. doi: 10.1371/journal.pone.0130517. PubMed PMID: 26107373; PMCID: PMC4479564.

23. Karron RA, Buonagurio DA, Georgiu AF, Whitehead SS, Adamus JE, Clements-Mann ML, Harris DO, Randolph VB, Udem SA, Murphy BR, Sidhu MS. Respiratory syncytial virus (RSV) SH and G proteins are not essential for viral replication in vitro: clinical evaluation and molecular characterization of a cold-passaged, attenuated RSV subgroup B mutant. Proc Natl Acad Sci U S A. 1997;94(25):13961-6. Epub 1998/02/12. doi: 10.1073/pnas.94.25.13961. PubMed PMID: 9391135; PMCID: PMC28415.

24. Behera AK, Matsuse H, Kumar M, Kong X, Lockey RF, Mohapatra SS. Blocking intercellular adhesion molecule-1 on human epithelial cells decreases respiratory syncytial virus infection. Biochem Biophys Res Commun. 2001;280(1):188-95. Epub 2001/02/13. doi: 10.1006/bbrc.2000.4093. PubMed PMID: 11162498.

25. Currier MG, Lee S, Stobart CC, Hotard AL, Villenave R, Meng J, Pretto CD, Shields MD, Nguyen MT, Todd SO, Chi MH, Hammonds J, Krumm SA, Spearman P, Plemper RK, Sakamoto K, Peebles RS, Jr., Power UF, Moore ML. EGFR Interacts with the Fusion Protein of Respiratory Syncytial Virus Strain 2-20 and Mediates Infection and Mucin Expression. PLoS Pathog. 2016;12(5):e1005622. Epub 2016/05/07. doi: 10.1371/journal.ppat.1005622. PubMed PMID: 27152417; PMCID: PMC4859522.

26. Tayyari F, Marchant D, Moraes TJ, Duan W, Mastrangelo P, Hegele RG. Identification of nucleolin as a cellular receptor for human respiratory syncytial virus. Nature Medicine. 2011;17(9):1132-5. doi: 10.1038/nm.2444.

27. Bose S, Basu M, Banerjee AK. Role of nucleolin in human parainfluenza virus type 3 infection of human lung epithelial cells. J Virol. 2004;78(15):8146-58. Epub 2004/07/16. doi: 10.1128/JVI.78.15.8146-8158.2004. PubMed PMID: 15254186; PMCID: PMC446124.

28. Su PY, Wang YF, Huang SW, Lo YC, Wang YH, Wu SR, Shieh DB, Chen SH, Wang JR, Lai MD, Chang CF. Cell surface nucleolin facilitates enterovirus 71 binding and infection. J Virol. 2015;89(8):4527-38. Epub 2015/02/13. doi: 10.1128/JVI.03498-14. PubMed PMID: 25673703; PMCID: PMC4442404.

29. Callebaut C, Blanco J, Benkirane N, Krust B, Jacotot E, Guichard G, Seddiki N, Svab J, Dam E, Muller S, Briand JP, Hovanessian AG. Identification of V3 loop-binding proteins as potential receptors implicated in the binding of HIV particles to CD4(+) cells. J Biol Chem. 1998;273(34):21988-97. Epub 1998/08/15. doi: 10.1074/jbc.273.34.21988. PubMed PMID: 9705340.

30. Anderson CS, Chirkova T, Slaunwhite CG, Qiu X, Walsh EE, Anderson LJ, Mariani TJ. CX3CR1 Engagement by Respiratory Syncytial Virus Leads to Induction of Nucleolin and Dysregulation of Cilia-related Genes. 2020.

31. Krzyzaniak MA, Zumstein MT, Gerez JA, Picotti P, Helenius A. Host cell entry of respiratory syncytial virus involves macropinocytosis followed by proteolytic activation of the F protein. PLoS Pathog. 2013;9(4):e1003309. Epub 2013/04/18. doi: 10.1371/journal.ppat.1003309. PubMed PMID: 23593008; PMCID: PMC3623752.

32. San-Juan-Vergara H, Sampayo-Escobar V, Reyes N, Cha B, Pacheco-Lugo L, Wong T, Peeples ME, Collins PL, Castano ME, Mohapatra SS. Cholesterol-rich microdomains as docking platforms for respiratory syncytial virus in normal human bronchial epithelial cells. J Virol. 2012;86(3):1832-43. Epub 2011/11/18. doi: 10.1128/JVI.06274-11. PubMed PMID: 22090136; PMCID: PMC3264380.

33. Connolly SA, Leser GP, Jardetzky TS, Lamb RA. Bimolecular complementation of paramyxovirus fusion and hemagglutinin-neuraminidase proteins enhances fusion: implications for the mechanism of fusion triggering. J Virol. 2009;83(21):10857-68. Epub 2009/08/28. doi: 10.1128/JVI.01191-09. PubMed PMID: 19710150; PMCID: PMC2772755.

34. Jardetzky TS, Lamb RA. Activation of paramyxovirus membrane fusion and virus entry. Curr Opin Virol. 2014;5:24-33. Epub 2014/02/18. doi: 10.1016/j.coviro.2014.01.005. PubMed PMID: 24530984; PMCID: PMC4028362.

35. Liljeroos L, Krzyzaniak MA, Helenius A, Butcher SJ. Architecture of respiratory syncytial virus revealed by electron cryotomography. Proc Natl Acad Sci U S A. 2013;110(27):11133-8. Epub 2013/06/19. doi: 10.1073/pnas.1309070110. PubMed PMID: 23776214; PMCID: PMC3703984.

36. McLellan JS, Yang Y, Graham BS, Kwong PD. Structure of respiratory syncytial virus fusion glycoprotein in the postfusion conformation reveals preservation of neutralizing epitopes. J Virol. 2011;85(15):7788-96. Epub 2011/05/27. doi: 10.1128/JVI.00555-11. PubMed PMID: 21613394; PMCID: PMC3147929.

37. Collins PL, Dickens LE, Buckler-White A, Olmsted RA, Spriggs MK, Camargo E, Coelingh KV. Nucleotide sequences for the gene junctions of human respiratory syncytial virus reveal distinctive features of intergenic structure and gene order. Proc Natl Acad Sci U S A. 1986;83(13):4594-8. Epub 1986/07/01. doi: 10.1073/pnas.83.13.4594. PubMed PMID: 3460060; PMCID: PMC323787.

38. Shi T, McAllister DA, O'Brien KL, Simoes EAF, Madhi SA, Gessner BD, Polack FP, Balsells E, Acacio S, Aguayo C, Alassani I, Ali A, Antonio M, Awasthi S, Awori JO, Azziz-Baumgartner E, Baggett HC, Baillie VL, Balmaseda A, Barahona A, Basnet S, Bassat Q, Basualdo W, Bigogo G, Bont L, Breiman RF, Brooks WA, Broor S, Bruce N, Bruden D, Buchy P, Campbell S, Carosone-Link P, Chadha M, Chipeta J, Chou M, Clara W, Cohen C, De Cuellar E, Dang D-A, Dash-Yandag B, Deloria-Knoll M, Dherani M, Eap T, Ebruke BE, Echavarria M, De Freitas Lázaro Emediato CC, Fasce RA, Feikin DR, Feng L, Gentile A, Gordon A, Goswami D, Goyet S, Groome M, Halasa N, Hirve S, Homaira N, Howie SRC, Jara J, Jroundi I, Kartasasmita CB, Khuri-Bulos N, Kotloff KL, Krishnan A, Libster R, Lopez O, Lucero MG, Lucion F, Lupisan SP, Marcone DN, McCracken JP, Mejia M, Moisi JC, Montgomery JM, Moore DP, Moraleda C, Moyes J, Munywoki P, Mutyara K, Nicol MP, Nokes DJ, Nymadawa P, Da Costa Oliveira MT, Oshitani H, Pandey N, Paranhos-Baccalà G, Phillips LN, Picot VS, Rahman M, Rakoto-Andrianarivelo M, Rasmussen ZA, Rath BA, Robinson A, Romero C, Russomando G, Salimi V, Sawatwong P, Scheltema N, Schweiger B, Scott JAG, Seidenberg P, Shen K, Singleton R, Sotomayor V, Strand TA, Sutanto A, Sylla M, Tapia MD, Thamthitiwat S, Thomas ED, Tokarz R, Turner C, Venter M, Waicharoen S, Wang J, Watthanaworawit W, Yoshida L-M, Yu H, Zar HJ, Campbell H, Nair H. Global,

regional, and national disease burden estimates of acute lower respiratory infections due to respiratory syncytial virus in young children in 2015: a systematic review and modelling study. The Lancet. 2017;390(10098):946-58. doi: 10.1016/s0140-6736(17)30938-8.

39. Hall CB, Weinberg GA, Iwane MK, Blumkin AK, Edwards KM, Staat MA, Auinger P, Griffin MR, Poehling KA, Erdman D, Grijalva CG, Zhu Y, Szilagyi P. The burden of respiratory syncytial virus infection in young children. N Engl J Med. 2009;360(6):588-98. doi: 10.1056/NEJMoa0804877. PubMed PMID: 19196675; PMCID: PMC4829966.

40. Falsey AR, Hennessey PA, Formica MA, Cox C, Walsh EE. Respiratory syncytial virus infection in elderly and high-risk adults. N Engl J Med. 2005;352(17):1749-59. Epub 2005/04/29. doi: 10.1056/NEJMoa043951. PubMed PMID: 15858184.

41. Bont L, Aalderen WM, Kimpen JL. Long-term consequences of respiratory syncytial virus (RSV) bronchiolitis. Paediatr Respir Rev. 2000;1(3):221-7. Epub 2003/01/18. doi: 10.1053/prrv.2000.0052. PubMed PMID: 12531083.

42. Sommer C. Risk Factors for Severe Respiratory Syncytial Virus Lower Respiratory Tract Infection. The Open Microbiology Journal. 2011;5(1):144-54. doi: 10.2174/1874285801105010144.

43. Blount RE, Jr., Morris JA, Savage RE. Recovery of cytopathogenic agent from chimpanzees with coryza. Proc Soc Exp Biol Med. 1956;92(3):544-9. doi: 10.3181/00379727-92-22538. PubMed PMID: 13359460.

44. Chanock R, Roizman B, Myers R. Recovery from infants with respiratory illness of a virus related to chimpanzee coryza agent (CCA). I. Isolation, properties and characterization. Am J Hyg. 1957;66(3):281-90. doi: 10.1093/oxfordjournals.aje.a119901. PubMed PMID: 13478578.

45. Hall CB, Walsh EE, Long CE, Schnabel KC. Immunity to and Frequency of Reinfection with Respiratory Syncytial Virus. Journal of Infectious Diseases. 1991;163(4):693-8. doi: 10.1093/infdis/163.4.693.

46. Mazur NI, Higgins D, Nunes MC, Melero JA, Langedijk AC, Horsley N, Buchholz UJ, Openshaw PJ, McLellan JS, Englund JA, Mejias A, Karron RA, Simoes EA, Knezevic I, Ramilo O, Piedra PA, Chu HY, Falsey AR, Nair H, Kragten-Tabatabaie L, Greenough A, Baraldi E, Papadopoulos NG, Vekemans J, Polack FP, Powell M, Satav A, Walsh EE, Stein RT, Graham BS, Bont LJ, Respiratory Syncytial Virus Network F. The respiratory syncytial virus vaccine landscape: lessons from the

graveyard and promising candidates. Lancet Infect Dis. 2018;18(10):e295-e311. Epub 2018/06/20. doi: 10.1016/S1473-3099(18)30292-5. PubMed PMID: 29914800.

47. Anderson LJ, Dormitzer PR, Nokes DJ, Rappuoli R, Roca A, Graham BS. Strategic priorities for respiratory syncytial virus (RSV) vaccine development. Vaccine. 2013;31 Suppl 2:B209-15. Epub 2013/04/26. doi: 10.1016/j.vaccine.2012.11.106. PubMed PMID: 23598484; PMCID: PMC3919153.

48. Kapikian AZ, Mitchell RH, Chanock RM, Shvedoff RA, Stewart CE. An epidemiologic study of altered clinical reactivity to respiratory syncytial (RS) virus infection in children previously vaccinated with an inactivated RS virus vaccine. Am J Epidemiol. 1969;89(4):405-21. Epub 1969/04/01. doi: 10.1093/oxfordjournals.aje.a120954. PubMed PMID: 4305197.

49. Kim HW, Canchola JG, Brandt CD, Pyles G, Chanock RM, Jensen K, Parrott RH. Respiratory syncytial virus disease in infants despite prior administration of antigenic inactivated vaccine. Am J Epidemiol. 1969;89(4):422-34. Epub 1969/04/01. doi: 10.1093/oxfordjournals.aje.a120955. PubMed PMID: 4305198.

50. Murphy BR, Walsh EE. Formalin-inactivated respiratory syncytial virus vaccine induces antibodies to the fusion glycoprotein that are deficient in fusion-inhibiting activity. J Clin Microbiol. 1988;26(8):1595-7. Epub 1988/08/01. doi: 10.1128/jcm.26.8.1595-1597.1988. PubMed PMID: 2459154; PMCID: PMC266671.

51. Huang K, Incognito L, Cheng X, Ulbrandt ND, Wu H. Respiratory syncytial virus-neutralizing monoclonal antibodies motavizumab and palivizumab inhibit fusion. J Virol. 2010;84(16):8132-40. doi: 10.1128/JVI.02699-09. PubMed PMID: 20519399; PMCID: PMC2916538.

52. Feltes TF, Cabalka AK, Meissner HC, Piazza FM, Carlin DA, Top FH, Connor EM, Sondheimer HM, for the Cardiac Synagis Study G. Palivizumab prophylaxis reduces hospitalization due to respiratory syncytial virus in young children with hemodynamically significant congenital heart disease. The Journal of Pediatrics. 2003;143(4):532-40. doi: 10.1067/s0022-3476(03)00454-2.

53. Palivizumab, a Humanized Respiratory Syncytial Virus Monoclonal Antibody, Reduces Hospitalization From Respiratory Syncytial Virus Infection in High-risk Infants. Pediatrics. 1998;102(3):531-7. doi: doi.org/10.1542/peds.102.3.531.

54. McLellan JS, Chen M, Joyce MG, Sastry M, Stewart-Jones GB, Yang Y, Zhang B, Chen L, Srivatsan S, Zheng A, Zhou T, Graepel KW, Kumar A, Moin S, Boyington JC, Chuang GY, Soto C, Baxa U, Bakker AQ, Spits H, Beaumont T, Zheng Z, Xia N, Ko SY, Todd JP, Rao S, Graham BS, Kwong PD. Structure-based design of a fusion glycoprotein vaccine for respiratory syncytial virus. Science.

2013;342(6158):592-8. doi: 10.1126/science.1243283. PubMed PMID: 24179220; PMCID: PMC4461862.

55. Crank MC, Ruckwardt TJ, Chen M, Morabito KM, Phung E, Costner PJ, Holman LA, Hickman SP, Berkowitz NM, Gordon IJ, Yamshchikov GV, Gaudinski MR, Kumar A, Chang LA, Moin SM, Hill JP, DiPiazza AT, Schwartz RM, Kueltzo L, Cooper JW, Chen P, Stein JA, Carlton K, Gall JG, Nason MC, Kwong PD, Chen GL, Mascola JR, McLellan JS, Ledgerwood JE, Graham BS, Team VRCS. A proof of concept for structure-based vaccine design targeting RSV in humans. Science. 2019;365(6452):505-9. doi: 10.1126/science.aav9033. PubMed PMID: 31371616.

56. Ruckwardt TJ, Morabito KM, Phung E, Crank MC, Costner PJ, Holman LA, Chang LA, Hickman SP, Berkowitz NM, Gordon IJ, Yamshchikov GV, Gaudinski MR, Lin B, Bailer R, Chen M, Ortega-Villa AM, Nguyen T, Kumar A, Schwartz RM, Kueltzo LA, Stein JA, Carlton K, Gall JG, Nason MC, Mascola JR, Chen G, Graham BS, Arthur A, Cunningham J, Eshun A, Larkin B, Mendoza F, Novik L, Saunders J, Wang X, Whalen W, Carter C, Hendel CS, Plummer S, Ola A, Widge A, Burgos Florez MC, Le L, Pittman I, Rothwell RSS, Trofymenko O, Vasilenko O, Apte P, Hicks R, Cartagena CT, Williams P, Requilman L, Tran C, Bai S, Carey E, Chamberlain AL, Chang Y-c, Chen M, Chen P, Cooper J, Fridley C, Ghosh M, Gollapudi D, Holland-Linn J, Horwitz J, Hussain A, Ivleva V, Kaltovich F, Leach K, Lee C, Liu A, Liu X, Manceva S, Menon A, Nagy A, O'Connell S, Ragunathan R, Walters J, Zhao Z. Safety, tolerability, and immunogenicity of the respiratory syncytial virus prefusion F subunit vaccine DS-Cav1: a phase 1, randomised, open-label, dose-escalation clinical trial. The Lancet Respiratory Medicine. 2021. doi: 10.1016/s2213-2600(21)00098-9.

57. Yamin D, Jones FK, DeVincenzo JP, Gertler S, Kobiler O, Townsend JP, Galvani AP. Vaccination strategies against respiratory syncytial virus. Proc Natl Acad Sci U S A. 2016;113(46):13239-44. Epub 2016/11/02. doi: 10.1073/pnas.1522597113. PubMed PMID: 27799521; PMCID: PMC5135296.

58. Diseases CoI. Use of Ribavirin in the Treatment of Respiratory Syncytial Virus Infection. Journal of the Academy of Pediatrics. 1993;92(3):501-4.

59. Kim JA, Seong RK, Kumar M, Shin OS. Favipiravir and Ribavirin Inhibit Replication of Asian and African Strains of Zika Virus in Different Cell Models. Viruses. 2018;10(2):72. Epub 2018/02/10. doi: 10.3390/v10020072. PubMed PMID: 29425176; PMCID: PMC5850379.

60. Antonini TM, Coilly A, Rossignol E, Fougerou-Leurent C, Dumortier J, Leroy V, Veislinger A, Radenne S, Botta-Fridlund D, Durand F, Houssel-Debry P, Kamar N, Canva V, Perre P, De Ledinghen V, Rohel A, Diallo A, Taburet AM, Samuel D, Pageaux GP, Duclos-Vallee JC, group ACCs. Sofosbuvir-Based Regimens in HIV/HCV Coinfected Patients After Liver Transplantation: Results From the ANRS

CO23 CUPILT Study. Transplantation. 2018;102(1):119-26. Epub 2017/08/29. doi: 10.1097/TP.0000000000001928. PubMed PMID: 28846559.

61. Hall CB, McBride JT, Walsh EE, Bell DM, Gala CL, Hildreth S, Ten Eyck LG, Hall WJ. Aerosolized ribavirin treatment of infants with respiratory syncytial viral infection. A randomized double-blind study. N Engl J Med. 1983;308(24):1443-7. Epub 1983/06/16. doi: 10.1056/NEJM198306163082403. PubMed PMID: 6343860.

62. Kenilworth NS-P. Rebetol (ribavirin). 2004.

63. Hoover J, Eades S, Lam WM. Pediatric Antiviral Stewardship: Defining the Potential Role of Ribavirin in Respiratory Syncytial Virus–Associated Lower Respiratory Illness. The Journal of Pediatric Pharmacology and Therapeutics. 2018;23(5):372-8. Epub 2018/11/16. doi: 10.5863/1551-6776-23.5.372. PubMed PMID: 30429691; PMCID: PMC6213624.

64. American Academy of Pediatrics Subcommittee on D, Management of B. Diagnosis and Management of Bronchiolitis. Pediatrics. 2006;118(4):1774-93. Epub 2006/10/04. doi: 10.1542/peds.2006-2223. PubMed PMID: 17015575.

65. Beaird OE, Freifeld A, Ison MG, Lawrence SJ, Theodoropoulos N, Clark NM, Razonable RR, Alangaden G, Miller R, Smith J, Young JAH, Hawkinson D, Pursell K, Kaul DR. Current practices for treatment of respiratory syncytial virus and other non-influenza respiratory viruses in high-risk patient populations: a survey of institutions in the Midwestern Respiratory Virus Collaborative. Transplant Infectious Disease. 2016;18(2):210-5. doi: 10.1111/tid.12510.

66. Behzadi MA, Leyva-Grado VH. Overview of Current Therapeutics and Novel Candidates Against Influenza, Respiratory Syncytial Virus, and Middle East Respiratory Syndrome Coronavirus Infections. Frontiers in Microbiology. 2019;10. doi: 10.3389/fmicb.2019.01327.

67. Kwakkenbos MJ, Diehl SA, Yasuda E, Bakker AQ, van Geelen CM, Lukens MV, van Bleek GM, Widjojoatmodjo MN, Bogers WM, Mei H, Radbruch A, Scheeren FA, Spits H, Beaumont T. Generation of stable monoclonal antibody-producing B cell receptor-positive human memory B cells by genetic programming. Nat Med. 2010;16(1):123-8. Epub 2009/12/22. doi: 10.1038/nm.2071. PubMed PMID: 20023635; PMCID: PMC2861345.

68. Tian D, Battles MB, Moin SM, Chen M, Modjarrad K, Kumar A, Kanekiyo M, Graepel KW, Taher NM, Hotard AL, Moore ML, Zhao M, Zheng ZZ, Xia NS, McLellan JS, Graham BS. Structural basis of respiratory syncytial virus subtype-dependent neutralization by an antibody targeting the fusion glycoprotein. Nat Commun.

2017;8(1):1877. Epub 2017/12/01. doi: 10.1038/s41467-017-01858-w. PubMed PMID: 29187732; PMCID: PMC5707411.

69. McLellan JS, Chen M, Leung S, Graepel KW, Du X, Yang Y, Zhou T, Baxa U, Yasuda E, Beaumont T, Kumar A, Modjarrad K, Zheng Z, Zhao M, Xia N, Kwong PD, Graham BS. Structure of RSV fusion glycoprotein trimer bound to a prefusion-specific neutralizing antibody. Science. 2013;340(6136):1113-7. Epub 2013/04/27. doi: 10.1126/science.1234914. PubMed PMID: 23618766; PMCID: PMC4459498.

70. Connor AL, Bevitt DJ, Toms GL. Comparison of human respiratory syncytial virus A2 and 8/60 fusion glycoprotein gene sequences and mapping of sub-group specific antibody epitopes. Journal of Medical Virology. 2001;63(2):168-77. doi: 10.1002/1096-9071(20000201)63:2<168::AID-JMV1012>3.0.CO;2-U.

71. Zhu Q, McLellan JS, Kallewaard NL, Ulbrandt ND, Palaszynski S, Zhang J, Moldt B, Khan A, Svabek C, McAuliffe JM, Wrapp D, Patel NK, Cook KE, Richter BWM, Ryan PC, Yuan AQ, Suzich JA. A highly potent extended half-life antibody as a potential RSV vaccine surrogate for all infants. Sci Transl Med. 2017;9(388). Epub 2017/05/05. doi: 10.1126/scitranslmed.aaj1928. PubMed PMID: 28469033.

72. Domachowske JB, Khan AA, Esser MT, Jensen K, Takas T, Villafana T, Dubovsky F, Griffin MP. Safety, Tolerability and Pharmacokinetics of MEDI8897, an Extended Half-life Single-dose Respiratory Syncytial Virus Prefusion F-targeting Monoclonal Antibody Administered as a Single Dose to Healthy Preterm Infants. Pediatr Infect Dis J. 2018;37(9):886-92. Epub 2018/01/27. doi: 10.1097/INF.0000000000001916. PubMed PMID: 29373476; PMCID: PMC6133204.

73. Griffin MP, Khan AA, Esser MT, Jensen K, Takas T, Kankam MK, Villafana T, Dubovsky F. Safety, Tolerability, and Pharmacokinetics of MEDI8897, the Respiratory Syncytial Virus Prefusion F-Targeting Monoclonal Antibody with an Extended Half-Life, in Healthy Adults. Antimicrob Agents Chemother. 2017;61(3). Epub 2016/12/14. doi: 10.1128/AAC.01714-16. PubMed PMID: 27956428; PMCID: PMC5328523.

74. Dall'Acqua WF, Kiener PA, Wu H. Properties of human IgG1s engineered for enhanced binding to the neonatal Fc receptor (FcRn). J Biol Chem. 2006;281(33):23514-24. Epub 2006/06/24. doi: 10.1074/jbc.M604292200. PubMed PMID: 16793771.

75. Rossey I, McLellan JS, Saelens X, Schepens B. Clinical Potential of Prefusion RSV F-specific Antibodies. Trends Microbiol. 2018;26(3):209-19. Epub 2017/10/22. doi: 10.1016/j.tim.2017.09.009. PubMed PMID: 29054341.

76. Mireia Pelegrin MN-G, and Marc Piechaczyk. Antiviral Monoclonal Antibodies: Can They Be More Than Simple Neutralizing Agents? Trends in Microbiology. 2015;23(10):653-65.

77. Berry JD, Gaudet RG. Antibodies in infectious diseases: polyclonals, monoclonals and niche biotechnology. N Biotechnol. 2011;28(5):489-501. doi: 10.1016/j.nbt.2011.03.018. PubMed PMID: 21473942.

78. Both L, Banyard AC, van Dolleweerd C, Wright E, Ma JK, Fooks AR. Monoclonal antibodies for prophylactic and therapeutic use against viral infections. Vaccine. 2013;31(12):1553-9. doi: 10.1016/j.vaccine.2013.01.025. PubMed PMID: 23370150; PMCID: PMC7115371.

79. Rijal P, Elias SC, Machado SR, Xiao J, Schimanski L, O'Dowd V, Baker T, Barry E, Mendelsohn SC, Cherry CJ, Jin J, Labbe GM, Donnellan FR, Rampling T, Dowall S, Rayner E, Findlay-Wilson S, Carroll M, Guo J, Xu XN, Huang KA, Takada A, Burgess G, McMillan D, Popplewell A, Lightwood DJ, Draper SJ, Townsend AR. Therapeutic Monoclonal Antibodies for Ebola Virus Infection Derived from Vaccinated Humans. Cell Rep. 2019;27(1):172-86 e7. doi: 10.1016/j.celrep.2019.03.020. PubMed PMID: 30943399.

80. Flego M, Ascione A, Cianfriglia M, Vella S. Clinical development of monoclonal antibody-based drugs in HIV and HCV diseases. BMC Med. 2013;11:4. doi: 10.1186/1741-7015-11-4. PubMed PMID: 23289632; PMCID: PMC3565905.

81. Tan Y, Ng Q, Jia Q, Kwang J, He F. A novel humanized antibody neutralizes H5N1 influenza virus via two different mechanisms. J Virol. 2015;89(7):3712-22. doi: 10.1128/JVI.03014-14. PubMed PMID: 25609802; PMCID: PMC4403434.

82. Quing Zhu JSM, Nicole L. Kallewaard, Nancy D. Ulbrandt, Susan Palaszynski, Jing Zhang, Brian M Moldt, Anis Khan, Catherine Svabek, Josephine M. McAuliffe, Daniel Wrapp, Nita K. Patel, Kimberly E. Cook, Bettina W. M. Richter, Patricia C. Ryan, Andy Q. Yuan and JoAnn A. Suzich. A highly potent extended half-life antibody as a potential RSV vaccine surrogate for all infants. Science Translational Medicine. 2017;9(388).

83. Johnson S, Oliver C, Prince GA, Hemming VG, Pfarr DS, Wang SC, Dormitzer M, O'Grady J, Koenig S, Tamura JK, Woods R, Bansal G, Couchenour D, Tsao E, Hall WC, Young JF. Development of a humanized monoclonal antibody (MEDI-493) with potent in vitro and in vivo activity against respiratory syncytial virus. J Infect Dis. 1997;176(5):1215-24. doi: 10.1086/514115. PubMed PMID: 9359721.

84. Salazar G, Zhang N, Fu TM, An Z. Antibody therapies for the prevention and treatment of viral infections. NPJ Vaccines. 2017;2(1):19. Epub 2017/12/22. doi: 10.1038/s41541-017-0019-3. PubMed PMID: 29263875; PMCID: PMC5627241.

85. Prince GA, Horswood RL, Chanock RM. Quantitative aspects of passive immunity to respiratory syncytial virus infection in infant cotton rats. J Virol. 1985;55(3):517-20. doi: 10.1128/JVI.55.3.517-520.1985. PubMed PMID: 4020957; PMCID: PMC254995.

86. Hammarstrom L, Smith CI. New and old aspects of immunoglobulin application. The use of intravenous IgG as prophylaxis and for treatment of infections. Infection. 1990;18(5):314-24. doi: 10.1007/BF01647018. PubMed PMID: 2125980.

87. Hemming VG, Prince GA, Horswood RL, London WJ, Murphy BR, Walsh EE, Fischer GW, Weisman LE, Baron PA, Chanock RM. Studies of passive immunotherapy for infections of respiratory syncytial virus in the respiratory tract of a primate model. J Infect Dis. 1985;152(5):1083-7. doi: 10.1093/infdis/152.5.1083. PubMed PMID: 4045247.

88. Larry J. Anderson PBaJCH. Neutralization of Respiratory Syncytial Virus by Individual Mixtures of F and G Protein Monoclonal Antibodies. Journal of Virology. 1988;62(11):4232-8.

89. Palivizumab, a humanized respiratory syncytial virus monoclonal antibody, reduces hospitalization from respiratory syncytial virus infection in high-risk infants. Pediatrics. 1998;102(3).

90. Young J. Development of a potent respiratory syncytial virus-specific monoclonal antibody for the prevention of serious lower respiratory tract disease in infants. Respiratory Medicine. 2002;96(Supplement 2):S31-S5.

91. Morris SK, Dzolganovski B, Beyene J, Sung L. A meta-analysis of the effect of antibody therapy for the prevention of severe respiratory syncytial virus infection. BMC Infect Dis. 2009;9:106. doi: 10.1186/1471-2334-9-106. PubMed PMID: 19575815; PMCID: PMC2720977.

92. Boyoglu-Barnum S, Chirkova T, Todd SO, Barnum TR, Gaston KA, Jorquera P, Haynes LM, Tripp RA, Moore ML, Anderson LJ. Prophylaxis with a respiratory syncytial virus (RSV) anti-G protein monoclonal antibody shifts the adaptive immune response to RSV rA2-line19F infection from Th2 to Th1 in BALB/c mice. J Virol. 2014;88(18):10569-83. Epub 2014/07/06. doi: 10.1128/JVI.01503-14. PubMed PMID: 24990999; PMCID: PMC4178873.

93. Anderson LJ, Hierholzer JC, Tsou C, Hendry RM, Fernie BF, Stone Y, McIntosh K. Antigenic characterization of respiratory syncytial virus strains with monoclonal antibodies. J Infect Dis. 1985;151(4):626-33. doi: 10.1093/infdis/151.4.626. PubMed PMID: 2579169.

94. Widjaja I, Wicht O, Luytjes W, Leenhouts K, Rottier PJM, van Kuppeveld FJM, Haijema BJ, de Haan CAM. Characterization of Epitope-Specific Anti-Respiratory Syncytial Virus (Anti-RSV) Antibody Responses after Natural Infection and after Vaccination with Formalin-Inactivated RSV. J Virol. 2016;90(13):5965-77. Epub 2016/04/22. doi: 10.1128/JVI.00235-16. PubMed PMID: 27099320; PMCID: PMC4907225.

95. Ngwuta JO, Chen M, Modjarrad K, Joyce MG, Kanekiyo M, Kumar A, Yassine HM, Moin SM, Killikelly AM, Chuang GY, Druz A, Georgiev IS, Rundlet EJ, Sastry M, Stewart-Jones GB, Yang Y, Zhang B, Nason MC, Capella C, Peeples ME, Ledgerwood JE, McLellan JS, Kwong PD, Graham BS. Prefusion F-specific antibodies determine the magnitude of RSV neutralizing activity in human sera. Sci Transl Med. 2015;7(309):309ra162. Epub 2015/10/16. doi: 10.1126/scitranslmed.aac4241. PubMed PMID: 26468324; PMCID: PMC4672383.

96. Tan L, Coenjaerts FE, Houspie L, Viveen MC, van Bleek GM, Wiertz EJ, Martin DP, Lemey P. The comparative genomics of human respiratory syncytial virus subgroups A and B: genetic variability and molecular evolutionary dynamics. J Virol. 2013;87(14):8213-26. doi: 10.1128/JVI.03278-12. PubMed PMID: 23698290; PMCID: PMC3700225.

97. Mufson MA, Orvell C, Rafnar B, Norrby E. Two distinct subtypes of human respiratory syncytial virus. J Gen Virol. 1985;66 (Pt 10):2111-24. Epub 1985/10/01. doi: 10.1099/0022-1317-66-10-2111. PubMed PMID: 2413163.

98. Hause AM, Henke DM, Avadhanula V, Shaw CA, Tapia LI, Piedra PA. Sequence variability of the respiratory syncytial virus (RSV) fusion gene among contemporary and historical genotypes of RSV/A and RSV/B. PLoS One. 2017;12(4):e0175792. Epub 2017/04/18. doi: 10.1371/journal.pone.0175792. PubMed PMID: 28414749; PMCID: PMC5393888.

99. Beeler JA vWCK. Neutralization epitopes of the F Glycoprotein of Respiratory Syncytial Virus: Effect of Mutation upon Fusion Function. Journal of Virology. 1989;63(7):2941-50.

100. Hicks SN, Chaiwatpongsakorn S, Costello HM, McLellan JS, Ray W, Peeples ME. Five Residues in the Apical Loop of the Respiratory Syncytial Virus Fusion Protein F2 Subunit Are Critical for Its Fusion Activity. J Virol. 2018;92(15). Epub

2018/05/11. doi: 10.1128/JVI.00621-18. PubMed PMID: 29743373; PMCID: PMC6052300.

101. Resch B. Product review on the monoclonal antibody palivizumab for prevention of respiratory syncytial virus infection. Hum Vaccin Immunother. 2017;13(9):2138-49. doi: 10.1080/21645515.2017.1337614. PubMed PMID: 28605249; PMCID: PMC5612471.

102. Wegzyn C, Toh LK, Notario G, Biguenet S, Unnebrink K, Park C, Makari D, Norton M. Safety and Effectiveness of Palivizumab in Children at High Risk of Serious Disease Due to Respiratory Syncytial Virus Infection: A Systematic Review. Infect Dis Ther. 2014;3(2):133-58. doi: 10.1007/s40121-014-0046-6. PubMed PMID: 25297809; PMCID: PMC4269625.

103. Homaira N, Rawlinson W, Snelling TL, Jaffe A. Effectiveness of Palivizumab in Preventing RSV Hospitalization in High Risk Children: A Real-World Perspective. Int J Pediatr. 2014;2014:571609. doi: 10.1155/2014/571609. PubMed PMID: 25548575; PMCID: PMC4274815.

104. Wu H, Pfarr DS, Johnson S, Brewah YA, Woods RM, Patel NK, White WI, Young JF, Kiener PA. Development of motavizumab, an ultra-potent antibody for the prevention of respiratory syncytial virus infection in the upper and lower respiratory tract. J Mol Biol. 2007;368(3):652-65. Epub 2007/03/17. doi: 10.1016/j.jmb.2007.02.024. PubMed PMID: 17362988.

105. Carbonell-Estrany X, Simoes EA, Dagan R, Hall CB, Harris B, Hultquist M, Connor EM, Losonsky GA, Motavizumab Study G. Motavizumab for prophylaxis of respiratory syncytial virus in high-risk children: a noninferiority trial. Pediatrics. 2010;125(1):e35-51. Epub 2009/12/17. doi: 10.1542/peds.2008-1036. PubMed PMID: 20008423.

106. Prescott WA, Jr., Doloresco F, Brown J, Paladino JA. Cost effectiveness of respiratory syncytial virus prophylaxis: a critical and systematic review. Pharmacoeconomics. 2010;28(4):279-93. doi: 10.2165/11531860-000000000-00000. PubMed PMID: 20131925.

107. Griffin MP, Yuan Y, Takas T, Domachowske JB, Madhi SA, Manzoni P, Simoes EAF, Esser MT, Khan AA, Dubovsky F, Villafana T, DeVincenzo JP, Nirsevimab Study G. Single-Dose Nirsevimab for Prevention of RSV in Preterm Infants. N Engl J Med. 2020;383(5):415-25. Epub 2020/07/30. doi: 10.1056/NEJMoa1913556. PubMed PMID: 32726528.

108. Lipsitch M, O'Hagan JJ. Patterns of antigenic diversity and the mechanisms that maintain them. J R Soc Interface. 2007;4(16):787-802. doi: 10.1098/rsif.2007.0229. PubMed PMID: 17426010; PMCID: PMC2394542.

109. Doud MB, Hensley SE, Bloom JD. Complete mapping of viral escape from neutralizing antibodies. PLoS Pathog. 2017;13(3):e1006271. doi: 10.1371/journal.ppat.1006271. PubMed PMID: 28288189; PMCID: PMC5363992.

110. Duffy S. Why are RNA virus mutation rates so damn high? PLoS Biol. 2018;16(8):e3000003. Epub 2018/08/14. doi: 10.1371/journal.pbio.3000003. PubMed PMID: 30102691; PMCID: PMC6107253.

111. Papenburg J, Carbonneau J, Hamelin ME, Isabel S, Bouhy X, Ohoumanne N, Dery P, Paes BA, Corbeil J, Bergeron MG, De Serres G, Boivin G. Molecular evolution of respiratory syncytial virus fusion gene, Canada, 2006-2010. Emerg Infect Dis. 2012;18(1):120-4. doi: 10.3201/eid1801.110515. PubMed PMID: 22264682; PMCID: PMC3310097.

112. Agoti CN, Otieno JR, Gitahi CW, Cane PA, Nokes DJ. Rapid spread and diversification of respiratory syncytial virus genotype ON1, Kenya. Emerg Infect Dis. 2014;20(6):950-9. Epub 2014/05/27. doi: 10.3201/eid2006.131438. PubMed PMID: 24856417; PMCID: PMC4036793.

113. Yasuhara A, Yamayoshi S, Soni P, Takenaga T, Kawakami C, Takashita E, Sakai-Tagawa Y, Uraki R, Ito M, Iwatsuki-Horimoto K, Sasaki T, Ikuta K, Yamada S, Kawaoka Y. Diversity of antigenic mutants of influenza A(H1N1)pdm09 virus escaped from human monoclonal antibodies. Sci Rep. 2017;7(1):17735. doi: 10.1038/s41598-017-17986-8. PubMed PMID: 29255273; PMCID: PMC5735164.

114. Gauger PC, Vincent AL. Serum Virus Neutralization Assay for Detection and Quantitation of Serum Neutralizing Antibodies to Influenza A Virus in Swine. Methods Mol Biol. 2020;2123:321-33. Epub 2020/03/15. doi: 10.1007/978-1-0716-0346-8_23. PubMed PMID: 32170698.

115. Gauger PC, Vincent AL. Serum virus neutralization assay for detection and quantitation of serum-neutralizing antibodies to influenza A virus in swine. Methods Mol Biol. 2014;1161:313-24. Epub 2014/06/06. doi: 10.1007/978-1-4939-0758-8_26. PubMed PMID: 24899440.

116. Nie J, Li Q, Wu J, Zhao C, Hao H, Liu H, Zhang L, Nie L, Qin H, Wang M, Lu Q, Li X, Sun Q, Liu J, Fan C, Huang W, Xu M, Wang Y. Quantification of SARS-CoV-2 neutralizing antibody by a pseudotyped virus-based assay. Nat Protoc. 2020;15(11):3699-715. Epub 2020/09/27. doi: 10.1038/s41596-020-0394-5. PubMed PMID: 32978602.

117. Cohen BJ, Doblas D, Andrews N. Comparison of plaque reduction neutralisation test (PRNT) and measles virus-specific IgG ELISA for assessing immunogenicity of measles vaccination. Vaccine. 2008;26(50):6392-7. Epub 2008/10/07. doi: 10.1016/j.vaccine.2008.08.074. PubMed PMID: 18834911.

118. Bewley KR, Coombes NS, Gagnon L, McInroy L, Baker N, Shaik I, St-Jean JR, St-Amant N, Buttigieg KR, Humphries HE, Godwin KJ, Brunt E, Allen L, Leung S, Brown PJ, Penn EJ, Thomas K, Kulnis G, Hallis B, Carroll M, Funnell S, Charlton S. Quantification of SARS-CoV-2 neutralizing antibody by wild-type plaque reduction neutralization, microneutralization and pseudotyped virus neutralization assays. Nat Protoc. 2021. Epub 2021/04/25. doi: 10.1038/s41596-021-00536-y. PubMed PMID: 33893470.

119. Matrosovich M, Matrosovich T, Garten W, Klenk HD. New low-viscosity overlay medium for viral plaque assays. Virol J. 2006;3(1):63. Epub 2006/09/02. doi: 10.1186/1743-422X-3-63. PubMed PMID: 16945126; PMCID: PMC1564390.

120. Kolawole AO, Li M, Xia C, Fischer AE, Giacobbi NS, Rippinger CM, Proescher JB, Wu SK, Bessling SL, Gamez M, Yu C, Zhang R, Mehoke TS, Pipas JM, Wolfe JT, Lin JS, Feldman AB, Smith TJ, Wobus CE. Flexibility in surface-exposed loops in a virus capsid mediates escape from antibody neutralization. J Virol. 2014;88(8):4543-57. doi: 10.1128/JVI.03685-13. PubMed PMID: 24501415; PMCID: PMC3993751.

121. Zhu Q, Lu B, McTamney P, Palaszynski S, Diallo S, Ren K, Ulbrandt ND, Kallewaard N, Wang W, Fernandes F, Wong S, Svabek C, Moldt B, Esser MT, Jing H, Suzich JA. Prevalence and Significance of Substitutions in the Fusion Protein of Respiratory Syncytial Virus Resulting in Neutralization Escape From Antibody MEDI8897. J Infect Dis. 2018;218(4):572-80. Epub 2018/04/05. doi: 10.1093/infdis/jiy189. PubMed PMID: 29617879.

122. Dykes C, Demeter LM. Clinical significance of human immunodeficiency virus type 1 replication fitness. Clin Microbiol Rev. 2007;20(4):550-78. doi: 10.1128/CMR.00017-07. PubMed PMID: 17934074; PMCID: PMC2176046.

123. Shrestha B, Austin SK, Dowd KA, Prasad AN, Youn S, Pierson TC, Fremont DH, Ebel GD, Diamond MS. Complex phenotypes in mosquitoes and mice associated with neutralization escape of a Dengue virus type 1 monoclonal antibody. Virology. 2012;427(2):127-34. doi: 10.1016/j.virol.2012.02.010. PubMed PMID: 22406169; PMCID: PMC3312934.

124. Miller CR, Johnson EL, Burke AZ, Martin KP, Miura TA, Wichman HA, Brown CJ, Ytreberg FM. Initiating a watch list for Ebola virus antibody escape mutations.

PeerJ. 2016;4:e1674. doi: 10.7717/peerj.1674. PubMed PMID: 26925318; PMCID: PMC4768679.

125. Matsuzaki Y, Sugawara K, Nakauchi M, Takahashi Y, Onodera T, Tsunetsugu-Yokota Y, Matsumura T, Ato M, Kobayashi K, Shimotai Y, Mizuta K, Hongo S, Tashiro M, Nobusawa E. Epitope mapping of the hemagglutinin molecule of A/(H1N1)pdm09 influenza virus by using monoclonal antibody escape mutants. J Virol. 2014;88(21):12364-73. doi: 10.1128/JVI.01381-14. PubMed PMID: 25122788; PMCID: PMC4248900.

126. Marissen WE, Kramer RA, Rice A, Weldon WC, Niezgoda M, Faber M, Slootstra JW, Meloen RH, Clijsters-van der Horst M, Visser TJ, Jongeneelen M, Thijsse S, Throsby M, de Kruif J, Rupprecht CE, Dietzschold B, Goudsmit J, Bakker AB. Novel rabies virus-neutralizing epitope recognized by human monoclonal antibody: fine mapping and escape mutant analysis. J Virol. 2005;79(8):4672-8. doi: 10.1128/JVI.79.8.4672-4678.2005. PubMed PMID: 15795253; PMCID: PMC1069557.

127. Lee CY, Kam YW, Fric J, Malleret B, Koh EG, Prakash C, Huang W, Lee WW, Lin C, Lin RT, Renia L, Wang CI, Ng LF, Warter L. Chikungunya virus neutralization antigens and direct cell-to-cell transmission are revealed by human antibody-escape mutants. PLoS Pathog. 2011;7(12):e1002390. doi: 10.1371/journal.ppat.1002390. PubMed PMID: 22144891; PMCID: PMC3228792.

128. Kugelman JR, Kugelman-Tonos J, Ladner JT, Pettit J, Keeton CM, Nagle ER, Garcia KY, Froude JW, Kuehne AI, Kuhn JH, Bavari S, Zeitlin L, Dye JM, Olinger GG, Sanchez-Lockhart M, Palacios GF. Emergence of Ebola Virus Escape Variants in Infected Nonhuman Primates Treated with the MB-003 Antibody Cocktail. Cell Rep. 2015;12(12):2111-20. doi: 10.1016/j.celrep.2015.08.038. PubMed PMID: 26365189.

129. Sourisseau M, Lawrence DJP, Schwarz MC, Storrs CH, Veit EC, Bloom JD, Evans MJ. Deep Mutational Scanning Comprehensively Maps How Zika Envelope Protein Mutations Affect Viral Growth and Antibody Escape. J Virol. 2019;93(23). doi: 10.1128/JVI.01291-19. PubMed PMID: 31511387; PMCID: PMC6854493.

130. Doud MB, Lee JM, Bloom JD. How single mutations affect viral escape from broad and narrow antibodies to H1 influenza hemagglutinin. Nat Commun. 2018;9(1):1386. doi: 10.1038/s41467-018-03665-3. PubMed PMID: 29643370; PMCID: PMC5895760.

131. Greaney AJ, Starr TN, Gilchuk P, Zost SJ, Binshtein E, Loes AN, Hilton SK, Huddleston J, Eguia R, Crawford KHD, Dingens AS, Nargi RS, Sutton RE, Suryadevara N, Rothlauf PW, Liu Z, Whelan SPJ, Carnahan RH, Crowe JE, Jr.,

Bloom JD. Complete Mapping of Mutations to the SARS-CoV-2 Spike Receptor-Binding Domain that Escape Antibody Recognition. Cell Host Microbe. 2021;29(1):44-57 e9. Epub 2020/12/02. doi: 10.1016/j.chom.2020.11.007. PubMed PMID: 33259788; PMCID: PMC7676316.

132. Starr TN, Greaney AJ, Addetia A, Hannon WW, Choudhary MC, Dingens AS, Li JZ, Bloom JD. Prospective mapping of viral mutations that escape antibodies used to treat COVID-19. Science. 2021;371(6531):850-4. Epub 2021/01/27. doi: 10.1126/science.abf9302. PubMed PMID: 33495308.

133. Crowe JE, Firestone CY, Crim R, Beeler JA, Coelingh KL, Barbas CF, Burton DR, Chanock RM, Murphy BR. Monoclonal antibody-resistant mutants selected with a respiratory syncytial virus-neutralizing human antibody fab fragment (Fab 19) define a unique epitope on the fusion (F) glycoprotein. Virology. 1998;252(2):373-5. doi: 10.1006/viro.1998.9462. PubMed PMID: 9878616.

134. Zhao X, Chen FP, Sullender WM. Respiratory syncytial virus escape mutant derived in vitro resists palivizumab prophylaxis in cotton rats. Virology. 2004;318(2):608-12. doi: 10.1016/j.virol.2003.10.018. PubMed PMID: 14972528.

135. Boivin G, Caouette G, Frenette L, Carbonneau J, Ouakki M, De Serres G. Human respiratory syncytial virus and other viral infections in infants receiving palivizumab. J Clin Virol. 2008;42(1):52-7. doi: 10.1016/j.jcv.2007.11.012. PubMed PMID: 18164233; PMCID: PMC7172843.

136. Zhu Q, McAuliffe JM, Patel NK, Palmer-Hill FJ, Yang CF, Liang B, Su L, Zhu W, Wachter L, Wilson S, MacGill RS, Krishnan S, McCarthy MP, Losonsky GA, Suzich JA. Analysis of respiratory syncytial virus preclinical and clinical variants resistant to neutralization by monoclonal antibodies palivizumab and/or motavizumab. J Infect Dis. 2011;203(5):674-82. doi: 10.1093/infdis/jiq100. PubMed PMID: 21208913; PMCID: PMC3072724.

137. Zhao X, Liu E, Chen FP, Sullender WM. In vitro and in vivo fitness of respiratory syncytial virus monoclonal antibody escape mutants. J Virol. 2006;80(23):11651-7. doi: 10.1128/JVI.01387-06. PubMed PMID: 17005645; PMCID: PMC1642624.

138. Zhao X, Sullender WM. In vivo selection of respiratory syncytial viruses resistant to palivizumab. J Virol. 2005;79(7):3962-8. doi: 10.1128/JVI.79.7.3962-3968.2005. PubMed PMID: 15767398; PMCID: PMC1061530.

139. Zhao X, Chen FP, Megaw AG, Sullender WM. Variable resistance to palivizumab in cotton rats by respiratory syncytial virus mutants. J Infect Dis. 2004;190(11):1941-6. doi: 10.1086/425515. PubMed PMID: 15529258.

140. Tome L, Frabasile S, Candia C, Pittini A, Farina N, Melero JA, Arbiza J. Selection and characterization of human respiratory syncytial virus escape mutants resistant to a polyclonal antiserum raised against the F protein. Arch Virol. 2012;157(6):1071-80. doi: 10.1007/s00705-012-1274-2. PubMed PMID: 22411099.

141. Morton CJ, Cameron R, Lawrence LJ, Lin B, Lowe M, Luttick A, Mason A, McKimm-Breschkin J, Parker MW, Ryan J, Smout M, Sullivan J, Tucker SP, Young PR. Structural characterization of respiratory syncytial virus fusion inhibitor escape mutants: homology model of the F protein and a syncytium formation assay. Virology. 2003;311(2):275-88. doi: 10.1016/s0042-6822(03)00115-6. PubMed PMID: 12842618.

142. Weiss GA, Watanabe CK, Zhong A, Goddard A, Sidhu SS. Rapid mapping of protein functional epitopes by combinatorial alanine scanning. Proc Natl Acad Sci U S A. 2000;97(16):8950-4. doi: 10.1073/pnas.160252097. PubMed PMID: 10908667; PMCID: PMC16802.

143. Burks EA, Chen G, Georgiou G, Iverson BL. In vitro scanning saturation mutagenesis of an antibody binding pocket. Proc Natl Acad Sci U S A. 1997;94(2):412-7. Epub 1997/01/21. doi: 10.1073/pnas.94.2.412. PubMed PMID: 9012796; PMCID: PMC19525.

144. Warren MS, Benkovic SJ. Combinatorial manipulation of three key active site residues in glycinamide ribonucleotide transformylase. Protein Eng. 1997;10(1):63-8. Epub 1997/01/01. doi: 10.1093/protein/10.1.63. PubMed PMID: 9051735.

145. Shortle D. Probing the determinants of protein folding and stability with amino acid substitutions. J Biol Chem. 1989;264(10):5315-8; PMCID: 2647715.

146. Labrou NE. Random mutagenesis methods for in vitro directed enzyme evolution. Curr Protein Pept Sci. 2010;11(1):91-100. Epub 2010/03/06. doi: 10.2174/138920310790274617. PubMed PMID: 20201809.

147. Mingo J, Erramuzpe A, Luna S, Aurtenetxe O, Amo L, Diez I, Schepens JT, Hendriks WJ, Cortes JM, Pulido R. One-Tube-Only Standardized Site-Directed Mutagenesis: An Alternative Approach to Generate Amino Acid Substitution Collections. PLoS One. 2016;11(8):e0160972. Epub 2016/08/23. doi: 10.1371/journal.pone.0160972. PubMed PMID: 27548698; PMCID: PMC4993582.

148. Wong TS, Roccatano D, Zacharias M, Schwaneberg U. A statistical analysis of random mutagenesis methods used for directed protein evolution. J Mol Biol. 2006;355(4):858-71. Epub 2005/12/06. doi: 10.1016/j.jmb.2005.10.082. PubMed PMID: 16325201.

149. Fowler DM, Araya CL, Fleishman SJ, Kellogg EH, Stephany JJ, Baker D, Fields S. High-resolution mapping of protein sequence-function relationships. Nature Methods. 2010;7(9):741-6. doi: 10.1038/nmeth.1492.

150. Ernst A, Gfeller D, Kan Z, Seshagiri S, Kim PM, Bader GD, Sidhu SS. Coevolution of PDZ domain-ligand interactions analyzed by high-throughput phage display and deep sequencing. Mol Biosyst. 2010;6(10):1782-90. Epub 2010/08/18. doi: 10.1039/c0mb00061b. PubMed PMID: 20714644.

151. Hietpas RT, Jensen JD, Bolon DN. Experimental illumination of a fitness landscape. Proc Natl Acad Sci U S A. 2011;108(19):7896-901. Epub 2011/04/06. doi: 10.1073/pnas.1016024108. PubMed PMID: 21464309; PMCID: PMC3093508.

152. Gaiotto T, Hufton SE. Cross-Neutralising Nanobodies Bind to a Conserved Pocket in the Hemagglutinin Stem Region Identified Using Yeast Display and Deep Mutational Scanning. PLoS One. 2016;11(10):e0164296. Epub 2016/10/16. doi: 10.1371/journal.pone.0164296. PubMed PMID: 27741319; PMCID: PMC5065140 antibodies described in this study has been filed. This does not alter adherence to all of the PLOS ONE policies on sharing data and information.

153. Dingens AS, Haddox HK, Overbaugh J, Bloom JD. Comprehensive Mapping of HIV-1 Escape from a Broadly Neutralizing Antibody. Cell Host & Microbe. 2017;21(6):777-87.e4. doi: 10.1016/j.chom.2017.05.003.

154. Kunkel TA. Rapid and efficient site-specific mutagenesis without phenotypic selection. Proc Natl Acad Sci U S A. 1985;82(2):488-92. Epub 1985/01/01. doi: 10.1073/pnas.82.2.488. PubMed PMID: 3881765; PMCID: PMC397064.

155. Kosuri S, Eroshenko N, Leproust EM, Super M, Way J, Li JB, Church GM. Scalable gene synthesis by selective amplification of DNA pools from high-fidelity microchips. Nat Biotechnol. 2010;28(12):1295-9. Epub 2010/11/30. doi: 10.1038/nbt.1716. PubMed PMID: 21113165; PMCID: PMC3139991.

156. Cadwell RC, Joyce GF. Mutagenic PCR. PCR Methods Appl. 1994;3(6):S136-40. Epub 1994/06/01. doi: 10.1101/gr.3.6.s136. PubMed PMID: 7920233.

157. Weile J, Sun S, Cote AG, Knapp J, Verby M, Mellor JC, Wu Y, Pons C, Wong C, van Lieshout N, Yang F, Tasan M, Tan G, Yang S, Fowler DM, Nussbaum R, Bloom JD, Vidal M, Hill DE, Aloy P, Roth FP. A framework for exhaustively mapping functional missense variants. Mol Syst Biol. 2017;13(12):957. Epub 2017/12/23. doi: 10.15252/msb.20177908. PubMed PMID: 29269382; PMCID: PMC5740498.

158. Roth JWFP. Multiplexed assays of variant effects contribute to a growing

genotype–phenotype atlas. Human Genetics. 2018. doi: 10.1007/s00439-018-1916.

159. Miller AD. pa317 Retrovirus Packaging Cells. Molecular Therapy. 2002;6(5):572-5. doi: 10.1006/mthe.2002.0728.

160. Ban J, First NL, Temin HM. Bovine leukaemia virus packaging cell line for retrovirus-mediated gene transfer. J Gen Virol. 1989;70 (Pt 8)(8):1987-93. Epub 1989/08/01. doi: 10.1099/0022-1317-70-8-1987. PubMed PMID: 2549178.

161. Burns JC, Friedmann T, Driever W, Burrascano M, Yee JK. Vesicular stomatitis virus G glycoprotein pseudotyped retroviral vectors: concentration to very high titer and efficient gene transfer into mammalian and nonmammalian cells. Proc Natl Acad Sci U S A. 1993;90(17):8033-7. Epub 1993/09/01. doi: 10.1073/pnas.90.17.8033. PubMed PMID: 8396259; PMCID: PMC47282.

162. Kovesdi I, Brough DE, Bruder JT, Wickham TJ. Adenoviral vectors for gene transfer. Curr Opin Biotechnol. 1997;8(5):583-9. Epub 1997/11/14. doi: 10.1016/s0958-1669(97)80033-x. PubMed PMID: 9353227.

163. Gaidukov L, Wroblewska L, Teague B, Nelson T, Zhang X, Liu Y, Jagtap K, Mamo S, Tseng WA, Lowe A, Das J, Bandara K, Baijuraj S, Summers NM, Lu TK, Zhang L, Weiss R. A multi-landing pad DNA integration platform for mammalian cell engineering. Nucleic Acids Res. 2018;46(8):4072-86. doi: 10.1093/nar/gky216. PubMed PMID: 29617873; PMCID: PMC5934685.

164. Matreyek KA, Stephany JJ, Chiasson MA, Hasle N, Fowler DM. An improved platform for functional assessment of large protein libraries in mammalian cells. Nucleic Acids Research. 2019. doi: 10.1093/nar/gkz910.

165. Matreyek KA, Stephany JJ, Fowler DM. A platform for functional assessment of large variant libraries in mammalian cells. Nucleic Acids Res. 2017;45(11):e102. Epub 2017/03/24. doi: 10.1093/nar/gkx183. PubMed PMID: 28335006; PMCID: PMC5499817.

166. Duportet X, Wroblewska L, Guye P, Li Y, Eyquem J, Rieders J, Rimchala T, Batt G, Weiss R. A platform for rapid prototyping of synthetic gene networks in mammalian cells. Nucleic Acids Res. 2014;42(21):13440-51. Epub 2014/11/08. doi: 10.1093/nar/gku1082. PubMed PMID: 25378321; PMCID: PMC4245948.

167. Chi X, Zheng Q, Jiang R, Chen-Tsai RY, Kong LJ. A system for site-specific integration of transgenes in mammalian cells. PLoS One. 2019;14(7):e0219842. Epub 2019/07/26. doi: 10.1371/journal.pone.0219842. PubMed PMID: 31344144; PMCID: PMC6657834 system (Kong, L.-J., Tsai, R., Site specific integration of

transgenes. PCT/US2017/027073). These do not alter our adherence to PLOS ONE policies on sharing data and materials.

168. Fowler DM, Fields S. Deep mutational scanning: a new style of protein science. Nature Methods. 2014;11(8):801-7. Epub 2014/07/31. doi: 10.1038/nmeth.3027. PubMed PMID: 25075907; PMCID: PMC4410700.

169. Whitehead TA, Chevalier A, Song Y, Dreyfus C, Fleishman SJ, De Mattos C, Myers CA, Kamisetty H, Blair P, Wilson IA, Baker D. Optimization of affinity, specificity and function of designed influenza inhibitors using deep sequencing. Nat Biotechnol. 2012;30(6):543-8. Epub 2012/05/29. doi: 10.1038/nbt.2214. PubMed PMID: 22634563; PMCID: PMC3638900.

170. Julius MH, Masuda T, Herzenberg LA. Demonstration that antigen-binding cells are precursors of antibody-producing cells after purification with a fluorescence-activated cell sorter. Proc Natl Acad Sci U S A. 1972;69(7):1934-8. Epub 1972/07/01. doi: 10.1073/pnas.69.7.1934. PubMed PMID: 4114858; PMCID: PMC426835.

171. Majithia AR, Tsuda B, Agostini M, Gnanapradeepan K, Rice R, Peloso G, Patel KA, Zhang XL, Broekema MF, Patterson N, Duby M, Sharpe T, Kalkhoven E, Rosen ED, Barroso I, Ellard S, Kathiresan S, O'Rahilly S, Chatterjee K, Florez JC, Mikkelsen T, Savage DB, Altshuler D, Consortium UMD, Con MIG, Consor UCL. Prospective functional classification of all possible missense variants in *PPARG*. Nature Genetics. 2016;48(12):1570-5. doi: 10.1038/ng.3700. PubMed PMID: WOS:000389011100019.

172. Schlinkmann KM, Honegger A, Tureci E, Robison KE, Lipovsek D, Pluckthun A. Critical features for biosynthesis, stability, and functionality of a G protein-coupled receptor uncovered by all-versus-all mutations. Proc Natl Acad Sci U S A. 2012;109(25):9810-5. Epub 2012/06/06. doi: 10.1073/pnas.1202107109. PubMed PMID: 22665811; PMCID: PMC3382542.

173. Bates JT, Keefer CJ, Slaughter JC, Kulp DW, Schief WR, Crowe JE, Jr. Escape from neutralization by the respiratory syncytial virus-specific neutralizing monoclonal antibody palivizumab is driven by changes in on-rate of binding to the fusion protein. Virology. 2014;454-455:139-44. doi: 10.1016/j.virol.2014.02.010. PubMed PMID: 24725940; PMCID: PMC4004766.

174. Forsyth CM, Juan V, Akamatsu Y, DuBridge RB, Doan M, Ivanov AV, Ma Z, Polakoff D, Razo J, Wilson K, Powers DB. Deep mutational scanning of an antibody against epidermal growth factor receptor using mammalian cell display and massively parallel pyrosequencing. MAbs. 2013;5(4):523-32. Epub 2013/06/15. doi: 10.4161/mabs.24979. PubMed PMID: 23765106; PMCID: PMC3906306.

175. Lee JM, Huddleston J, Doud MB, Hooper KA, Wu NC, Bedford T, Bloom JD. Deep mutational scanning of hemagglutinin helps predict evolutionary fates of human H3N2 influenza variants. Proc Natl Acad Sci U S A. 2018;115(35):E8276-E85. Epub 2018/08/15. doi: 10.1073/pnas.1806133115. PubMed PMID: 30104379; PMCID: PMC6126756.

176. Starr TN, Greaney AJ, Hilton SK, Ellis D, Crawford KHD, Dingens AS, Navarro MJ, Bowen JE, Tortorici MA, Walls AC, King NP, Veesler D, Bloom JD. Deep Mutational Scanning of SARS-CoV-2 Receptor Binding Domain Reveals Constraints on Folding and ACE2 Binding. Cell. 2020;182(5):1295-310 e20. Epub 2020/08/26. doi: 10.1016/j.cell.2020.08.012. PubMed PMID: 32841599; PMCID: PMC7418704.

177. Mehlhoff JD, Ostermeier M. Biological fitness landscapes by deep mutational scanning. Elsevier; 2020. p. 203-24.

178. Naldini L. Lentiviruses as gene transfer agents for delivery to non-dividing cells. Current Opinion in Biotechnology. 1998;9(5):457-63. doi: 10.1016/s0958-1669(98)80029-3.

179. Collins PL, Hill MG, Camargo E, Grosfeld H, Chanock RM, Murphy BR. Production of infectious human respiratory syncytial virus from cloned cDNA confirms an essential role for the transcription elongation factor from the 5' proximal open reading frame of the M2 mRNA in gene expression and provides a capability for vaccine development. Proc Natl Acad Sci U S A. 1995;92(25):11563-7. Epub 1995/12/05. doi: 10.1073/pnas.92.25.11563. PubMed PMID: 8524804; PMCID: PMC40442.

180. Anthony John Mason USPT, Victoria (AU), Paul R Young, Queensland (AU), inventorMethod of Expression and Agents Identified Thereby2004 Aug. 19, 2004

181. Katzen F. Gateway((R)) recombinational cloning: a biological operating system. Expert Opin Drug Discov. 2007;2(4):571-89. Epub 2007/04/01. doi: 10.1517/17460441.2.4.571. PubMed PMID: 23484762.

182. Shin J-H, Yue Y, Duan D. Recombinant Adeno-Associated Viral Vector Production and Purification. Humana Press; 2012. p. 267-84.

183. Reiser J. Production and concentration of pseudotyped HIV-1-based gene transfer vectors. Gene Ther. 2000;7(11):910-3. doi: 10.1038/sj.gt.3301188. PubMed PMID: 10849549.

184. Mendell JR, Rodino-Klapac LR, Rosales-Quintero X, Kota J, Coley BD, Galloway G, Craenen JM, Lewis S, Malik V, Shilling C, Byrne BJ, Conlon T, Campbell KJ, Bremer WG, Viollet L, Walker CM, Sahenk Z, Clark KR. Limb-girdle

muscular dystrophy type 2D gene therapy restores alpha-sarcoglycan and associated proteins. Ann Neurol. 2009;66(3):290-7. Epub 2009/10/03. doi: 10.1002/ana.21732. PubMed PMID: 19798725; PMCID: PMC6014624.

185. Bainbridge JW, Smith AJ, Barker SS, Robbie S, Henderson R, Balaggan K, Viswanathan A, Holder GE, Stockman A, Tyler N, Petersen-Jones S, Bhattacharya SS, Thrasher AJ, Fitzke FW, Carter BJ, Rubin GS, Moore AT, Ali RR. Effect of gene therapy on visual function in Leber's congenital amaurosis. N Engl J Med. 2008;358(21):2231-9. Epub 2008/04/29. doi: 10.1056/NEJMoa0802268. PubMed PMID: 18441371.

186. Killikelly AM, Kanekiyo M, Graham BS. Pre-fusion F is absent on the surface of formalin-inactivated respiratory syncytial virus. Scientific Reports. 2016;6(1):34108. doi: 10.1038/srep34108.

187. Sultana A, Lee JE. Measuring protein-protein and protein-nucleic Acid interactions by biolayer interferometry. Curr Protoc Protein Sci. 2015;79:19 25 1-19 25 6. Epub 2015/02/03. doi: 10.1002/0471140864.ps1925s79. PubMed PMID: 25640894.

188. Petersen RL. Strategies Using Bio-Layer Interferometry Biosensor Technology for Vaccine Research and Development. Biosensors (Basel). 2017;7(4):49. Epub 2017/11/01. doi: 10.3390/bios7040049. PubMed PMID: 29088096; PMCID: PMC5746772.

189. Kumaraswamy S, Tobias R. Label-free kinetic analysis of an antibody-antigen interaction using biolayer interferometry. Methods Mol Biol. 2015;1278:165-82. Epub 2015/04/11. doi: 10.1007/978-1-4939-2425-7_10. PubMed PMID: 25859949.

190. Hearty S, Leonard P, O'Kennedy R. Measuring antibody-antigen binding kinetics using surface plasmon resonance. Methods Mol Biol. 2012;907:411-42. Epub 2012/08/22. doi: 10.1007/978-1-61779-974-7_24. PubMed PMID: 22907366.

191. Chenail G, Brown NE, Shea A, Feire AL, Deng G. Real-time analysis of antibody interactions with whole enveloped human cytomegalovirus using surface plasmon resonance. Anal Biochem. 2011;411(1):58-63. Epub 2010/12/21. doi: 10.1016/j.ab.2010.12.017. PubMed PMID: 21167121.

192. Lad L, Clancy S, Kovalenko M, Liu C, Hui T, Smith V, Pagratis N. High-throughput kinetic screening of hybridomas to identify high-affinity antibodies using bio-layer interferometry. J Biomol Screen. 2015;20(4):498-507. Epub 2014/11/27. doi: 10.1177/1087057114560123. PubMed PMID: 25425568.

193. Xiong X, Martin SR, Haire LF, Wharton SA, Daniels RS, Bennett MS, McCauley JW, Collins PJ, Walker PA, Skehel JJ, Gamblin SJ. Receptor binding by an H7N9 influenza virus from humans. Nature. 2013;499(7459):496-9. Epub 2013/06/22. doi: 10.1038/nature12372. PubMed PMID: 23787694.

194. Selvarajah S, Sexton NR, Kahle KM, Fong RH, Mattia KA, Gardner J, Lu K, Liss NM, Salvador B, Tucker DF, Barnes T, Mabila M, Zhou X, Rossini G, Rucker JB, Sanders DA, Suhrbier A, Sambri V, Michault A, Muench MO, Doranz BJ, Simmons G. A neutralizing monoclonal antibody targeting the acid-sensitive region in chikungunya virus E2 protects from disease. PLoS Negl Trop Dis. 2013;7(9):e2423. Epub 2013/09/27. doi: 10.1371/journal.pntd.0002423. PubMed PMID: 24069479; PMCID: PMC3772074.

195. Tian G, Tang F, Yang C, Zhang W, Bergquist J, Wang B, Mi J, Zhang J. Quantitative dot blot analysis (QDB), a versatile high throughput immunoblot method. Oncotarget. 2017;8(35):58553-62. Epub 2017/09/25. doi: 10.18632/oncotarget.17236. PubMed PMID: 28938578; PMCID: PMC5601674.

196. Georgiou G. Analysis of large libraries of protein mutants using flow cytometry. Advances in protein chemistry. 2001;55:293-315. doi: 10.1016/S0065-3233(01)55007-X.

197. Daugherty PS, Iverson BL, Georgiou G. Flow cytometric screening of cell-based libraries. J Immunol Methods. 2000;243(1-2):211-27. Epub 2000/09/15. doi: 10.1016/s0022-1759(00)00236-2. PubMed PMID: 10986416.

198. Hotard AL, Shaikh FY, Lee S, Yan D, Teng MN, Plemper RK, Crowe JE, Jr., Moore ML. A stabilized respiratory syncytial virus reverse genetics system amenable to recombination-mediated mutagenesis. Virology. 2012;434(1):129-36. Epub 2012/10/16. doi: 10.1016/j.virol.2012.09.022. PubMed PMID: 23062737; PMCID: PMC3492879.

199. Miller CR, Lee KH, Wichman HA, Ytreberg FM. Changing folding and binding stability in a viral coat protein: a comparison between substitutions accessible through mutation and those fixed by natural selection. PLoS One. 2014;9(11):e112988. Epub 2014/11/19. doi: 10.1371/journal.pone.0112988. PubMed PMID: 25405628; PMCID: PMC4236103.

200. Mitra R, Baviskar P, Duncan-Decocq RR, Patel D, Oomens AG. The human respiratory syncytial virus matrix protein is required for maturation of viral filaments. J Virol. 2012;86(8):4432-43. Epub 2012/02/10. doi: 10.1128/JVI.06744-11. PubMed PMID: 22318136; PMCID: PMC3318654.

Appendix A: Copyright Letter for Permission

ELSEVIER LICENSE
TERMS AND CONDITIONS

Jul 14, 2021

This Agreement between University of Idaho -- Laura Hutchison ("You") and Elsevier ("Elsevier") consists of your license details and the terms and conditions provided by Elsevier and Copyright Clearance Center.

License Number	5094421025315
License date	Jun 22, 2021
Licensed Content Publisher	Elsevier
Licensed Content Publication	Trends in Microbiology
Licensed Content Title	Clinical Potential of Prefusion RSV F-specific Antibodies
Licensed Content Author	Iebe Rossey,Jason S. McLellan,Xavier Saelens,Bert Schepens
Licensed Content Date	Mar 1, 2018
Licensed Content Volume	26
Licensed Content Issue	3
Licensed Content Pages	11
Start Page	209
End Page	219
Type of Use	reuse in a thesis/dissertation
Portion	figures/tables/illustrations